2018-11-29

Mutual Diffusivity of Bitumen and Liquid Hydrocarb

Grimaldos Aguilar, Franklin Aldemar

UNIVERSITY OF CALGARY

Mutual Diffusivity of Bitumen and Liquid Hydrocarbons

by

Franklin Aldemar Grimaldos Aguilar

A THESIS

SUBMITTED TO THE FACULTY OF GRADUATE STUDIES

IN PARTIAL FULFILMENT OF THE REQUIREMENTS FOR THE

DEGREE OF MASTER OF SCIENCE

GRADUATE PROGRAM IN CHEMICAL AND PETROLEUM ENGINEERING

CALGARY, ALBERTA

NOVEMBER, 2018

Abstract

The objective of this study was to determine the mutual diffusivity for bitumen and maltenes with liquid hydrocarbons at ambient conditions. A new apparatus was designed and commissioned to measure the mass transfer in these systems based on the density profiles established over time in a column of solvent over bitumen. A one dimensional numerical model based on molecular diffusion was developed to determine the mutual diffusivity from the concentration profiles. The model accounted for the dependence of diffusivity on viscosity through a correlation based on the infinite dilution diffusivities of the solvent and the oil. Diffusivities were determined for Athabasca bitumen and maltenes with toluene, n-heptane, and n-pentane at ambient conditions and diffusion times from 3 to 15 days. The model matched the measured concentration profiles to within ±2% for bitumen and ±7% for maltenes. In addition, the effect of asphaltene precipitation of the mass transfer rate was assessed.

Dedication

A Dios por haberme dado tanto.

A mi mama Rubiela y a mi Papa Jesús Martin, por ustedes hago todo.

A mi hermano José Daniel, siempre orgulloso de usted.

A mi novia Yuli, por todo su amor y apoyo incondicional.

A mi abuelo José Aristóbulo, siempre presente en todos mis logros.

Table of Contents

List of Tables

List of Figures and Illustrations

xiii

List of Symbols, Abbreviations and Nomenclature

Upper Case Symbols

A : An arbitrary component

A_P : Proportionality constant in diffusivity-viscosity relationship

A^∞ : Proportionality constant in Equation 6.2

A_p^∞ : Proportionality constant in Equation 6.10

A^* : Bitumen specific parameter in density correlation [kg/m^3]

A_0 : Fitting parameter for dilute gas viscosity

A_{xo} : Cross-sectional area [cm²]

B : An arbitrary component

B_0 : Fitting parameter for dilute gas viscosity

B^* : Bitumen specific parameter in density correlation [kg/m^{3}K]

B_p : Proportionality constant in Equation 6.1

C : Mass concentration of any component [g/cm^3]

C^* : Any value of concentration between 0 and initial concentration of the Component [g/cm^3]

C_{Aeq} : Maximum solubility of the diffusing gas A in B [g/cm^3]

$C_{s,eq}$: Maximum solubility of the diffusing gas solvent in bitumen [g/cm^3]

D^* : Bitumen specific parameter in density empirical correlation[1/K]

D : Diffusivity of any component [cm^2/s]

D_0 : Concentration dependent molecular diffusivity averaged from solvent and solute infinite dilution diffusion coefficients [cm^2/s]

D_{AB} : Diffusivity of species A in B [cm^2/s]

D_{BA} : Diffusivity of species B in A [cm^2/s]

D_{sb} : Diffusivity of solvent in bitumen [cm^2/s]

D_{bs} : Diffusivity of bitumen in solvent [cm^2/s]

$(D_{sb}^\infty)^*$: Predicted infinite dilution diffusivity [cm^2/s].

D_{AA} : Self-diffusivity of a molecule of Component A in Pure A [cm^2/s]

D_{BB} : Self-diffusivity of a molecule of Component B in Pure B [cm^2/s]

D_{AB}^0 : Infinite dilution diffusivity of species A in B [cm^2/s]

D_{BA}^o : Infinite dilution diffusivity of species B in A [cm^2/s]

$D_{AB}^{o}{}^{Ideal}$: Infinite dilution diffusivity of A in B for an ideal solution [cm^2/s]

$\overline{D}_{sb}^{j}$: Average mutual diffusivity between neighbor layers where the diffusion process occurs. Used for the numerical model [cm²/s]

E_0 : Fitting parameter for dilute gas viscosity

F_0 : Fitting parameter for dilute gas viscosity

F^* : Bitumen specific parameter in density empirical correlation [1/MPa]

G : Calibration constant for the density meter.

J : Calibration constant for the density meter.

M : Initial Mass of any component [g]

$M_{b,i}^{j}$: Mass of bitumen for layer i and time j [g]

$M_{s,i}^{j}$: Mass of solvent for layer i and time j[g]

MW_B : Molecular weight of component B [g/mol]

N : Avogadro's number

P : Pressure [MPa]

P_N : Normalized pressure

R : Ideal gas constant [J/kmol.K]

R_A : Radius of the diffusing particle [m]

S : Slope in the linear region for a plot of solvent mass diffused versus square root of time [g/t$^{-0.5}$]

SG : Specific gravity of the bitumen

T : Temperature [K]

T_b : Normal boiling point of the bitumen [K]

V_A : Molar volume of component A [cm³/mol]

V : Volume [cm³]

V_{cum} : Cumulative volume [cm³]

X : Position with respect the initial interface of two liquids in contact[cm]

Z : Compressibility factor

Lower Case Symbols

a_A : Activity coefficient of component A

a_1^* : Fluid specific parameter in effective density correlation [kg/m^3]

a_2^* : Fluid specific parameter in effective density correlation [kg/m^{3}K]

b_1^* : Fluid specific parameter in effective density correlation [kg/m^{3}MPa]

b_2^* : Fluid specific parameter in effective density correlation [kg/m^{3}MPaK]

c_2 : Fluid specific parameter in Expanded Fluid viscosity model

c_3 : Fluid specific parameter in Expanded Fluid viscosity model

h : Slope value for slope and intercept technique Equation 2.33

h_{oil} : Height of oil column [cm]

h_{sol} : Height of solvent column [cm]

h_{total} : Total height of the oil column [cm]

Δh : Element thickness in the gas-liquid numerical model [cm]

$\vec{j}$: Mass flux of component A [g/cm²s]

k : Intercept value for slope and intercept technique Equation 2.33

k_B : Boltzmann constant [m^{2}kg/s^{2}K]

m_{oil} : Mass of oil in a gas-liquid diffusion experiment[g]

$\dot{m}$: Mass flow of any component [g/min]

m_{total}^j : Total amount of solvent diffused [g]

$m_s(t)$: Mass of solvent dissolved at a given time [g]

$m_{s,corr}$: Corrected solvent mass diffused [g]

$m_{s,shifted}$: Mass of solvent diffused corrected through the origin [g]

nc : Number of components in a system

p : Oscillating period

r : Rate of mass addition per unit volume due to reaction of any component [g/cm^3. s]

r_{leak} : Leak rate from gas diffusion apparatus [g/min]

t : Time [s]

Δt   : Time step in the liquid-liquid numerical model [min]

u : Straight line equation for slope and intercept technique Equation 2.33.

$\check{v}_b$: Molar volume of the bitumen at its normal boiling [cm³/mol]

v_s^{298} : Specific volume of solvent at 298 K [cm³/gr]

v_b^{298} : Specific volume of bitumen at 298 K [cm³/gr]

w : Mass fraction

x : Mole fraction of bitumen.

Δx : Element thickness in the liquid-liquid numerical model [cm]

$\overline{\Delta x}^j$: Average thickness between neighbor layers where the diffusion process occurs [cm]

Greek Symbols

α : Activity coefficient

β : Parameter in Expanded Fluid viscosity model

β_{SB} : Binary interaction parameter between solvent and bitumen in density equation

β_{SB}^{298} : Binary interaction parameter between solvent and bitumen at 298 Kelvin

δ_{ij} : Parameter in mixing rule for dilute gas viscosity

λ : Boltzmann parameter [cm/s$^{0.5}$]

μ : Viscosity of a single fluid [mPa·s]

Φ : Association factor of component B

ρ : Mass density [g/cm^3]

ρ_s^0 : Compressed state density [kg/m^3]

ρ_s^* : Parameter in Expanded Fluid viscosity model [kg/m^3]

ρ_{meas} : Measured mass density [g/cm^3]

θ_{ij} : Binary interaction parameter between in EF viscosity model

Superscripts

j : Time coordinate index in numerical models

298   : At 298 Kelvin

∞ : Infinite dilution

n : Constant specific to the diffusing species

m : Constant specific to the diffusing species

Subscripts

A   : An arbitrary component

AB0   : Initial amount of Component A in B

A0   : Initial amount of Component A in a of a mixture of A and B

BA0   : Initial amount of Component B in A

B   : An arbitrary component

B0   : Initial amount of Component A in a of a mixture of A and B

b : Bitumen

D   : Refer to dilute gas of a single fluid

$diff$: In the diffusion cell

i : Space coordinate index in numerical models

j : An arbitrary phase

$meas$: measured value

m : Position coordinate index in numerical models

$malt$: Maltenes

mix : Of a mixture

n : Position coordinate index in numerical models

$nmax$: Maximum position coordinate index in numerical models

0   : At the initial state

s : Solvent

S0   : Initial solvent amount in the solvent phase

SB0   : Initial solvent amount in the bitumen phase

$supply$: In the supply cylinder

Abbreviations

ARD   : Absolute Relative Deviation

AARD   : Average Absolute Relative Deviation

EF   : Expanded Fluid model

MAARD   : Maximum Absolute Relative Deviation

CHAPTER ONE: INTRODUCTION

Heavy oil and bitumen are crude oils with a specific gravity below 20 and 10° API, respectively (Johnston *et al.*, 2017). Canada has large deposits of heavy oil and bitumen with proven reserves of 163 billion barrels as of 2017 of which 22.1 billion of barrels are under active development (BP Statistical Review of World Energy, 2018; Energy Fact Book of Natural Resources Canada, 2016-2017). Approximately 80% of these reserves are *in situ* heavy oil and bitumen and 20% are mineable oil sands. Oil sand production is currently 3.1 million of barrels per day.

Heavy oil and bitumen are considered unconventional resources due to their high viscosity which ranges from 1000 to over 1 million mPa·s at ambient conditions (Gray, 2015). The lower viscosity heavy oils can be recovered through conventional methods including cold production, waterflooding, and polymer flooding. However, the higher viscosity oils are immobile at reservoir pressures and temperatures and cannot be recovered using conventional methods. Instead, thermal methods, such as steam flooding, cyclic steam stimulation (CSS) and steam assisted gravity drainage (SAGD) are used. In all of these methods, the steam heats the oil, reducing its viscosity so that it will flow. However, these methods use large volumes of water, use considerable energy to heat the water to steam, and emit significant quantities of greenhouse gases. In addition, they are not effective for thin, shallow, or carbonate reservoirs.

Solvent-based or solvent-assisted processes are a potential alternative or supplement to thermal processes. In these processes, the injected solvent diffuses into the heavy oil, reducing its viscosity so that it can flow. These processes use less water and are less energy intensive than pure thermal methods. Examples of solvent-based processes include cyclic solvent injection and the vapor extraction process (VAPEX). Examples of solvent-assisted processes include expanding solvent-SAGD (ES-SAGD) and the N-Solv condensing solvent process. These processes have been tested in pilot projects with mixed results (Bayestehparvin *et al*., 2017, 2018; Castellanos-Diaz, 2016; Chen *et al.,* 2018; Gagliano *et al.,* 1994; Gupta and Gittins, 2006; Lin *et al*., 2014; Perlau *et al*.,

2013; Verlaan *et al*., 2015). Currently, only the LASER process (cyclic solvent injection post SAGD) has been implemented on a commercial scale (Stark, 2013).

In situ recovery processes with solvent involve a combination mass transfer and drainage (Figure 1.1). Sufficient mass transfer rates are required to obtain economical oil rates. Mass transfer also affects the residence time of the solvent in the reservoir and the amount of solvent that is recovered at the end of the process. Therefore, an understanding of the mass transfer and drainage mechanisms that control the solvent/bitumen mixing process is required to design commercially successful processes. One of the key variables that controls the mass transfer rate between solvents and bitumen is dispersivity which depends significantly on diffusivity.
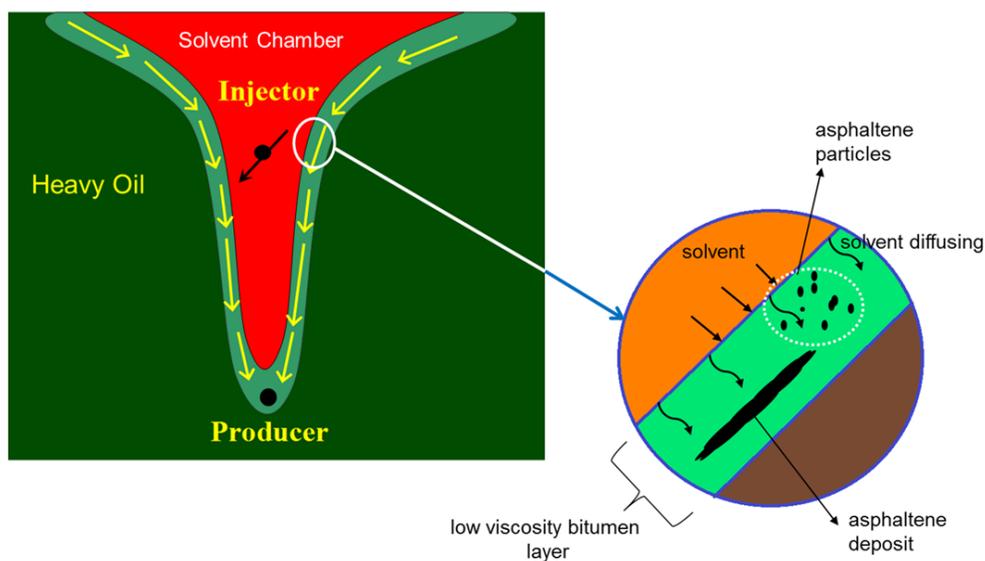
Figure 1.1. Scheme of the mechanisms involved in *In-situ* recovery processes with solvent.

The focus of this thesis is on the mutual diffusivity of liquid hydrocarbons and heavy oils because lab scale experiments and some field and lab scale simulations have shown that liquid phase hydrocarbons, such as pentane, can significantly increase oil recovery (Nourozieh *et al.*, 2014). The determination of diffusivity in liquid-liquid systems usually involves the measurement of concentration profiles over time. However, the measurement of concentration profiles in liquid solvent-bitumen mixtures is challenging because the mixtures can be viscous and opaque, and may

contain associating material such as asphaltenes (Zhang and Shaw, 2007). Therefore, techniques such as X-ray tomography (Wen *et al.*, 2004; Zhang and Shaw, 2007), infrared (Oballa and Butler, 1989), visible light absorption (Fadaei *et al.*, 2013) and nuclear magnetic resonance (Wen *et al.*, 2005) have been used in these types of systems. However, these techniques are expensive and involve complex data analysis (Cussler, 2009).

Diffusivity cannot be measured directly; rather, it is determined from a model fitted to the measured concentration profiles. Typically, the measured mass transfer process is between a solvent layer and a heavy oil layer and it is modeled as one-dimensional molecular counter diffusion of two components at fixed temperature, pressure, and volume (Oballa and Butler, 1989; Wen and Kantzas, 2005; Zhang *et al.*, 2007; Fadaei *et al.*, 2013; Fayazi *et al.*, 2017). Even with this simple geometry, it is challenging to model mass transfer in liquid solvent-bitumen systems because bitumen is a multi-component mixture, the mixtures have non-zero excess volumes of mixing, asphaltene precipitation may occur, and the diffusivity likely depends on composition.

To obtain a tractable mass transfer model, the solvent-bitumen mixture is usually treated as a pseudo-binary mixture; that is, the bitumen is treated as a single component (Oballa and Butler, 1989; Wen and Kantzas, 2005; Zhang *et al.*, 2007; Fadaei *et al.*, 2013; Fayazi *et al.*, 2017). It is assumed that the preferential diffusion of light bitumen components versus heavy bitumen components is either negligible or causes some spreading of the diffusion front but does not significantly alter the bulk diffusion rate. The volume change in mixing is also usually assumed to be negligible because the excess volume of mixing is low for hydrocarbon mixtures (Oballa and Butler, 1989; Wen and Kantzas, 2005; Zhang *et al.*, 2007; Fadaei *et al.*, 2013; Fayazi *et al.*, 2017).

Asphaltene precipitation can occur in sufficient concentrations of an *n*-alkane solvent (Johnston *et al.*, 2017). If asphaltenes precipitate and settle, they can induce convection and accelerate the mass transfer rate. If the precipitated particles accumulate, they may form a barrier to mass transfer. In either case, a model based only on molecular diffusion is inadequate. Typically, mass transfer rates have only been modeled for aromatic solvents which do not cause asphaltene precipitation or the

models have ignored any effects of the precipitation (Wen and Kantzas, 2005; Zhang *et al*., 2007; Guerrero-Aconcha *et al*., 2008; Diedro *et al*., 2015).

Even though it has been known since 1989 that the diffusivity of liquid hydrocarbons in bitumen is strongly dependent on the solvent concentration (Oballa and Butler, 1989), some studies treat the diffusivity in these systems as a constant concentration independent parameter (Wen *et al*., 2004, 2005; Salama and Kantzas, 2005; Afsahi and Kantzas, 2006). While this approach may provide an "average" diffusivity, it does not match the concentration profile exactly and will provide incorrect mass transfer rates for regions of different solvent concentration.

Oballa and Butler (1989) evaluated the diffusivity of toluene in bitumen as a function of toluene concentration using the Boltzmann-transformation modeling technique. They found a local maximum in diffusivity at a bitumen volume concentration of approximately 50%. However, there is no apparent physical reason for a maximum to occur suggesting that the analysis may be flawed. Since then, at least 16 studies have been performed using different measurement and modeling techniques for a variety of liquid hydrocarbons solvents (*n*-alkane, toluene, kerosene, benzene and others) diffusing in bitumens and heavy oils with viscosities ranging from 6 to 12000 mPa·s (Oballa and Butler, 1989; Wen and Kantzas, 2005; Zhang *et al*., 2007; Guerrero-Aconcha *et al.,* 2008; Fadaei *et al.,* 2013; Diedro *et al.,* 2015 Fayazi *et al*., 2017). A consistent relationship between diffusivity and solvent concentration has not been established for these systems.

1.1 Objectives
The overall goals of this thesis are to:
1. develop a straightforward method to determine the mutual diffusivities of liquid hydrocarbons (toluene, *n*-pentane, and *n*-heptane) and a Western Canadian bitumen
2. establish a consistent relationship between diffusivity and the solvent concentration or mixture viscosity.

The specific objectives are as follows:

1. Design and commission an apparatus to measure mass transfer in hydrocarbon/bitumen systems. The apparatus will measure the density profile of a column of liquid solvent over bitumen after diffusion has occurred for a specified time. The solvent concentration profile will be calculated from the density profile based on the known densities of the bitumen and solvent.

2. Construct a numerical model of the mass transfer experiments to determine the diffusivity. The one dimensional model will treat the solvent-bitumen system as a pseudo-binary with no excess volume of mixing. The mutual diffusivity will be incorporated as a function of solvent concentration or mixture viscosity.

3. Collect liquid-liquid mass transfer data for pseudo-binary systems with solvents including toluene, *n*-heptane, and *n*-pentane, and oils including maltenes and bitumen at ambient conditions

4. Measure gas-liquid mass transfer rates of toluene, *n*-heptane, and *n*-pentane in bitumen and maltenes at temperatures at 150°C.

5. Adapt or develop a correlation for concentration dependent diffusivity based on the systems with no asphaltene precipitation.

6. Evaluate the possible correlation between liquid-liquid and gas-liquid mass transfer data.

7. Qualitatively assess the impact of asphaltene precipitation on the mass transfer rates.

1.2 Thesis Structure

This thesis is divided into five remaining chapters, as outlined below.

- *Chapter 2* reviews mass transfer theory for gases and liquids and summarizes the most common theoretical solutions and semi-analytical methods used to predict diffusivity in binary gas-liquid and liquid mixtures. The experimental methods and models used to determine the diffusivity of liquid hydrocarbon/bitumen systems are discussed. Published diffusivities of liquid hydrocarbon in heavy oils are summarized and briefly discussed.

- *Chapter 3* describes the apparatus and experimental procedures used in this thesis with a focus on the existing gas-liquid diffusivity apparatus and the liquid-liquid diffusivity apparatus designed and commissioned as part of this thesis. The tests used to commission the diffusivity apparatus are also presented.

- *Chapter 4* summarizes the existing numerical model for the diffusion of gas into bitumen and the model developed in this thesis for the diffusion in a liquid solvent/bitumen system. The density, viscosity, and diffusivity models used within the mass transfer model are provided. The methodology to fit the model to concentration profile data is discussed.

- *Chapter 5* presents the results from the liquid-liquid diffusivity experiments. The mutual diffusivity is determined for each of the systems using the numerical model developed in Chapter 4 and the results are compared with literature data. The effects of the initial masses of solvent and oil, diffusion time, type of solvent, initial oil viscosity, and asphaltene precipitation on the mutual diffusivity are discussed.

- *Chapter 6* presents the results from the gas-liquid diffusivity experiments. The diffusivity of the gaseous solvent in oil is determined for each of the systems using the numerical model presented in Chapter 4 and the results are compared with literature data. The gas-liquid and liquid-liquid are compared and the collective dataset is used to develop a correlation for the mutual diffusivity as a function of the mixture viscosity.

- *Chapter 7* summarizes the major results and conclusions from this thesis and provides recommendations for future work in this area.

CHAPTER TWO: LITERATURE REVIEW

In this chapter, a summary of the mass transfer theory of gases and liquid is provided starting from Fick´s First law. Relevant concepts of diffusion in gas-liquid and liquid-liquid systems are discussed including the mathematical framework for representing mass transfer and calculating the diffusivity. Finally, the most common methods for measuring the diffusivity of gaseous and liquid hydrocarbons in oil are described. Previous results reported in these areas are also provided.

2.1 Mass Transfer Theory

2.1.1 Diffusion Concept

At the molecular level, diffusion is defined as the mass transfer process by which matter is transported from one point to another due to random molecular motion (Crank, 1975). At the macroscale, diffusion is known as the net transport of matter within a single phase in the absence of external mechanical mixing or convection (Poling *et al*., 2001). It has been shown that diffusion can occur as a result of pressure and temperature gradients, external force fields and concentration gradients (Poling *et al.*, 2001). For this study, only the latter form of diffusion will be considered.

The concept of diffusion can be easily illustrated by a classic mass transfer experiment (Crank, 1975), as shown in Figure 2.1. In this case, a column of a tinted substance A is placed on top of a clear substance B in a closed vessel. Initially, a well-defined interface separates the fluids. As time passes the top substance become clearer, while the bottom one becomes tinted. In other words, molecules of substance A are being transfer to the bottom, while molecules of B are being transferred to the top. Therefore, it can be said that substance A is diffusing into substance B and *vice versa*. For a binary mixture that is isotropic (*i.e*., no preferential paths), isothermal, isobaric with no external force or field gradients, the only driving force for diffusion is the concentration gradient.
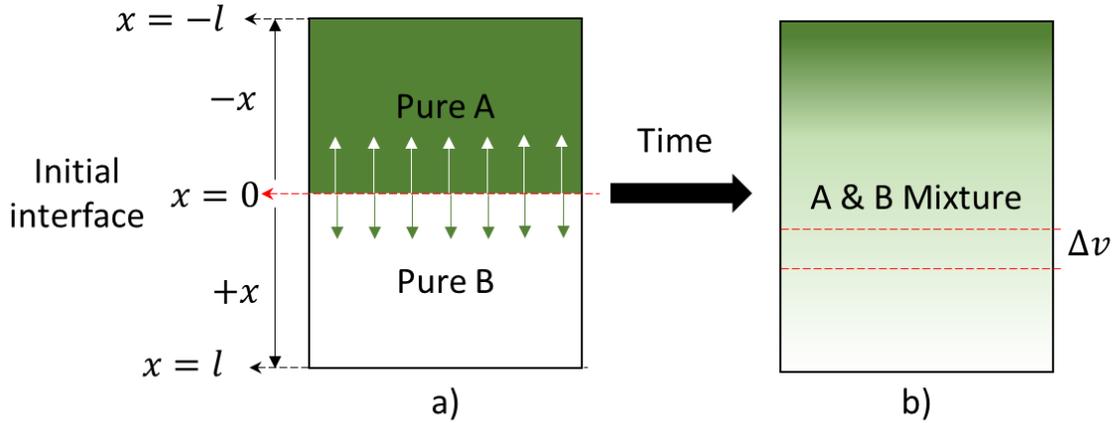
Figure 2.1. Schematic of a mass transfer experiment for an isotropic medium under isothermal and isobaric conditions with no external force or field gradients: a) initial condition; b) condition after the diffusion process has taken place for a fixed time.

A mass balance including the mass transferred due to flow, diffusion and reaction is performed on a control volume, Δv, in Figure 2.1b, to obtain the continuity equation, given by (Bird *et al.*, 1960):

$$\frac{d(\rho \cdot w_A)}{dt} = -(\nabla \cdot \overrightarrow{j_A}) + r_A \tag{2.1}$$

where w_A is the mass fraction of component A, t is time in s, r_A is the rate of mass addition per unit volume due to reaction in g/cm³s, ρ is the density of the mixture in g/cm³, and j_A is the mass flux in g/cm²s. The mass flux term can be expressed by the Fick's First Law of Diffusion (Bird *et al.*, 1960) which states that the rate of transfer of a diffusing substance through a unit cross-sectional area is proportional to the concentration gradient (Crank, 1975) and is given by:

$$\overrightarrow{j_A} = -\rho D_{AB} \nabla w_A \tag{2.2}$$

where D_{AB} is the mutual diffusivity or diffusivity in cm²/s between components A and B, defined as the proportionality constant between the mass flux and the concentration gradient (Bird *et al.*, 1960). Depending on the system, diffusivity can be treated as a constant or as a function or concentration (Crank, 1975). Assuming a one-dimensional, isothermal, isobaric diffusion system without reaction and bulk flow, and combining Eqs. 2.1 and 2.2 (Bird *et al.*, 1960), the continuity equation simplifies to:

$$\frac{\partial(\rho \cdot w_A)}{\partial t} = \frac{\partial}{\partial x}\left(\rho D_{AB} \frac{\partial w_A}{\partial x}\right) \tag{2.3}$$

where x is the position along the path of diffusion in cm. If D_{AB} and ρ are constant, Eq. 2.3 reduces to the Fick's Second Law, given by:

$$\frac{\partial C_A}{\partial t} = D_{AB} \frac{\partial^2 C_A}{\partial x^2} \tag{2.4}$$

where C_A is the concentration of component A in g/cm³. The solution of either Eq. 2.3 or Eq. 2.4 depends on the nature, geometry, initial condition and boundary conditions of the system. If it is assumed that the experiment depicted in Figure 2.1 is performed in a cylindrical vessel where diffusion occurs only in one direction (*i.e.*, along the vertical axis), one initial condition and two boundary conditions are required to solve the equations. However, the type of the boundary conditions depends on the phase of the fluids; that is, the conditions are different if the diffusing substances are both in the same phase (*e.g.*, liquid-liquid) or in different phase (*e.g.*, gas-liquid). The conditions and the solutions of the continuity equation for liquid-liquid and gas-liquid systems will be discussed later.

2.1.2 Mass Fluxes and Diffusivities

As shown in Figure 2.1, across the plane $x = 0$ substance B is diffusing upwards, while substance A is diffusing downwards. Considering a one-dimension diffusion process, the mass flux for each substance is giving by:

$$\overrightarrow{J_B} = -D_{BA} \frac{dC_B}{dx} \tag{2.5}$$

$$\overrightarrow{J_A} = -D_{AB} \frac{dC_A}{dx} \tag{2.6}$$

where D_{BA} is a measure of how fast Component B diffuses through Component A and D_{AB} is a measure of how fast Component A diffuses through Component B. If there is no volume change upon mixing in either side of the plane $x = 0$, it can be proved (Crank, 1975) that:

$$D_{AB} = D_{BA} \tag{2.7}$$

This means that the behavior of a binary system with no volume change upon mixing can be described using a single mutual diffusivity, which is a function of the composition of each component, temperature and pressure (Crank, 1975; Oballa and Butler, 1989).

Special cases of the mutual diffusivity are the infinite dilution diffusivities and self-diffusion coefficients given by Poling *et al.* (2001) and Crank (1975). Figure 2.2 shows the different types of diffusivity for a binary mixture of A (*n*-octane) and B (*n*-dodecane). The mutual diffusivity (D_{AB} or D_{BA}) represents the diffusion of each component in a binary mixture (line in Figure 2.2). The limiting values for the mutual diffusivity are the infinite dilution diffusivities. When the concentration of A tends to zero, the mutual diffusivity of A goes to the infinite dilution diffusivity of A in B, D_{AB}^{o}, which represents the diffusion of a molecule of A in a medium of pure B. Similarly, D_{BA}^{o} is the infinite dilution diffusivity of a molecule of B in pure A. Some correlations for the mutual and infinite dilution diffusivities for gas-liquid and liquid-liquid system will be discussed later. The self-diffusion coefficients (symbols in Figure 2.2) represents the diffusivity of a given molecule in its own medium. Although, the self-diffusion coefficient cannot be correlated to the mutual diffusivity (Cussler, 2009), the mutual diffusivity must be lower than the maximum self-diffusion coefficient and higher than the minimum self-diffusion coefficient (Crank, 1975; Oballa and Butler, 1989).
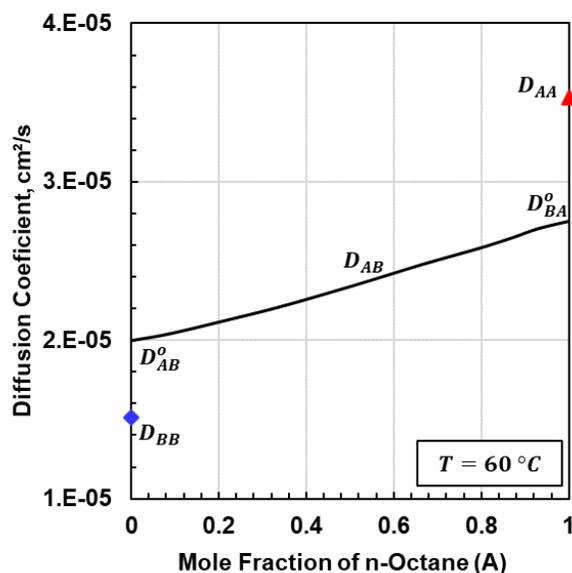
Figure 2.2. Mutual, self, and infinite diffusivity in a binary mixture of *n*-octane and *n*-dodecane. Adapted from Poling *et al.* (2001).

2.1.3 Gas-Liquid Systems: Solving the Continuity Equation

Initial Conditions

There are two initial conditions that can be used to model the systems of interest in this thesis. Consider the system shown in Figure 2.1. The first condition applies if at time zero there is no initial concentration of Component A in Component B. The initial condition is then given by:

$$C_A(x, t = 0) = 0 \tag{2.8}$$

The second initial condition applies if a given concentration of Component A is uniformly distributed in a mixture of *A* and *B*, and is given by:

$$C_A(x, t = 0) = C_{A0} \tag{2.9}$$

where C_{A0} is the initial concentration of Component A in the mixture.

Boundary Conditions

If Component A is in the gas phase and Component B is a stagnant non-volatile liquid, A will diffuse into B, but there will be negligible diffusion of B into A. For these types of systems, it is common to apply one boundary condition at the initial interface of the fluids ($x = 0$ in Figure 2.1) and another at the bottom of the cell ($x = l$ in Figure 2.1) because it is at these points where the most information regarding the diffusing gas is available (Richardson, 2017).

There are three types of boundary conditions that can be applied at the interface of a gas and liquid: the Dirichlet, Neumann and Robin (or Cauchy) conditions. In this thesis, a Dirichlet equilibrium boundary condition is used since this type of condition has been successfully used to fit experimental data of hydrocarbon gas solvents diffusing into heavy oil/ bitumen (Tharanivasan *et al*., 2004; Richardson, 2017). The Dirichlet equilibrium boundary condition is given by:

$$C_A(x = 0, t) = C_{Aeq} \tag{2.10}$$

where C_{Aeq} is the maximum solubility of the diffusing gas A in B at the system pressure and temperature (Richardson, 2017). The solubility can be found experimentally.

There are two common conditions that are applied at the bottom of the column (Richardson, 2017). The first is the infinite acting boundary condition where it is assumed that the column of

Component B is infinitely deep. This boundary condition is valid if the substance A has not reached the bottom of the substance B column, and is given by:

$$C_A(x \to \infty, t) = 0 \tag{2.11}$$

The second is the finite acting boundary condition and applies before and after the Component A has reached the bottom of the column. Since there is no diffusion of the substance A beyond this position, the concentration gradient must be zero and the boundary condition is given by:

$$\frac{dC_A}{dx}\bigg|_{x=l} = 0 \tag{2.12}$$

The mass transfer system depicted in Figure 2.1 is now completely defined. Analytical solutions for the continuity equation can be obtained as long as the diffusivity is assumed to be constant (*i.e.*, independent of concentration) and the height of the liquid column does not change with time (*i.e.*, negligible swelling) (Richardson, 2017). These two conditions apply in dilute systems.

Dilute Systems: Infinite Acting Solution

The Dirichlet equilibrium boundary condition (Eq. 2.10) is applied at the interface and the infinite acting boundary condition (Eq. 2.11) at the bottom of the liquid column. With no initial concentration of A in B (Eq. 2.8), the solution of Eq. 2.4 is given by (Crank, 1975):

$$\frac{C_A}{C_{Aeq}} = 1 - erf\left(\frac{x}{\sqrt{4D_{AB}t}}\right) \tag{2.13}$$

where *erf* is the error function. Eq 2.13 is valid for an isotropic medium, one-dimensional, isothermal, isobaric diluted diffusion system (constant diffusivity), without reaction and bulk flow, with no volume change upon mixing, where the diffusing substance has not reached the bottom of the liquid column; that is, early time.

Dilute Systems: Finite Acting Solution

The Dirichlet equilibrium boundary condition (Eq. 2.10) is applied at the interface and the finite acting boundary condition (Eq. 2.12) at the bottom of the liquid column. With no initial concentration of A in B (Eq. 2.8), the solution of Eq. 2.4 is given by (Crank, 1975):

$$\frac{c_A}{c_{A\,eq}} = 1 - \frac{4}{\pi}\sum_{n=1}^{\infty}\frac{1}{(2n-1)}\sin\left(\left(\frac{2n-1}{2}\right)\frac{\pi}{l}x\right)exp\left(-\left(\left(\frac{2n-1}{2}\right)\frac{\pi}{l}\right)^2 D_{AB}t\right) \quad (2.14)$$

The finite and infinite acting solutions are the same before the diffusing substance reaches the bottom of the oil column, but then only the finite acting solution is valid. Eq. 2.14 is valid for an isotropic medium, one-dimensional, isothermal, isobaric diluted diffusion system (constant diffusivity), without reaction and bulk flow, with no volume change upon mixing, at any time in the diffusion process.

Non-Dilute Systems

Solutions for gas-liquid systems with concentration dependent diffusivity and swelling are not provided in this thesis. Typically, a numerical model is required. In Chapter 4, a briefly description of a numerical model developed by Richardson (2017) will be provided.

2.1.4 Liquid-Liquid Systems: Solving the Continuity Equation

Initial Conditions

If Components A and B are both liquids (here termed Liquid A and Liquid B), the initial condition must be specified above and below the initial interface of the fluids ($x = 0$ in Figure 2.1):

$$C_A(x < 0, t = 0) = C_{A0} \quad (2.15)$$

$$C_A(x > 0, t = 0) = 0 \quad (2.16)$$

where C_{A0} is the initial concentration of pure A. If the Liquid B contains an evenly distributed initial concentration of A, then Eq. 2.16 becomes:

$$C_A(x > 0, t = 0) = C_{AB0} \quad (2.17)$$

Similarly, if Liquid A contains an evenly distributed initial concentration of B, then Eq. 2.15 becomes:

$$C_A(x > 0, t = 0) = C_{BA0} \quad (2.18)$$

where C_{BA0} is the initial concentration of B in A.

Boundary Conditions

For liquid-liquid systems where a clear interface between the substance disappear with time, it is convenient to set up the boundary conditions at the top ($x = -l$ in Figure 2.1) and at the bottom of

the cell ($x = l$ in Figure 2.1). There are two boundary conditions that are commonly applied at the bottom and top of the cell. The first option is the infinite acting boundary condition where it is assumed that the liquid columns of A and B are infinitely long. This boundary condition is valid if Component A has not reached the bottom of Liquid B column and Component B has not reached the top of Liquid A. The infinite acting boundary condition is given by:

$$C_A(x \rightarrow \infty, t) = 0 \qquad (2.19)$$

$$C_B(x \rightarrow -\infty, t) = 0 \qquad (2.20)$$

The second option is the finite acting boundary condition and can be applied before and after Component A has reached the bottom of Liquid B and Component B has reached the top of the Liquid A and is given by:

$$\frac{dC_A}{dx}\bigg|_{x=l} = 0 \qquad (2.21)$$

$$\frac{dC_B}{dx}\bigg|_{x=-l} = 0 \qquad (2.22)$$

Analytical solutions for the continuity equation can be obtained as long as the diffusivity is assumed to be constant (*i.e.*, independent of concentration) and if there is no volume change upon mixing. These two conditions apply in dilute systems.

Dilute Systems: Infinite Acting Solution

The infinite acting boundary conditions (Eqs. 2.19 and 2.20) are applied at the bottom and top of the cell. With no initial concentration of Component A in Liquid B or Component B in Liquid A (Eqs. 2.15 and 2.16), the solution is given by(Crank, 1975):

$$\frac{C_A}{C_{Ao}} = \frac{1}{2} \cdot \left[1 - erf \left(\frac{x}{\sqrt{4D_{AB}t}} \right) \right] \qquad (2.23)$$

Eq. 2.23 is valid for a fixed volume system with an isotropic medium, one-dimensional, isothermal, isobaric diluted diffusion system (constant diffusivity), without reaction and bulk flow, with no volume change upon mixing, where neither Component A has reached the bottom nor Component B has reached the top of the cell.

Finite Acting Boundary Conditions

Analytical solutions for finite boundary conditions in liquid-liquid systems require an extensive mathematical procedure, which is outside the scope of this project. A numerical method is presented in Chapter 4.

Non-Dilute Systems

Analytical solutions for liquid-liquid systems with a concentration dependent diffusivity are not available. Two semi-analytical methods for determining concentration dependent diffusivities from measured concentration profiles are provided below. A numerical method is presented in Chapter 4.

Boltzmann-Transformation Approach:

Boltzmann (1984) proved that, if the diffusivity is only a function of concentration, the variables x and t can be combined in one variable called the Boltzmann parameter and given by (Crank, 1975):

$$\lambda = \frac{x}{2\sqrt{t}} \tag{2.24}$$

The λ expression is substituted into the Eq. 2.3 to obtain the following ordinary differential equation for a constant density system:

$$\frac{d}{d\lambda}\left(D\frac{dC}{d\lambda}\right) = -2\lambda\frac{dC}{d\lambda} \tag{2.25}$$

The above transformation is valid if the diffusion occurs in an infinite medium and the concentration is initially constant above and below the initial interface of the fluids (Crank, 1975). For instance, if Liquids A and B in Figure 2.1 are brought together at $t = 0$, the initial and boundary conditions to solve Eq. 2.25 in terms of Component A are given by:

$$C_A = C_{A0} \quad x < 0, \quad t = 0 \tag{2.26}$$

$$C_A = 0 \quad x > 0, \quad t = 0 \tag{2.27}$$

$$C_A = C_{A0} \quad x \to -\infty, \quad t > 0 \tag{2.28}$$

$$C_B = C_{B0} \quad x \to \infty, \quad t > 0 \tag{2.29}$$

where C_{A0} and C_{B0} are the initial concentration of A and B, respectively. Assuming that there is no overall change in volume upon mixing, the solution of Eq. 2.25 in terms of diffusivity is given by(Crank, 1975):

$$D_{AB}(C_A) = \frac{1}{2t}\left(\frac{\partial x}{\partial C_A}\right)_{t,C=C^*}\int_0^{C^*} x\,dC_A \tag{2.30}$$

where C^* is any value of C_A between 0 and C_{A0}. It can be proved that to fulfill the boundary conditions, the origin from which x is measured must satisfy:

$$\int_0^{C_{A0}} x\,dC_A = 0 \tag{2.31}$$

In a constant volume system, Eq. 2.31 is the conservation of mass and it is satisfied if x is measured from the initial interface between the two substance; that is, at the plane $x = 0$ (Crank, 1975). However, in real systems where the concentration profile is not symmetric, Eq. 2.31 cannot be satisfied at the initial interface and the origin from which x is measured must be found (Mohsen Ghanavati, 2013).

Once a concentration-distance plot is available (*i.e.,* from a diffusion experiment), the plane $x = 0$ is located using the Eq. 2.31, and then the diffusivity is calculated at different concentrations (C^*) using Eq. 2.30. The integrals and gradients can be calculated numerically or graphically. This technique was first used by Matano (1933) in metal systems and since then it has been applied to other systems (Crank, 1975). For instance, Oballa and Butler (1989) and Wen and Kantzas (2005) used this technique to evaluate the concentration dependent diffusivity of hydrocarbon solvents in bitumen and heavy oil.

Slopes and Intercept Technique:
Due to errors inherent to the numerical or graphical integration and derivations, the Boltzmann-transformation approach shows considerable uncertainty at concentrations near the limiting values (Crank, 1975). Hall (1953) proposed an alternative method to improve the accuracy of the calculations at high and low concentration range. He noticed that when concentration is plotted against $x/\sqrt{t}$ on a probability plot, the curve becomes linear at the two ends of the concentration range. He proposed an analytical solution which was later modified by Crank (1975) who observed

the same linear behavior when concentration is plotted versus the Boltzmann parameter. The diffusivity can then be determined as follows:

$$\frac{C}{C_o} = \frac{1}{2}(1 + \text{erf}(u)) \tag{2.32}$$

$$u = k + h\lambda \tag{2.33}$$

$$D(C) = \frac{1}{h^2} + k\frac{\pi^{1/2}}{h^2}(1 + \text{erf}(u))(\exp(u^2)) \tag{2.34}$$

where h and k are the slopes and intercept, respectively, of the linear portion of the probability plot of the concentration curve against λ. These equations only apply to the component with a concentration increasing from zero to C_o. This technique is valid at high and low concentration ranges where u behaves linearly with λ. Sarafianos (1986) proposed a modification which include intermediate concentration range and for the concentration of the component which steps down from C_o to zero. This technique has been also widely applied and was first used for bitumen and hydrocarbon solvent systems by Guerrero-Aconcha (2009). However, this method gave unrealistically high diffusivities at high solvent contents. Recently, Babak *et al*, (2018) developed a new iterative slope and intercept method which incorporated the slope and intercept method into the integral representation of the diffusion equation (Babak et al., 2018). The new method provided physically plausible diffusivities over the entire range of solvent contents.

2.2 Models for Diffusivity in Liquids

In this section some theoretical and empirical equations for estimating the diffusivity in gas-liquid and liquid-liquid systems will be provided. The diffusivity can be related to the Brownian motion of the molecules, the properties of the molecules (such as molecular diameter and shape) and molecular interaction forces (Cussler, 2009; Coelho *et al*., 2002). However, for diffusion in liquids where molecules are strongly packed and molecular interactions creates robust force fields between them (Poling *et al.*, 2001), the theoretical relationships for diffusivity are mathematically complex (unless simplifying assumptions are made) and are not practical for modeling purposes (Cussler, 2009). Instead, many semi-empirical and empirical correlations have been developed for diffusivities in liquids in terms of more easily measured properties such as viscosity and molar volume (Bird *et al.*, 1960). The most common models to calculate the diffusivity in liquids are presented below.

2.2.1 Theoretical Models

Hydrodynamic Theory

The hydrodynamic theory is based on a single rigid spherical solute molecule moving through a medium of low molecular weight liquid solvent, first expressed as the Stokes-Einstein equation, given by (Cussler, 2009; Bird *et al.*, 1960):

$$D_{AB}^o = \frac{k_B T}{6\pi R_A \mu_B} \tag{2.35}$$

where D_{AB}^o is the infinite dilution diffusivity of A in B, k_B is the Boltzmann constant in $m^2 kg/s^2 K$, R_A is the radius of the diffusing particle in m, and μ_B is the viscosity of the continuous phase in Pa·s. This equation is limited to calculate infinite dilution diffusivity and should not be used for calculating diffusivity in concentrating systems (Bird *et al.*, 1960). The diffusivity calculated with this equation typically can have an error up to 20% (Cussler, 2009), but if the radius of the solute is less than five times the radius of the solvent, the error increases (Chen *et al.*, 1981). To improve the accuracy of the Equation 2.35 for small solutes, the factor 6π can be reduced to 4π or 2π (Cussler, 2009).

Kinetic Theory

Arnold (1930) adapted the kinetic theory of gases to diffusion in liquid systems by assuming that the resistance to diffusion in liquids is caused only by binary collisions. The diffusivity according to this theory is given by:

$$D_{AB} = \frac{A_P}{\mu_B^{1/2}} \tag{2.36}$$

where A_P is a proportionality constant that depends on the solute and the solvent properties (Arnold, 1930).

Eyring's Theory

Eyring's theory describe the diffusion process in terms of an activated unimolecular rate process (Bird *et al.*, 1960). Since this theory is based on an extremely simplified model of the liquid state, the conditions required for its validity are not clear (Bird *et al.*, 1960). However, the theory can be

applied in dilute conditions with uniform concentration (Ghai *et al.*, 1973) or ideal solutions. For a simple cubic molecular arrangement (Li and Chang, 1955), the diffusivity according Eyring's theory is given by:

$$D_{AB}^{o}{}^{Ideal} = \frac{k_B T}{6\mu_B} \left(\frac{N}{V_A}\right)^{1/3}$$
(2.37)

where $D_{AB}^{o}{}^{Ideal}$ is the infinite dilution diffusivity of A in B for an ideal solution, N is Avogadro's number, and V_A is the molar volume of A. For a nonideal solution Eq. 2.37 becomes:

$$D_{AB}^{o} = D_{AB}^{o}{}^{Ideal} \left(\frac{d \ln a_A}{d \ln x_A}\right)$$
(2.38)

where x_A and a_A are the molar fraction and activity coefficient, respectively, of Component A. The thermodynamic correction factor (the derivative term) is equal to unity for ideal solutions or pure components. Equilibrium composition data are needed to estimate the activity coefficient in mixtures (Richardson, 2017).

A more complete list and a detailed discussion of theories of diffusion in liquids can be found elsewhere (Poling *et al.*, 2001; Ghai *et al.*, 1973). However, due to their oversimplified nature no existing theory can effectively represent the nature of diffusion (Bird *et al.*, 1960). Thus, most of the calculations of diffusivities rely on empirical and semi-empirical expressions.

2.2.2 Empirical Diffusivity Models at Infinite Dilution.

In this section, three common equations for estimating infinite dilution diffusivities are presented. Recall that, at infinite dilution, the diffusivity can be treated as constant and independent of the concentration. For engineering proposes, infinite dilution diffusivities are assumed to be representative at solute concentrations of 5 to 10 mol% (Poling *et al.*, 2001).

Wilke-Chang Correlation

Wilke and Chang (1955) performed an empirical modification of the Stokes-Einstein equation, given by:

$$D_{AB}^{0} = \frac{7.4 * 10^{-8}\sqrt{\phi MW_B}T}{\mu_B V_A^{0.6}}$$
(2.39)

where MW_B is the molecular weight of solvent B in g/mol, T is the temperature in K, V_A is the molar volume of solute A at its normal boiling temperature in cm²/mol, and ϕ is the association factor of solvent B. The ϕ parameter has values of 2.6, 1.9, 1.5, 1.0 for water, methanol, ethanol, and unassociated solutes, respectively (Wilke and Chang, 1955). The Wilke-Chang equation can effectively estimate diffusion coefficients in dilute solutions with an average error of 10%, based on the 251 systems tested by the authors (Poling *et al.*, 2001).

Hayduk and Minhas Correlation

Hayduk and Minhas (1982) developed four different correlations for diffusivities at infinite dilution: the first for non-polar solvents, the second for normal paraffin solutions, the third for diffusivity in water and the fourth a general correlation. For this thesis, only the equation for normal paraffin solutions is provided and is given by:

$$D_{AB}^0 = \frac{13.3 * 10^{-8} T^{1.47} \mu_B^{\left(10.2/V_A - 0.791\right)}}{V_A^{0.71}} \tag{2.40}$$

Eq. 2.40 can estimate diffusivities in dilute solutions with an average error of 3.4%, based on 58 data points of normal paraffin solutes from C5 to C32 and solvents from C5 to C16 (Hayduk and Minhas, 1982).

Hayduk and Cheng Correlation

Hayduk and Cheng (1971) developed the following power law correlation of diffusivity to viscosity based on detailed observations of experimental data:

$$D_{AB}^0 = \frac{A_P}{\mu_B^n} \tag{2.41}$$

where A_P and n are dependent only on the properties of the diffusing component. They stated that this relationship is independent of temperature and solvent composition. Eq. 2.41 should be used for extrapolation proposes for a given solute and solvent, when at least two diffusivities of the same solute in other solvents are known (Hayduk and Cheng, 1971).

2.2.3 Empirical Diffusivity Correlations for Concentrated Systems.

In liquids where molecules are closely packed and there are strong molecular interactions, the diffusivity cannot be considered invariant with composition (Poling *et al*., 2001). Diffusivities in liquids can vary significantly with the solute concentration (Cussler, 2009). In this case, the diffusivity can be expressed as follows (Cussler, 2009; Bird *et al.*, 1960):

$$D_{AB}(C) = D_0(C) \left(\frac{d \ln a_A}{d \ln x_A} \right)$$
(2.42)

where $D_{AB}(C)$ is the diffusivity for a concentrated solution and $D_0(C)$ is the concentration dependent molecular diffusivity averaged from solvent and solute infinite dilution diffusivities. Many empirical correlations have been developed to calculate $D_0(C)$ by applying different averaging formulas to the solvent and solute infinite dilution diffusivities (Cussler, 2009) and the most well-known ones are listed below.

Modified Darken Equation

Darken (1948) developed a correlation for binary diffusion in metals. His equation is based on an arithmetic average of the tracer diffusivities of the two components. However, data for tracer diffusivities are not available; instead, the Darken equation is expressed in terms of the infinite dilution diffusivities Poling et al., (2001):

$$D_{AB} = (D_{AB}^0 x_B + D_{BA}^0 x_A) \left(\frac{d \ln a_A}{d \ln x_A} \right)$$
(2.43)

Vignes Equation

Vignes (1966) developed an empirical correlation for ideal systems, non-ideal systems and associated solutions (*e.g.*, alcohols and benzene or chloroform and acetone). Vignes found that the diffusivity does not vary linearly with the composition, and that the deviation from linearity increases as the difference between the mutual diffusivity and diluted diffusivities increases (Vignes, 1966). He suggested that, except for associated solutions, a molar geometric average can be used to calculate the diffusivity at dilute conditions to obtain the following expression:

$$D_{AB} = (D_{AB}^0)^{x_B} (D_{BA}^0)^{x_A} \left(\frac{d \ln a_A}{d \ln x_A} \right)$$
(2.44)

The Vignes equation was found to be accurate for ideal systems, but not always for non-ideal systems (Dullien, 1971).

Leffler and Cullinan Equation

Leffler and Cullman (1970) modified the Vignes equation to include the effect of viscosity on the diffusivity as follows:

$$D_{AB}\mu_{mix} = (D_{AB}^0\mu_B)^{x_B}(D_{BA}^0\mu_A)^{x_A}\left(\frac{d\ln a_A}{d\ln x_A}\right) \tag{2.45}$$

where subscript *mix* indicates the mixture. The Leffler and Cullman equation was found to be slightly better in fitting experimental data than the Vignes equation (Poling *et al*., 2001).

The empirical models discussed above all require the thermodynamic correction factor to calculate the concentration dependent diffusivity. However, for systems such as hydrocarbon solvents and heavy oil where there are limited or no available thermodynamic data, this term may not be known (Richardson, 2017). Instead correlations that avoid the need for the correction factor have been proposed for mixtures of heavy oil and solvent and are provided below.

Modified Hayduk and Cheng Equation

The modified Hayduk and Cheng equation (1971) include the mixture viscosity and a temperature dependence as follows:

$$D_{AB} = \frac{A_p T}{\mu_{mix}^n} \tag{2.46}$$

where A_p and *n* are fitting parameters.

2.3 Methods for Measuring Diffusivity of Solvents in Heavy Oil

Diffusivity measurement methods can be divided in two categories: direct methods and indirect methods (Sheikha *et al.*, 2005). Direct methods obtain the diffusivity by measuring the concentration profile of the diffusing component, while indirect methods measure another property of the system, such as a pressure drop (Richardson, 2017). Since there are no standard methods to obtain the diffusivity of one substance in another, many methods have been used to measure gas

or liquid solvent diffusing into heavy oil (or bitumen). The most commonly used methods are discussed below.

2.3.1 Methods for Measuring Diffusivity of Gas into Heavy Oil

There are many indirect and direct methods that have been developed to measure the diffusivity of gaseous solvent into heavy oil/bitumen. The pressure decay method is used in this thesis and is discussed briefly below and in more detail in Chapters 3 and 4. A more detailed review of other methods used to measure the diffusivity of gaseous solvent into heavy oil/bitumen can be found elsewhere (Richardson, 2017).

Pressure Decay Method

Pressure decay is an indirect technique in which the diffusivity of a gaseous solvent is obtained by measuring the pressure drop in the system. The change of pressure is proportional to the mass of gas that diffuses into the oil. The diffusivity can be obtained by fitting the mass of gas diffused over time with a suitable diffusion model (Richardson, 2017). Lundberg *et al.* (1963) developed the pressure decay method for methane in polystyrene and it was first applied to hydrocarbon systems by Riazi (1996).

2.3.2 Methods for Measuring Diffusivity of Liquid Solvents in Heavy Oil

Since this thesis is focused on liquid-liquid diffusion, a brief summary of all of the commonly used methods for measuring diffusivity in these systems is provided below. A more detailed review can be found elsewhere (Ghanavati *et al.,* 2014).

Spinning Disk Method

Funk (1979) used the spinning disk method to measure the diffusivity of low molecular weight paraffin solvents in oil sand bitumen at ambient conditions. In this technique, a disk uniformly coated with bitumen is submerged into a receptacle containing a known volume of liquid solvent. The disk is rotated at a constant speed and the concentration of the bitumen in the solvent are measured versus time. A constant diffusivity can be calculated from the analysis of the bitumen

concentration. This technique can be applied if the bitumen dissolution is a diffusion controlled process (Cussler, 2009).

Transpiration Technique

Fu and Phillips (1979) developed this technique to measure diffusivities of volatile hydrocarbons in semisolid bitumen. In this technique, a homogenous solution of bitumen and a volatile hydrocarbon (with known initial concentration) is placed into a diffusion cell, where the hydrocarbon can escape from the solution to a continuously flowing nitrogen stream or water stream (Tang and Zhang, 2000). The concentration of volatile hydrocarbon at the nitrogen-bitumen interface is assumed to be zero and, therefore, the diffusion of the hydrocarbon out of the homogenous solution is controlled only by the resistance in the liquid phase (Fu and Phillips, 1979). The mass diffused is determined from the concentration of the hydrocarbon in the nitrogen and a constant diffusivity is calculated from the analysis of the mass transferred over time.

Taylor Dispersion Method

The Taylor dispersion technique was originally designed to determinate the diffusivity in gases and liquids (Cussler, 2009) and was first applied to bitumen in liquid solvents by Nortz *et al.* (1990). In this method, a small amount of bitumen is injected in one end of a long tube through which a hydrocarbon solvent is flowing in the laminar regime. As the bitumen moves, its shape changes due to diffusion and dispersion (Taylor, 1953, 1954). The shape of the bitumen phase is measured at the end of the tube and then used to calculate the diffusivities (Ghanavati *et al.*, 2014a; Cussler, 2009). In highly viscous and opaque systems, such as hydrocarbon and bitumen, the Taylor dispersion technique is limited to nearly infinitely dilute conditions.

Nuclear Magnetic Resonance

Nuclear magnetic resonance (NMR) is a technique that can be used to obtain diffusivities in highly viscous systems without requiring a high initial concentration difference and with an accuracy of around five percent (Cussler, 2009). In this method, the response of hydrogen protons to a magnetic field is measured and correlated to the concentration of the solvent in the bitumen (Bryan *et al.*, 2002; Wen *et al.*, 2005). This technique has been widely used to measure diffusivities in

hydrocarbon solvent and bitumen systems (Guerrero-Aconcha *et al.*, 2008; Luo *et al.*, 2007; Luo and Kantzas, 2008; Salama and Kantzas, 2005; Wen and Kantzas, 2005; Wen *et al.*, 2004; Zhang *et al.*, 2007; Zhang and Shaw, 2007). To apply this method, a bitumen sample is placed in a cylindrical cell and a known mass of liquid or gaseous solvent is placed on the oil and left to diffuse for a set time. The diffusivity is determined by fitting a diffusion model to the concentration profiles measured at each time Fayazi *et al.* (2017).

Light Transmission Absorption

This technique is an optical method in which concentration profiles are measured by light absorption through a column of diffusing fluids. Oballa and Butler (1989) measured the diffusion of toluene and bitumen in a thin glass cell located between a near-infrared light source and a detector. The concentration profiles were measured over time and the diffusivity determined by fitting a diffusion model to the measured profiles.

X-Ray Tomography

X-ray computer tomography scan (CT) measures the density distribution within a fluid. In solvent/bitumen applications, the density of a column of bitumen and solvent is measured along the length of the column (Guerrero-Aconcha and Kantzas, 2009; Guerrero-Aconcha *et al.*, 2008; Luo *et al.*, 2007; Luo and Kantzas, 2008; Salama and Kantzas, 2005; Wen and Kantzas, 2005; Wen *et al.*, 2004). The density profiles are transformed into a solvent concentration profile using a density mixing rule. As with other methods, the diffusivity is determined by fitting a model to the measured concentration profiles.

Microfluidics: Visible Light Transmission Imaging

Microfluidics was first used to measure diffusivities of carbon dioxide in bitumen/heavy oil systems by Fadaei *et al.* (2011). Later, Fadaei *et al.* (2013) modified this approach to measure concentration dependent diffusivities of toluene in Athabasca bitumen. A few microliters of bitumen and toluene are brought into contact in a Teflon microcell. At the micro-scale, the bitumen was semitransparent and visible light transmission imaging was used to measure the concentration

profile of the solvent in the solvent/bitumen column over time. The diffusivity was again determined by fitting a diffusion model to the measured concentration profiles.

2.4 Gas and Liquid Diffusivity in Bitumen

Diffusivities of hydrocarbons such as methane, ethane, propane and butane, from the gas phase into bitumen (or heavy oil) have been measured over a range of pressures and temperatures. A detailed summary about these studies can be found elsewhere (Richardson, 2017). No data were found for diffusion from the gas phase into bitumen for the solvents considered in this thesis (toluene, *n*-pentane and *n*-heptane). Data were available for the diffusion of liquid hydrocarbons into bitumen and are summarized below. Since diffusivity must be determined from a model applied to the data, diffusion modeling is also discussed.

2.4.1 Data for Liquid Hydrocarbon Diffusivity in Bitumen

Table 2.1 summarizes the solvents and conditions for the data from the literature. All the data were collected at atmospheric pressure and temperatures between 20 and 35°C. There are a few data points at higher temperatures for 1-methylnaphthalene diffusion in Athabasca bitumen vacuum bottoms (ABVB) and a blend of vacuum residues from Western Canada (BVR).

Table 2.1. Literature data for liquid hydrocarbon diffusivity in bitumen (DME = dimethylether, MN = 1-methylnaphthalene).

Author	Solvent	Oil (Viscosity)	T (^{o}C)	Measurement Method	Data Analysis Approach	Conc. Dependent
Funk (1979)	*n*-pentane	Athabasca bitumen	25	spinning disk	analytical solution	no
	n-heptane					
	n-decane					
Fu and Phillips (1979)	*n*-pentane	bitumen 56.5 Pa·s @ 25°C	23±1.5	transpiration technique	analytical solution	no
	n-hexane					
	n-heptane					
	isohexane					
	dimethylbutane					
	cyclohexane					
	benzene					
	toluene					
	octane					

Oballa and Butler (1989)	toluene	bitumen 31.1 Pa·s @ 20°C	20±0.5	light transmission	Boltzmann-transformation	yes
Nortz et al. (1990)	MN	ABVB & BVR	50	Taylor dispersion method	Taylor dispersion	no
			70			
Tang and Zhang (2000)	phenol	bitumen 48.5 Pa·s @ 22°C	22	transpiration technique	analytical solution	no
Tang (2001)	n-hexane isohexane cyclohexane toluene	bitumen 56.5 Pa·s @ 25°C	23±1.5	transpiration technique	analytical solution	no
Wen et al. (2004) Wen et al. (2005)	n-heptane n-hexane n-pentane toluene naphtha kerosen	Cold Lake bitumen 130 Pa·s @ 25°C Atlee Buffalo heavy oil 6 Pa·s @ 25°C Peace River bitumen 671 Pa·s @ 25°C	22	NMR	analytical solution	no
Wen et al. (2004) Wen and Kantzas (2005)	n-heptane	Peace River bitumen 671 Pa·s @ 25°C	22	NMR+CT	Boltzmann-transformation	yes
Salama and Kantzas (2005)	n-octane n-heptane n-hexane n-pentane	heavy oil 21.4 Pa·s @ 20°C	22±2	NMR+CT	Boltzmann-transformation	yes
Afsahi and Kantzas (2006)	n-heptane n-hexane n-pentane toluene naphtha kerosene	Cold Lake bitumen 130 Pa·s @ 25°C Atlee Buffalo heavy oil 6 Pa·s @ 25°C Peace River bitumen 671 Pa·s @ 25°C	22	NMR	analytical solution	no
Zhang and Shaw (2007)	n-heptane	Cold Lake bitumen 130 Pa·s @ 25°C	22	CT	semi-analytical solution,	yes

Zhang *et al.* (2007)	*n*-pentane	Athabasca bitumen 18 Pa·s @ 25°C			variable density	
Luo *et al.* (2007) Luo and Kantzas (2008)	*n*-heptane	heavy oil 21.4 Pa·s @ 20°C	22	CT	modified Boltzmann-transformation with excess volume of mixing	yes
Guerrero-Aconcha *et al.* (2008)	*n*-octane *n*-heptane *n*-hexane	heavy oil 6 Pa·s @ 25°C	24	CT	slopes and intercept technique	yes
Sadighian *et al.* (2011)	*n*-heptane *n*-heptane	Athabasca Bitumen 18 Pa·s @ 25°C Athabasca atm. residue 2600 Pa·s @ 25°C	24	CT	semi-analytical solution, variable density	yes
Fadaei *et al.* (2013)	toluene	Athabasca Atm. residue 2000 Pa·s @ 21°C	21	microfluids: visible light transmission imaging	semi-analytical solution, variable density.	yes
Ghanavati *et al.* (2014)	*n*-hexane	Athabasca Atm. residue 20 Pa·s @ 42°C	30	Taylor dispersion method	Taylor dispersion	yes
Diedro *et al.* (2015)	*n*-pentane *n*-propane toluene DME	Peace River bitumen 55 Pa·s @ 22°C Grosmont heavy oil 12000 Pa·s @ 25°C	22	CT	slopes and intercept technique	yes
Fayazi *et al.* (2017)	toluene	heavy oil 47 Pa·s @ 15.6°C	35	NMR imaging	slopes and intercept technique	yes
Babak *et al.*, (2018)	toluene	Peace River bitumen 55 Pa·s @ 22°C	22	CT	iterative slope and intercept method	yes

2.4.2 Modeling of Liquid Hydrocarbon Diffusion in Bitumen

Constant Diffusivity

Diffusion of liquid hydrocarbons into bitumen has usually been modeled assuming a constant diffusivity. Funk (1979) used the solution to Fick's Second Law for unsteady state diffusion in a spinning disk given by Crank (1975). He estimated the diffusivity of bitumen in solvent at bitumen concentrations of approximately 0.0015 g/mL. Fu and Phillips (1979), Tang and Zhang (2000) and Tang (2001) used the solution to Fick's Second Law for an infinite medium (Eq. 2.23) to analyze their experiments within a concentration range of 0.05-0.012 g/mL. The constant diffusivity could be taken as constant because the solute concentrations were low; that is, approaching the infinite dilution condition.

Later, Wen *et al.* (2003) used the same assumption along with the same equation (Eq. 2.23) to evaluate average diffusivities for concentrated systems of liquid hydrocarbon solvent in bitumen. However, the assumption of constant diffusivity may not be valid for these systems where strong intermolecular forces exist and asphaltene precipitation can occur during the diffusion process. Many other authors have modeled the diffusion of hydrocarbon solvents in bitumen with a constant diffusivity. They justified the assumption based on the narrow distance, small concentration range and short diffusion times used in their experiments (Wen *et al.*, 2004, 2005; Wen and Kantzas, 2005; Salama and Kantzas, 2005; Afsahi and Kantzas, 2006) .

In later studies, the diffusivity was found to depend on the initial amounts of solvent and oil, the solvent-oil-ratio (SOR), and the experimental time. Zhang and Shaw, (2007) suggested that these dependences occur when the spatial gradients for density are non-negligible. Eq. 2.23 neglects density gradients and may predict erroneous diffusivities for mixtures with a strong density dependence on the concentration (Wen *et al.*, 2005).

Concentration Dependent Diffusivity

The diffusivity of liquid hydrocarbons in heavy oil in concentrated systems should not be treated as a constant. In liquids, molecules are packed close together and there are strong molecular interactions (Poling *et al.*, 2001). These interactions vary markedly with the solute concentration

and, therefore, diffusivities in liquids vary significantly with the solute concentration (Cussler, 2009). More complex analysis and modeling are required to account for the concentration dependence of the diffusivity.

The first concentration dependent diffusivity of liquid hydrocarbons in heavy oil was determined by Oballa and Butler in 1989 using a free diffusion method. They used the change in monochromatic infrared light intensity to determine concentration profiles for toluene-bitumen systems at ambient conditions. They estimated the concentration dependent diffusivity from the measured concentration profiles using the Boltzmann-Transformation approach (Eq. 2.30) and found that the diffusivity shows a maximum at volume concentrations of bitumen of approximately 50%, Figure 2.3.
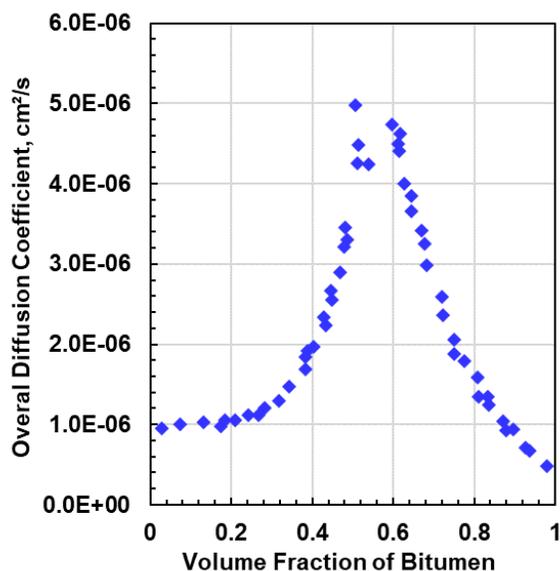
Figure 2.3. Diffusivity dependence on concentration for toluene-bitumens system at ambient conditions. Adapted from (Oballa and Butler, 1989).

Other authors have reported a similar counterintuitive concentration dependence using the same Boltzmann-Transformation approach applied to concentration profiles measured with different methods: Wen *et al*. (2004) and Wen and Kantzas (2005) for *n*-heptane in Peace River bitumen, Salama and Kantzas (2005) for *n*-octane, *n*-heptane and *n*-pentane in heavy oil, and; Fadaei *et al*.

(2013) for toluene in Athabasca atmospheric residue. It appears that the counterintuitive concentration dependency is related to the data analysis method (*i.e.* it is model dependent).

Zhang *et al*. (2007) and Zhang and Shaw (2007) studied the diffusion of *n*-pentane in Athabasca bitumen using x-rays to measure concentration profiles. They noted that the Boltzmann-Transformation approach considers spatial density gradients to be negligible or zero. Therefore, using this assumption in system such as hydrocarbon and heavy oil system (where density gradients are high at early times) might affect the diffusivity calculations. To account for these gradients Zhang and Shaw solved the continuity equation with a variable density to obtain the diffusivity from the concentration profiles. Their calculated diffusivity still showed counterintuitive trends versus concentration; however, based on the narrow range of diffusivities observed (1 to $2x10^{-6}$ cm²/s), they concluded that this behavior was due to measurement errors. They also established that the diffusivities at ambient condition were nearly constant over the composition range studied (10 to 90 wt% *n*-pentane). They reinterpreted concentration profiles obtain by Wen *et al*. (2004) and found nearly constant diffusivities. Finally, they concluded that the apparent dependence of the diffusivity on experimental time was caused by ignoring the density gradients.

Using the same approach developed by Zhang *et al*. (2007) and Zhang and Shaw (2007), Sadighian *et al.* (2011) evaluated the diffusivity for *n*-pentane in two different oils. They reported the diffusivity to be a quadratic function of the concentration of solvent in the range of concentrations studied (10 to 90 wt% *n*-pentane in Athabasca bitumen and 66 to 77 wt% for *n*-pentane in Athabasca atmospheric residue). They recommended a constant value of $5.7x10^{-7}$ cm²/s outside the measured range. Later, Fadaei *et al*. (2013) used the same technique, but reported a counterintuitive concentration dependence for the diffusivity of toluene in bitumen. Nonetheless, they found that a constant value of $2x10^{-6}$ cm²/s could be used for diffusivity of toluene in bitumen between 20 to 80 wt% toluene.

Luo *et al.* (2007) evaluated the effect of the volume change of mixing on the diffusivity for *n*-heptane in heavy oil. They measured and reported a negative volume change upon mixing with a

maximum value of -0.02 cm³/g at ambient conditions. They obtained the diffusivity as a function of the concentration using a modified Boltzmann-Transformation which included the volume change of mixing. They compared the diffusivity values obtained with the new technique with those obtained from the usual Boltzmann-Transformation approach (Eq. 2.30) and concluded that including volume exchange of mixing into the concentration profiled analyses improved the trend for concentration dependence and eliminated the time dependence of the diffusivity.

Guerrero-Aconcha *et al*. (2008) measured concentration profiles with the x-ray technique for three different *n*-alkanes in heavy oil. They used the slope and intercept technique (Eqs. 2.32 to 2.34) to determine concentration dependent diffusivity coefficients. They eliminated the abnormal trend in the concentration dependency and reported that the diffusivity monotonically decreased as the concentration of bitumen increased in the studied range of concentration (0 to 80 vol% solvent). They showed that their results were consistent with the Vignes equation (Eq. 2.44). However, at high solvent concentration the diffusivity goes above the self-diffusion coefficient of the solvent.

Diedro *et al*. (2015) also used concentration profiles from the x-ray technique and the slopes and intercept method to determine the diffusivity of four different solvents into two different bitumens. They also reported a monotonic change of the diffusivity with concentration. They found that for solvent concentrations below 50 vol%, the diffusivity can be taken as a constant. However, Fayazi *et al*. (2017) obtained abnormal trends in the concentration dependence for toluene diffusion into bitumen system using the slope and intercept technique. The inconsistences in the results from this method may occur because one of the main conditions to apply this technique cannot be fulfilled. To use the slope and intercept technique, the plot of concentration against distance on a semi-probability paper must lead to a curve with straight-line in the regions of low and high concentrations (Sarafianos, 1986). However, in hydrocarbon solvent-bitumen the plot is curved in these regions. In fact, this method is applicable mostly for systems with constant diffusion coefficients (Ahmed *et al.,* 2015a-b).

Ghanavati *et al*. (2014) used the Taylor dispersion technique to determine the concentration dependent diffusivity of *n*-hexane in Athabasca bitumen at different temperatures. They reported

that the diffusivity increased as the solvent concentration in the mixture increased from 0 to 33 vol%. They could not evaluate higher solvent concentrations due to limitations in their equipment. They also measured the infinite dilutivities of bitumen in n-hexane at different temperatures and compared them with some theoretical models. They found that the Wilke-Chang (Eq. 2.39) and Hayduk and Minhas (Eq. 2.40) correlations performed poorly for these systems.

In summary, both the measurement and modeling required to determine the mutual diffusivity in mixtures of liquid hydrocarbons and heavy oil or bitumen are challenging. The main challenge is that the mutual diffusivity in these systems is strongly dependent on the concentration of the solvent even though most of the literature report only a constant diffusivity. No clear relationship has been established between concentration and diffusivity (Poling et al., 2001) and the reported data are scattered partly because this relationship has not been correctly accounted for. In addition, the available measurement methods are expensive and involve complex data analysis (Cussler, 2009). Some the methods are applicable under very specific assumptions and can lead to unexpected values of the diffusivity when the assumptions are violated.

CHAPTER 3: EXPERIMENTAL METHODS

This chapter summarizes the materials and experimental methods used in this thesis. The existing pressure decay apparatus and procedure for gas diffusion into bitumen measurements are described. The new apparatus and procedure for liquid-liquid diffusivity measurement are discussed in detail including the design key parameters and the tests used to validate the method.

3.1 Materials

The Western Canadian bitumen sample (WC-B-A3) used in this thesis was provided by Nexen and was obtained from a Jacos SAGD process where it had been treated to remove water. The residual water content was less than 1 wt%. The molecular mass, density, viscosity, and SARA assay of the WC-B-A3 bitumen are listed in Table 3.1.

Table 3.1. Selected properties of WC-B-A3 bitumen and maltenes.

Property	WC-B-A3 Bitumen	WC-B-A3 Maltenes
Density, g/cm³ at 20°C	1.009	0.98157
Viscosity at 20°C and 1 atm, mPa.s	357560	12674
Molecular weight, g/mol	571.6	-
Saturates, wt%	19.5	-
Aromatics, wt%	41.7	-
Resins, wt%	18.5	-
C5-asphaltenes, wt%	20.2	-

The following hydrocarbons were purchased from VWR International LLC and used for the diffusivity experiments: toluene (99.5% purity) and *n*-pentane (>98% purity) from Fisher Chemical and *n*-heptane (technical, mixture of isomers) from Anachemia. The *n*-pentane and *n*-heptane were also used to obtain the asphaltene yield curves. Additionally, deionized boiled water and toluene were used to calibrate the density meter.

3.2 Bitumen Fractionation and Property Measurement

3.2.1 Asphaltene Yield and Onset

Bitumen is fully soluble in toluene but asphaltenes may precipitate from the bitumen when it is mixed with liquid *n*-alkanes. The yield is defined as the mass of precipitated asphaltenes divided by the mass of bitumen. The onset of precipitation is defined as the precipitant content at which asphaltenes first precipitate. The onsets are required to help interpret the liquid-liquid diffusion data with bitumen and *n*-heptane or *n*-pentane. The onsets were determined by extrapolating asphaltene yield measurements to zero yield as shown in Figure 3.1. This method has been shown to be consistent with micrographic observations of the onset of precipitation from bitumen titrated with the same *n*-alkane (Agrawal, P *et al.,* 2012; Casas, 2017).

Asphaltene yields were measured following the procedure described by Mancilla-Polanco (2018). Known masses of *n*-pentane or *n*-heptane and bitumen are added to series of 30 mL vials to obtain solvent contents from 20 to 90 wt%. The mixtures are sonicated and agitated for 1 hour and left to settle for 24 hours. Then, the vials are centrifuged for 5 minutes at 4000 rpm and the supernatant is removed. The residue (asphaltenes with some trapped maltenes) is washed with 20 cm³ of solvent, then sonicated for 60 minutes and left to settle for 18 hours. The vials are then centrifuged for 5 minutes at 4000 rpm and the supernatant is removed. The vials are left to dry for 1 day in a fume hood at ambient conditions and then for 6 days at 60°C in a vacuum oven (70 kPa of vacuum). Finally, the residual (precipitate) mass in each vial is measured and the yield is calculated. The asphaltene yields were repeatable to ±0.37 wt% for *n*-pentane and ±0.45 wt% for *n*-heptane, based on a 95% confident interval.
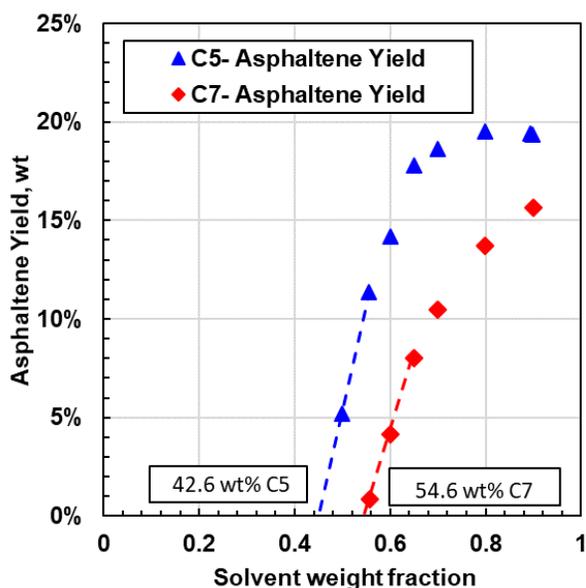
Figure 3.1. C7 and C5 asphaltene yield curves for WC-B-A3 bitumen at 22 °C and 0.1 MPa**.**

3.2.2 Fractionation into Maltenes

WC-B-A3 was de-asphalted using *n*-pentane to obtain maltenes following the procedure provided by Alboudwarej (2003). The maltenes recovered with the deasphalting procedure are soluble in *n*-pentane and *n*-heptane and were used in some diffusivity experiments with *n*-alkanes to avoid asphaltene precipitation during the diffusion process. To recover the maltenes, *n*-pentane was mixed with bitumen at a 40:1 volume ratio of *n*-pentane to bitumen. The mixture was sonicated for 60 minutes and left to equilibrate and settle in a water bath for 24 hours at 21°C. The mixture was filtered through a VWR 413 filter paper (particle retention of 5µm) to remove the precipitated asphaltenes. The *n*-pentane was evaporated from the recovered filtrate in a roto-evaporator at 80°C until the mass of the liquid sample remained constant. The residual pentane content in the maltenes is expected to be less than 3.5% (Sanchez-Lemus, 2015). The maltenes made up 79 wt% of the original bitumen.

3.2.3 SARA Fractionation

The ASTM D4124 method was used to fractionate the bitumen in saturates, aromatics, resins, and asphaltenes. Briefly, asphaltenes and solids are precipitated with *n*-pentane and removed from the

bitumen. Then, the maltenes (de-asphalted oil) are fractionated into saturates, aromatics and resins using liquid chromatography. A detailed explanation of this method is found elsewhere (Rodriguez-Leon, 2018). The SARA fractionation was performed by Elaine Baydak at the University of Calgary and is reported in Table 3.1. The SARA composition is repeatable to 0.9 wt%. (Rodriguez-Leon, 2018).

3.2.4 Molecular Weight

The molecular weight of the bitumen was measured with a Jupiter Model 833 Vapor Pressure Osmometer. A detailed explanation of this equipment and the procedure to measure the molecular weight is provided elsewhere (Rodriguez-Leon, 2018). The molecular weight measurement was performed by Elaine Baydak at the University of Calgary and is reported in Table 3.1. The molecular weight is repeatable to ±52 g/mol based on a 95% confident interval.

3.2.5 Density and Viscosity Measurements

Density and viscosity for Athabasca bitumen (WC-B-A3) were measured from 50 to 175 °C and 0.1 to 10 MPA using an in-house capillary viscometer equipped with an Anton Paar DMA-HPM density meter. A detailed explanation of the apparatus and procedure is provided elsewhere (Motahhari, 2013d; Ramos-Pallares, 2017). The capillary viscometer measurements were performed by Florian Schoeggl at the University of Calgary and are reported in Appendix A. The experimental data for density were fitted with an empirical correlation from Saryazdi *et al.* (2013) and the viscosity data were fitted with the Expanded Fluid viscosity correlation (Yarranton and Satyro, 2009). The correlations are presented in Chapter 4. Values at 20°C and 0.1 MPa were determined from the fitted correlations and are reported in Table 3.1

The density and viscosity of the maltenes were measured from 15 to 80°C at atmospheric pressure. The properties at 20°C are reported in Table 3.1. The densities were measured with an Anton Paar DMA 4500M density meter. The precision and repeatability of the density measurements are reported to be ±0.01 kg/m³ and ± 0.05 kg/m³ respectively (Ramos-Pallares, 2017). The viscosity was measured with an Anton Paar MCR-52 Cone and Plate Rheometer. The repeatabilities for oils and maltenes are ±5% and ±4%, respectively (Ramos-Pallares, 2017). A detailed explanation of the

apparatus and procedures for the density and viscosity measurements is provided elsewhere (Ramos-Pallares, 2017).

3.3 Gas-Liquid Diffusivity

3.3.1 Apparatus and Procedure

The diffusivities of gaseous toluene, *n*-pentane and *n*-heptane in bitumen and maltenes were determined with the pressure decay method. In this method, the pressure of the gas above a liquid is measured while the gas diffuses into the liquid. The change in the mass of the gas is calculated from the real gas law. This change in mass is equal to the mass of gas that diffuses into the bitumen. Hence, a pressure decay experiment gives the mass of gas diffused over time. The diffusivity is determined by modeling the mass transfer rate. If the experiment is run to completion, the liquid becomes saturated with the gas and the pressure reaches a constant value. The solubility of the gas in the liquid can be determined from the mass of gas diffused to reach the saturation condition.

The in house pressure decay apparatus used in this thesis is described in detail elsewhere (Richardson, 2017) and is shown in Figure 3.2. It consists of a cylindrical diffusion cell and a gas supply cylinder both submerged in an oil bath. The vessels are connected by a block valve, V2. This valve is used for traditional pressure decay experiments where the pressure in both the cell and supply cylinder decreases with diffusion.

Valves V1, V3, V4, and Regulator R2 are used to initialize the experiments. All the lines between valves and vessels are covered with an electrical heating tape. The oil bath is heated by a VWR refrigerated/heating circulation system and the temperature within the bath is measured with a thermocouple with an accuracy of $\pm 2^{\circ}$C. The pressure in the system is measured with two pressure transducers (PT1 and PT2) with an accuracy of ± 21 kPa. This equipment can measure gas-liquid diffusivities up to 180°C and 6.8 MPa.
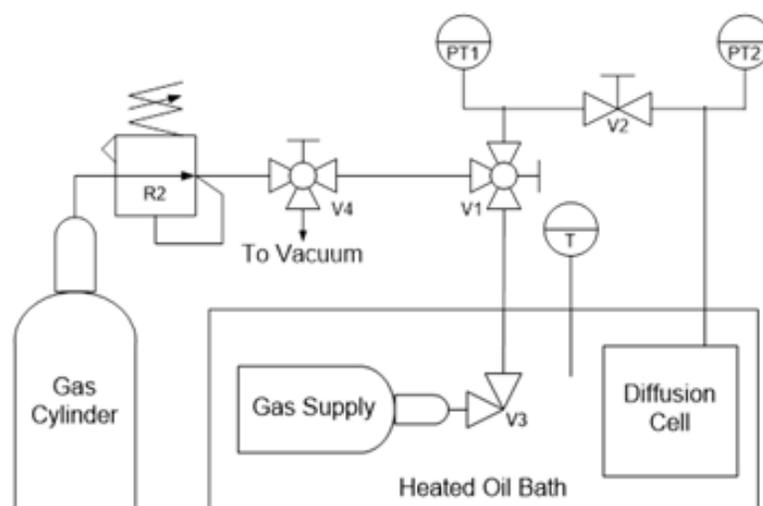
Figure 3.2. Schematic of the pressure decay diffusivity apparatus. Adapted from (Richardson, 2017).

To set up a gas-liquid diffusivity experiment, the diffusion cell is cleaned, dried, and weighed. Approximately 30 mL of bitumen is placed into the cell and it is reweighed to determine the mass of the bitumen. The cell is then placed in the oil bath and connected to the system. The gas supply cylinder is cleaned, dried, vacuumed, and purged with the solvent vapor three times. The cylinder is then filled with a specified mass of liquid solvent, placed in the oil bath, and connected to the system. Valve V3 is closed and the whole system is heated to the desired temperature and left under vacuum for 24 hours.

The whole system is then vacuumed and purged with the solvent gas three times. The diffusion cell with the oil under vacuum is isolated from the supply cylinder by closing Valve V2. The heating tape is turned on to heat the lines to the same temperature as the oil bath. Finally, Valve V3 is opened and the system is left until the temperature and pressure are stable for at least 2 hours (Richardson, 2017). During equilibration, the pressure and temperature are recorded every 15 minutes.

To perform a diffusion experiment, the diffusion cell and the gas supply cylinder are connected by gradually opening Valve V2. The pressure and temperature of the gas supply cylinder and the diffusion cell are each measured at the following intervals: 30 s for one hour, 1 min. for next 1 hour, 5 min. for next 10 hours, and 15 min. for the rest of the experiment. The experiment is completed when the pressure becomes constant (the saturation condition).

3.3.2 Processing of Pressure Decay Data

The mass of gas diffused is calculated from the measured change in pressure in the diffusion cell and the gas supply cylinder using the real gas law as follows (Richardson, 2017):

$$m_s(t) = \left[\frac{MW_s V_0 P_0}{RZ_0 T_0} - \frac{MW_s V(t)P(t)}{RZ(t)T(t)}\right]_{diff} + \left[\frac{MW_s V_0 P_0}{RZ_0 T_0} - \frac{MW_s V_0 P(t)}{RZ(t)T(t)}\right]_{supply} \qquad (3.1)$$

where m_s is the mass of gas diffused, t is time in minutes, R is the ideal gas constant in cm^3-kPa/mol-K, MW_s is the molar mass of Solvent in g/mol, P is the pressure in kPa, Z is the compressibility factor of the gas, and T is the temperature in K. The subscript 0 indicates the initial condition in the cell, $diff$ refers to the diffusion side of the system, and $supply$ refers to the gas supply side of the apparatus.

The volume of the gas phase in the diffusion cell is calculated by:

$$V(t)_{diff} = V_0 - \left(V(t)_{mix} - \frac{m_{oil}}{\rho_b}\right) \qquad (3.2)$$

where V_0 is the initial gas phase volume in the diffusion cell, $V(t)_{mix}$ is the volume of the bitumen-solvent mixture in cm^3 at time t, m_{oil} is the initial mass of bitumen in g, and ρ_b is the density of the bitumen in g/cm^3 at the initial pressure and temperature. Here, "solvent" indicates the dissolved gas. The volume of the bitumen-solvent mixture is given by:

$$V(t)_{mix} = \frac{m_s(t) + m_{oil}}{\rho_{mix}} \qquad (3.3)$$

where ρ_{mix} is the density of the bitumen-solvent mixture. It is determined from the empirical non-ideal mixing rule given by (Saryazdi *et al.*, 2013):

$$\rho_{mix} = \left(\frac{w_s}{\rho_s} + \frac{1 - w_s}{\rho_b} - w_s(1 - w_s)\left(\frac{1}{\rho_s} + \frac{1}{\rho_b}\right)\beta_{sb}\right)^{-1} \qquad (3.4)$$

where w_s the mass fraction of solvent in the oil phase, ρ_s the effective density of the solvent in g/cm³, and β_{sb} is a binary interaction parameter between the solvent and the oil. A detailed explanation on how to calculate the binary interaction parameter is given in *Chapter 4*. The solvent mass fraction is given by:

$$w_s(t) = \frac{m_s(t)}{m_s(t) + m_{oil}}$$

(3.5)

The effective density and binary interaction parameter are discussed in Chapter 4.

There are two main sources of error in the calculation of the mass diffused over time: 1) leaks; 2) non-equilibrium effects when the valve is opened between the diffusion cell and the supply cylinder (Richardson, 2017). Small leak rates cause an approximately linear loss of gas mass over time. The leak rate (mass loss per time) is determined from a plot of mass diffused versus time and the mass diffused is then corrected as follows:

$$m_{s,corr}(t) = m_s(t) - r_{leak}t$$

(3.6)

where $m_{s,corr}(t)$ is the leak corrected mass diffused in g, r_{leak} is the leak rate in g/min, and t is the time in minutes. If the leak rate is too large to clearly identify the final pressure plateau, the experiment is abandoned.

To account for the non-equilibrium start up effects (particularly temporary condensation of gas in the pressure gauge lines), a plot mass diffused ($m_{s,corr}(t)$) versus square root of time is required. The initial mass transferred must equal zero at time equal to zero. Therefore, if the data do not pass through the origin, they are shifted by the non-zero intercept as follows:

$$m_{s,shifted}(t) = m_{s,corr}(t) - intercept$$

(3.7)

where $m_{s,shifted}(t)$ is the corrected mass diffused in g and $intercept$ is the deviation from the origin in the original plot. This correction can be applied if the deviation from the origin is small and a clear linear trend in the early time data is observed. A detailed explanation of these corrections can be found elsewhere (Richardson, 2017).

3.4 Liquid-Liquid Diffusivity

3.4.1 Apparatus

A new apparatus was designed to measure the mutual diffusivity of liquid hydrocarbons (toluene, *n*-pentane and *n*-heptane) and bitumen or maltenes. The apparatus was based on a concept proposed by Maini (2016). A column of solvent is placed above a column of bitumen and left to diffuse for a specified time. The combined liquid column is displaced through a density meter and the density is measured over a series of height intervals. At each height, the solvent content is determined from the measured density and the known density of the components. The diffusivity is determined from a numerical model tuned to match the measured solvent concentration profile.

The apparatus is shown in Figure 3.3. The main components are a cylindrical diffusion cell equipped with a piston, a pump, a density meter, a data logging computer, and a sampling vessel. Other components include a hydraulic fluid supply cylinder, and a transfer cylinder for injecting cleaning fluid (usually toluene). The pump is connected to the bottom of the diffusion cell and moves the piston with hydraulic fluid. The density meter is connected to the top of the diffusion cell. The sampling vessel is connected to the outlet of the density meter. The main components are described in more detail below:

- The diffusion cell has an internal diameter of 3.8 cm and a height of 11.7 cm with a maximum fluid capacity of 135 cm³.
- The Quizix SP-5200 pump delivers metered flow rates in the range of 0.01 to 15 cm³/min, accurate to 0.005 cm³/min. The pump discharge pressure is measured with a built-in sensor with an accuracy of ±0.005 MPa.
- The Anton Paar DMA-HPM oscillating Hastelloy C-276 tube density meter is rated for fluids with densities up to 3 g/cm³, temperatures from 20 up to 200°C, and pressures up to 140 MPa. The temperature of the sample is measured with a built-in sensor, accurate to ± 0.1°C. The density measurements are repeatable to $\pm 1 \cdot 10^{-4}$ g/cm³ at static conditions. The upper limit of the sampling frequency for the density meter is 1 data point per second. The error at flowing conditions is discussed later.
- Sampling vessel is a 100 cm³ glass vial. It could be changed for vials up to 5cm³.

The pumping pressure, sample temperature, and oscillating period are recorded directly on a computer with a maximum recording rate of 1 measurement per second.
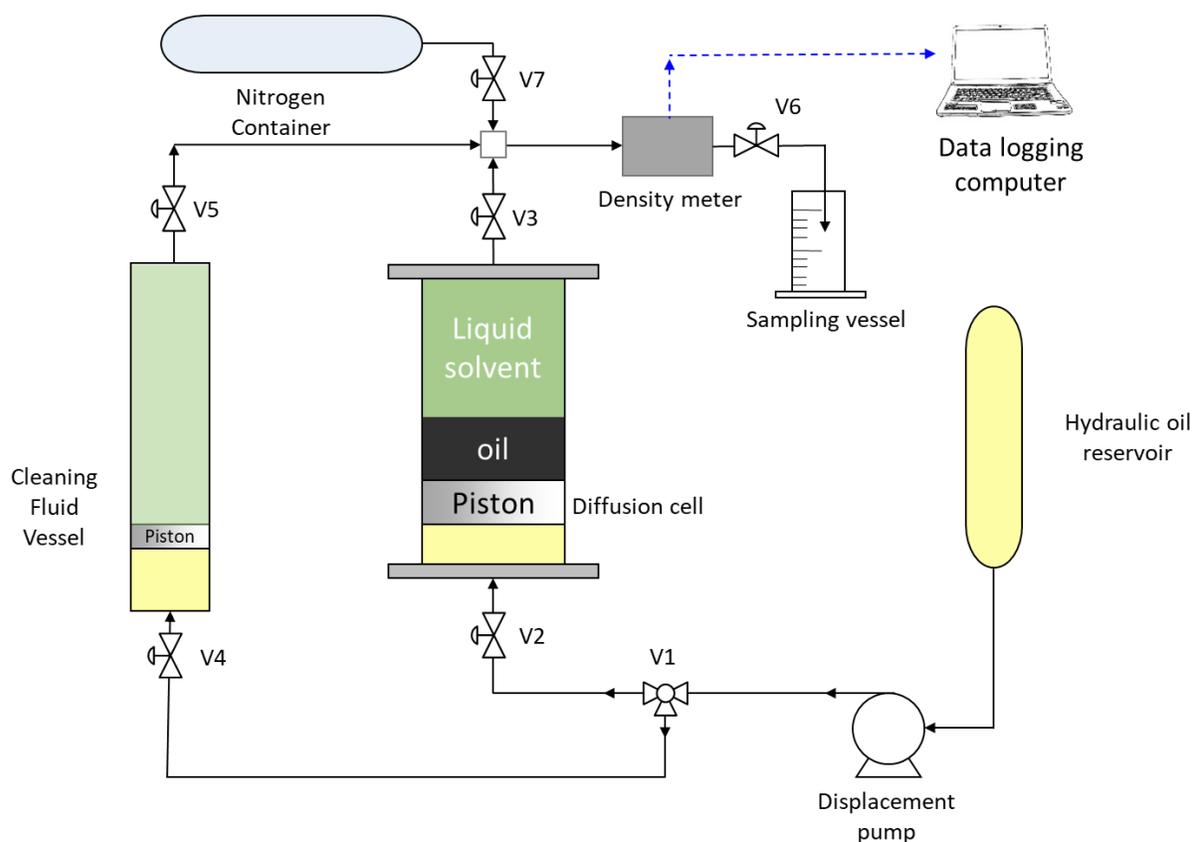
Figure 3.3. Schematic of the liquid-liquid diffusivity apparatus.

3.4.2 Procedure for Diffusivity Experiments

To perform an experiment, the piston is set in a cleaned and dried diffusion cell at the pre-determined total height (measured from the top of the cell to the top of the piston). To determine the required height, the height of the bitumen and solvent layers are calculating from the specified mass and known density of each fluid. The total height is simply the sum of the component heights.

The lower section of the cell (underneath the piston) is filled with hydraulic oil and closed. The specified mass of bitumen is placed on the top of the piston. To expel any air bubbles from the

bitumen, the cell is wrapped with an electrical heating tape and the cell is heated up to 40°C for 24 hours. Then, the heating tape is removed and the bitumen is left to cool for 24 hours. After cooling, the cell is weighed. Solvent is poured down the inside wall until the cell is filled. The cell is reweighed and the final mass of solvent is calculated from the change in the cell mass.

The cell is closed and left in a vertical position at ambient conditions for the desired diffusion time. Then, cell is connected to the pump and density meter. Valves V1, V2, V3 and V6 are opened and the fluid is displaced through the density meter at a rate of 1 or 2 cm³/min. The pumping pressure, sample temperature, and oscillating period are recorded at a rate of 1 measurement every second until all of the sample is displaced. If necessary, Valve V6 can be operated as a back-pressure valve to keep the pressure within the density meter above the vapor pressure of the solvent.

To clean the outlet lines and the density meter, Valves V2 and V3 are closed, Valve V1 is set to redirect the hydraulic oil to the cleaning vessel, and Valves V4 and V5 are opened. Toluene is displaced through the density meter at 10 cm³/min until only toluene is collected in the sampling vessel. Finally, Valve V7 is opened and nitrogen is used to displace the toluene out of the apparatus.

3.4.3 Design Checks

Some factors that may prevent the collection of representative, accurate, and usable density/concentration profiles are:

- Unrepresentative density measurement at flowing conditions
- Disruption of the bitumen/solvent interface when filling the apparatus
- Disruption of the solvent concentration profile while displacing the contents of the diffusion cell
- Continued diffusion while displacing the contents of the diffusion cell

Each factor is discussed below.

Density Measurement at Flowing Conditions

Three potential sources of error when using a vibrating Hastelloy C-276 tube density meter for measurements of mixtures of bitumen and solvent at flowing conditions are:

- applicability of calibration constants to different solvent and mixtures
- effect of flow on density measurement
- effect of density gradient on density measurement

Each source of error is discussed below.

Typically, with the Anton Paar density meter, a homogenous 1 cm³ sample is pumped into the Hastelloy C-276 tube and then it is left static while the oscillating period is measured. The density is calculated from the period of the oscillation as follows:

$$\rho = Gp^2 - J \qquad (3.8)$$

where p is the oscillating period, ρ is the density, and G and J are the calibration constants (functions of temperature and pressure but not density). In this thesis, water and toluene (99.5% purity) were used to determine the calibration constants at atmospheric pressure and 15, 20, and 25°C. The repeatability of the density measurement is expected to be ±0.1 kg/m³.

After calibration, static density measurements were taken for 4 different solvents and a series of bitumen/toluene mixtures with different toluene contents. The measured solvent densities were compared with reference values from the NIST Chemistry Book (2018). The measured bitumen/toluene mixture densities were compared with reference values obtained from another density meter (Anton Paar DMA 4500M). Figure 3.4 shows the deviation of the measurements. The absolute average deviation (AAD) was $5.8 \cdot 10^{-4}$ g/cm³ for pure solvents and $5.9 \cdot 10^{-4}$ g/cm³ for mixtures. The bias in the measurement was $-3.1 \cdot 10^{-4}$ g/cm³ for pure solvents and $3.1 \cdot 10^{-4}$ g/cm³ for mixtures.
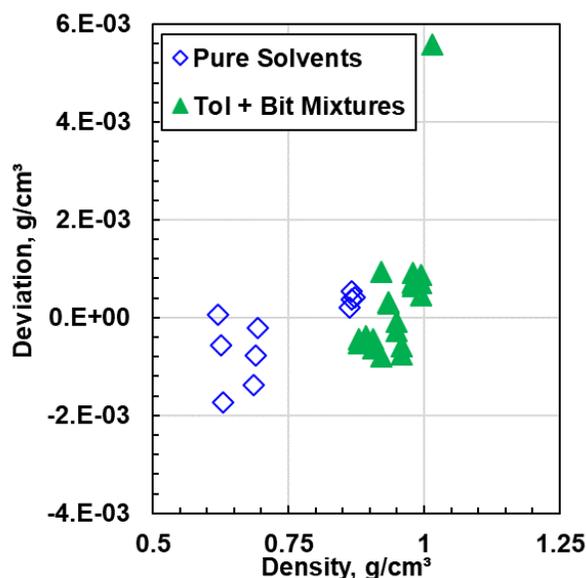
Figure 3.4. Density meter error for static measurements.

The vibrating Hastelloy C-276 tube density meter is designed for static measurements. To assess the effect of flow on the density measurement, the densities of toluene, *n*-pentane, and *n*-heptane were individually measured at flow rates of 1, 2, 5, 10, 15 cm³/min at ambient temperature and atmospheric pressure. The density was recorded each second and compared with the values reported in NIST Chemistry Book (2018) at the same conditions. Below 2 cm³/s, the measured densities were within $\pm 5.8 \cdot 10^{-4}$ g/cm³ of the standard; that is, within the experiment error. Above 2 cm³/min, the density values became erratic.

A similar test was performed on a series of bitumen/solvent mixtures at a flow rate of 1 cm³/min at ambient temperature and atmospheric pressure. Higher flow rates could not be tested because the higher viscous samples (bitumen content above 80 wt%) could not be pumped through the density meter at these rates. The density was again recorded each second and compared with the values measured at static conditions in a reference density meter. Figure 3.5 shows the deviation of the measurements. The increase in the error was almost negligible with an absolute deviation of $6.0 \cdot 10^{-4}$ g/cm³ compared with $5.9 \cdot 10^{-4}$ g/cm³ for the static measurements.
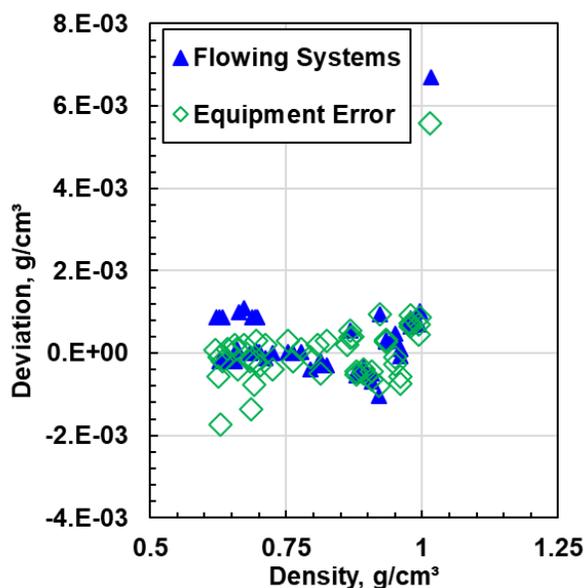
Figure 3.5. Density meter error for flowing measurements of mixtures of bitumen and toluene each with a uniform composition.

Finally, the effect of flowing with a density gradient on the density measurements was tested. With a density gradient, the fluid in the density meter does not have a uniform composition and it was not certain that the density meter would give the average density of the fluid. Several diffusion experiments were performed with bitumen or maltenes with solvent (toluene, *n*-pentane, or *n*-heptane) to generate fluid columns with solvent concentration profiles. Each column of fluid was displaced through the density meter at 1 or 2 cm³/min and the density was recorded every second. After the density meter, 5 cm³ samples were collected in sampling vessels. Each sample was manually shaken to homogenized and its density were measured at static conditions in a reference density meter (Anton Paar DMA 4500M). The flowing measurements are compared with the static sample measurements in Figure 3.6. The flowing measurements are consistent with the static measurements throughout the concentration profile. The average absolute deviation was $6.8 \cdot 10^{-4}$ g/cm³ with a bias of $-2.6 \cdot 10^{-4}$ g/cm³. In general, the flowing density was slightly lower than the static density. It is possible that some solvent evaporated while the 5 cm³ samples were collected, reducing their solvent content and increasing their density.
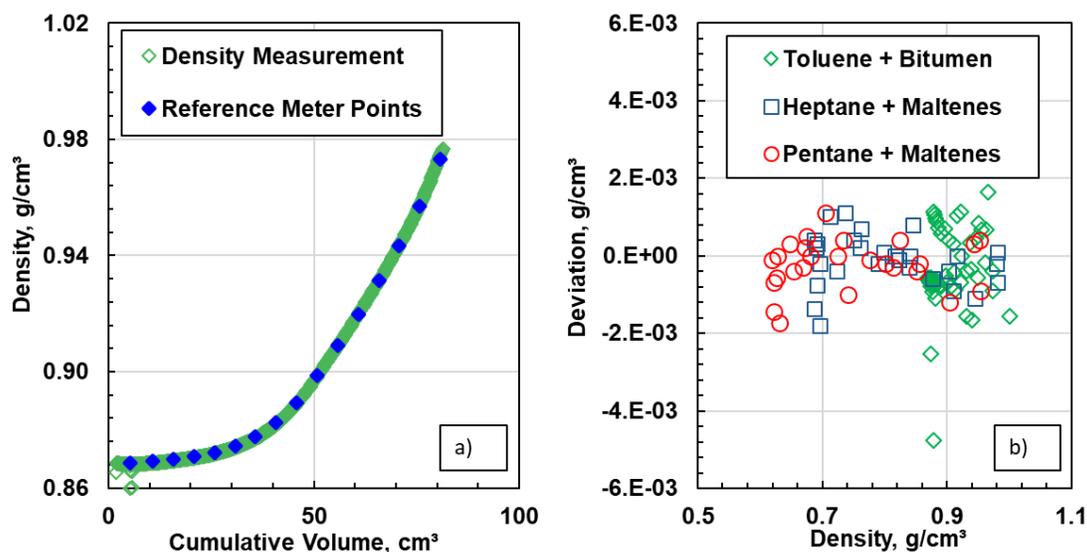
Figure 3.6. Density meter error for flowing system with density profile: a) comparison of flowing and static sample densities for a toluene-bitumen system after 5 days of diffusion at ambient conditions: b) deviation versus density for the systems evaluated in this thesis.

Filling Effects

If filling disturbs the bitumen/solvent interface, it may cause convective mixing leading to erroneous diffusivity calculations. To evaluate the sensitivity to filling, two different solvent filling methods were compared using the same amount of bitumen in each diffusion cell. In one cell, toluene was placed on top of the bitumen using a needle right above the interface. In the other cell, toluene was gently poured down the wall of cell. Then, both cells were closed and left to diffuse for a specified time. Figure 3.7 compares the measured density profiled for the two filling methods. The density profile is identical for both methods and there is no evidence of a mixing effect (irregular density profile). Therefore, either filling method can be used.
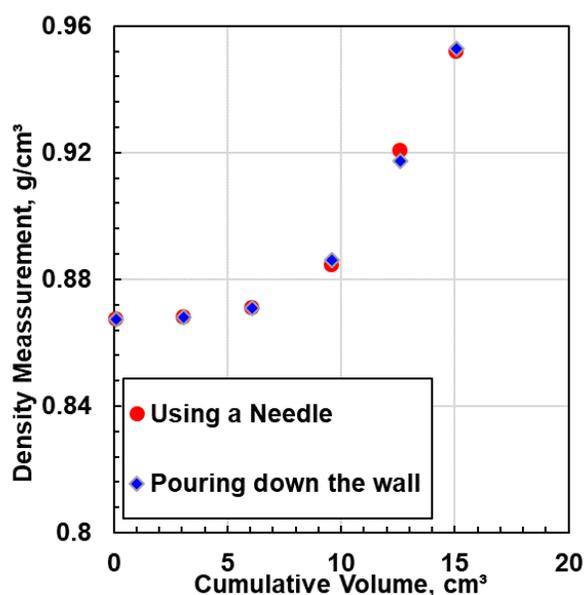
Figure 3.7. Comparison of the density profiles for two different filling methods for a toluene-bitumen system after 5 days of diffusion time.

Displacement Effects

It is possible that the solvent concentration profile is disrupted when the column of fluid is displaced from the diffusion cell; for example, if plug flow is not obtained. To assess the effect of displacement, concentration profiles were compared for the same system at the same conditions with and without displacement. The concentration profile with displacement was measured as described previously. To obtain a profile without displacement, the static fluid column after the set diffusion time was opened at the top and sampled with a pipette at 5 cm³ intervals. Each sample was homogenized and its density was measured at static conditions in a reference density meter. Figure 3.8 shows that the solvent concentration profiles with and without displacement for a toluene/bitumen system are consistent throughout the concentration profile. The average absolute deviation was $6.9 \cdot 10^{-4}$ g/cm³, almost within the expected error of a density measurement for a bitumen solvent mixture ($5.9 \cdot 10^{-4}$ g/cm³). The slight increase in the average error may be caused by local mixing or solvent evaporation when the 5 cm³ samples were taken.
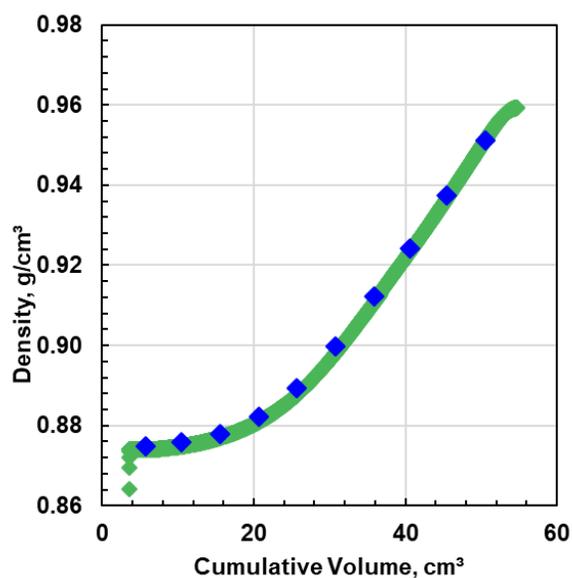
Figure 3.8. Effect of the displacement method in the density profile for a bitumen + toluene system at ambient conditions after 5 days of diffusion time.

Displacement Time

In the proposed method, the fluid column is displaced while there is still a concentration gradient. Hence, diffusion continues during the displacement. If the displacement is slow relative to diffusion, the concentration profile may change within the time required to displace the fluid column. In this case, the fluid displaced from the top of the column would reflect a different concentration profile than the fluid displaced from the bottom of the column. The measured profile would then be a distorted profile with pieces from different diffusion times.

To minimize the error caused by the displacement time, the displacement time must be much less than the time for diffusion to alter the concentration profile. Displacement time depend on how much fluid is displaced and the displacement rate. For the experiments performed in this thesis, the displacement times ranged from 40 to 135 minutes. The time for diffusion to alter the concentration profile depends on the concentration gradient and the diffusivity. The largest concentration gradient is at the initial bitumen/solvent interface. This interface disappears as diffusion takes place and a smooth concentration profile is established from the top to the bottom

of the column. In general, 3 days was sufficient to establish a smooth concentration profile for solvent/bitumen systems. Diffusion times of 3 to 15 days were used in this thesis.

The error due to displacement time was assessed by comparing two diffusion profiles for a toluene/bitumen system at ambient conditions: one measured after 3 days of diffusion and one after 3 days and 140 minutes. The displacement rate was 1 cm³/min in both cases. Figure 3.9 shows that the deviation between the two density profiles is small. The absolute deviation (AD) is $\pm 1.4 \cdot 10^{-2}$ g/cm³ based on a confidence interval of 95%; that is, within the repeatability of the measurements (also $\pm 1.4 \cdot 10^{-2}$ g/cm³ based on a confidence interval of 95%). A similar experiment was performed for a n-heptane/maltenes system at ambient conditions after 5 days of diffusion and with a 300 minute displacement time. The AD was $\pm 1.0 \cdot 10^{-2}$ g/cm³ based on a confidence interval of 95%. The deviations are expected to be even smaller at longer diffusion times.
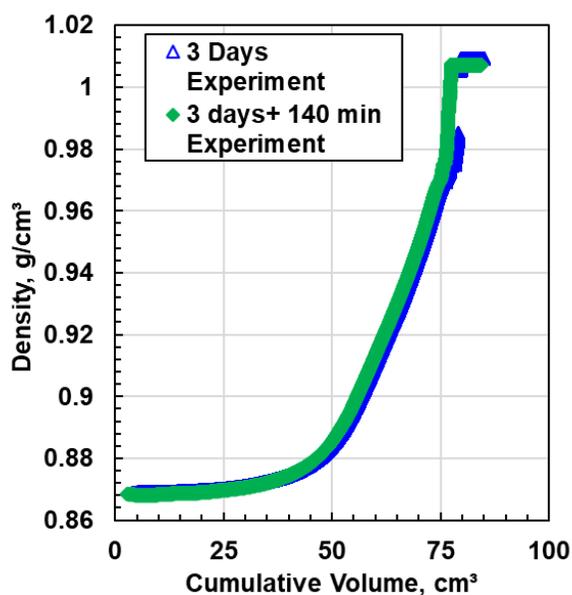
Figure 3.9. Effect of displacement time on two density profiles at 19.7 °C for toluene + bitumen systems after 3 days of diffusion time.

Accuracy and Resolution

The proposed liquid-liquid diffusivity apparatus measures density profiles for flowing system (< 2 cm³/min) with a maximum deviation of $6.9 \cdot 10^{-4}$ g/cm³ and a repeatability of $\pm 1.4 \cdot 10^{-2}$ g/cm³ based on a 95% confidence interval. To determine the repeatability, two diffusion cells with the same amounts of bitumen and solvent were left for the same experimental time. Then, the cells were displaced at 1 cm³/min and the density profile were obtained. The deviation between each point (density at each volume displacement) of the two profiles and the average absolute deviation was calculated to obtain the repeatability.

The spatial resolution of the measurement (height represented with each density measurement) is also important when modeling the data to match the concentration profile. The less the height, the better the resolution. The spatial resolution depends on the cross-sectional area of the diffusion cell, the displacement rate, and the data sampling rate. For a displacement rate of 1 cm³/min, a cell diameter of 3.8 cm, and a data sampling rate of 1 measurement per second, the spatial resolution is 1 density measurement per 0.0015 cm. For a 2 cm³/min displacement rate, the spatial resolution is 1 density measurement per 0.003 cm. The resolution of 0.0015 to 0.003 cm is finer than reported for other methods (0.015 to 0.05 cm) (Diedro *et al*., 2015; Fadaei *et al*., 2013; Fayazi *et al*., 2017; Guerrero-Aconcha *et al*., 2008; Oballa and Butler, 1989; Zhang *et al*., 2007).

Possible Source of Error

The main source of error using the liquid-liquid diffusivity apparatus is the possibility of mixing due to convection during the filling and displacement steps. However, the average absolute deviation due to the displacement effects was almost within the expected error of the density measurement. It was also shown that there was no evidence of a mixing effect while the cell was filled. Another source of error is the fluctuation in room temperature. However, this variation is less than ±2 °C, therefore the mixing due to heat convection is expected to be low. In Section 3.4.5, it will be show that the mixing caused by any type of convection is negligible compared to the mixing due to molecular diffusion.

3.4.4 Processing of Density Data

Eliminating Outliers

Figure 3.10a shows the raw measured density profile for a toluene/bitumen system after 3 days of diffusion at ambient conditions. There are several localized dips in the measured profile. These dips are random and do not appear in all of the measured profiles. They are considered to outliers caused when the pressure drop in the u-tube of the density meter was large enough to allow the formation of solvent gas bubbles. The outliers were eliminated from the profile as shown in Figure 3.10b. Eliminating the points slightly reduced the local spatial resolution but did not affect the analysis of the data.
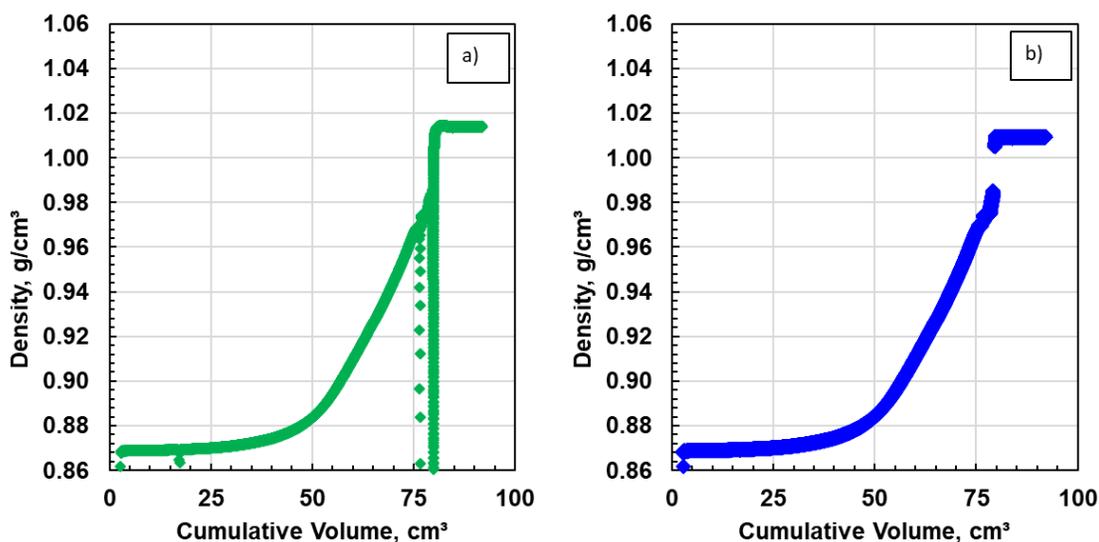
Figure 3.10. Density profile data processing for a toluene/bitumen system at 20°C after 3 days of diffusion time: a) raw measured density profile. b) density profile after eliminating outliers.

Converting from Density to Solvent Concentration

Mass transfer is more naturally and conveniently examined in terms of a concentration profile versus height rather than a density profile versus displaced volume. Therefore, the displaced volumes were converted to their relative position with respect to the initial interface. In addition, all of the measured densities were converted to solvent mass concentrations expressed in grams of solvent per volume of solution (g/cm³).

The cumulative volume was converted to the relative position with respect to the initial interface as follows:

$$X(t) = \frac{V_{cum}(t)}{A_{xo}} - h_{sol} \tag{3.9}$$

where $X(t)$ is the relative position with respect to the initial interface in cm, $V_{cum}(t)$ is the cumulative volume at time t in cm³, A_{xo} is the cross-sectional area in cm², and h_{sol} is the distance from the top of the cell to the initial top of the bitumen layer in cm. $X(t)$ is negative above the initial interface (solvent side) and positive below the interface (bitumen side).

The mass concentration of the solvent in the mixture, C_s is given by:

$$C_s = w_s \rho_{meas} \tag{3.10}$$

where w_s is the mass fraction of the solvent and ρ_{meas} is the measured density of the mixture in g/cm³. The solvent mass fraction was calculated from the measured density by rearranging the excess volume mixing rule (Eq. 3.4) as follows:

$$w_s{}^2 \left(\frac{1}{\rho_s} + \frac{1}{\rho_b} \right) \beta_{sb} + w_s \left(\frac{1}{\rho_s} - \frac{1}{\rho_b} - \left(\frac{1}{\rho_s} + \frac{1}{\rho_b} \right) \beta_{sb} \right) + \frac{1}{\rho_b} - \frac{1}{\rho_{meas}} = 0 \tag{3.11}$$

where ρ_s is the effective density of the solvent in g/cm³, ρ_b is the density of bitumen in g/cm³, and β_{sb} is the binary interaction parameter. A detailed explanation of this correlation and the method to calculate β_{sb} is presented in Chapter 4. Finally, it is common to normalize the concentration by the initial concentration of solvent, C_o. In pure solvent, the initial concentration is equivalent to the solvent density.

3.4.5 Validation of Concentration Profiles

The concentration profiles were first examined to determine if they followed the trends expected for mass transfer between solvent and bitumen. Figure 3.11 shows some normalized solvent concentration profiles for a bitumen-toluene system after 3, 5, and 12 days of diffusion. As expected, as time passes and more diffusion occurs, the bitumen content increases monotonically on the solvent side (X<0) and the solvent content increases monotonically on the bitumen side (X>0). After 3 to 5 days, the bitumen reached the top of the solvent side (a distance of 6 cm) but

the solvent did not reach the bottom of the bitumen (a distance of 2 cm). In other words, the bitumen moved significantly faster through the solvent than the solvent did through the bitumen. Faster diffusion is expected through the low viscosity solvent than through the high viscosity bitumen and this difference has been observed by others (Fayazi *et al*., 2017; Oballa and Butler, 1989). Finally, the concentration profile did not follow a perfect S-shape. Deviations from an S-shape profile are expected in systems where the diffusion coefficient is concentration dependent.
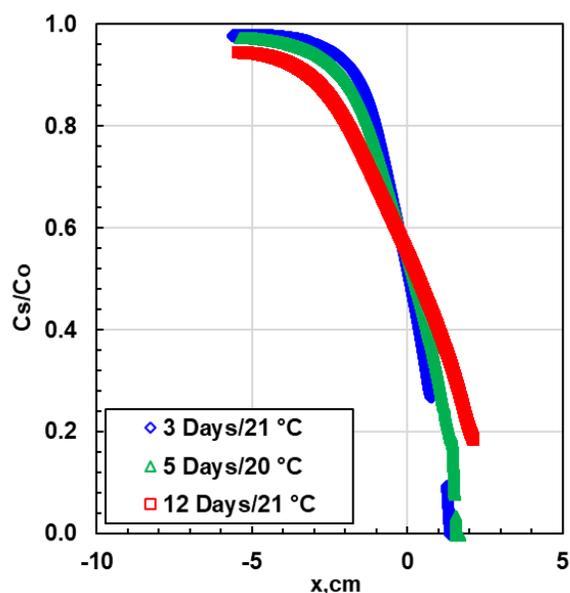
Figure 3.11. Concentration profiles for toluene-bitumen systems at ambient conditions and diffusion times of 3, 15, and 12 days.

For mass transfer processes dominated by molecular diffusion, the concentration profiles are all expected to follow the same "master" curve when plotted against the Boltzmann parameter $(X/\sqrt{t})$. Figure 3.12 shows that the data from this thesis for toluene/bitumen systems all collapse onto a single master curve. Hence, the mass transfer in the toluene/bitumen system measured in this thesis is a diffusion dominated process and there was no mixing or convection in these experiments. Comparable results were obtained for all of the systems and a detailed discussion in presented in Chapter 5.
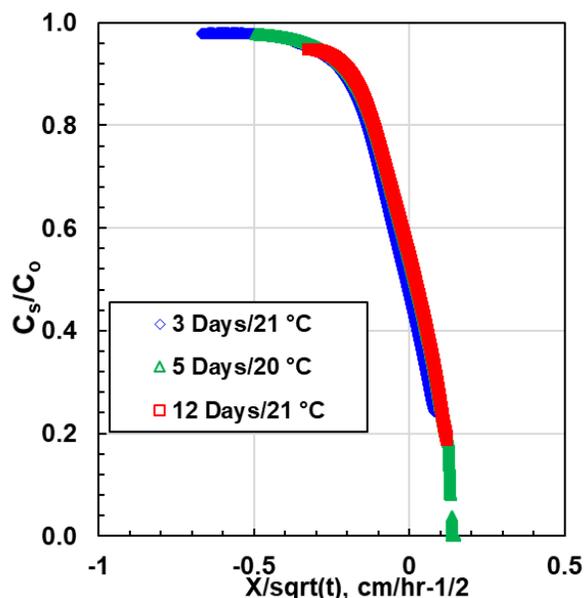
Figure 3.12. Concentration profiles for toluene/bitumen systems at ambient conditions and diffusion times of 3, 15, and 12 days plotted against the Boltzmann parameter ($X/\sqrt{t}$).

Finally, the concentration profiles measured in this thesis were compared with concentration profiles available in the literature for similar systems. In all cases the form of the solvent concentration was adjusted to match the form in which the original authors presented the data; that is, as normalized solvent concentration, solvent mass fraction, or bitumen volume fraction. Figure 3.13 shows that the concentration profiles measured in this thesis for toluene-bitumen systems overlap the concentration profiles measured with a CAT scanner (Diedro *et al*., 2015), with magnetic resonance imaging (Fayazi *et al*., 2017), with microfluidic visible light absorption (Fadaei et al., 2013) and with light transmission absorption (Oballa and Butler, 1989.) Similarly, the concentration profiles measured in this thesis for *n*-pentane/bitumen (Figure 3.14a) and *n*-heptane (Figure 3.14b) overlap the concentration profiles measured with a CAT scanner by Diedro *et al.* (2015) and Wen *et al*., (2004), respectively. There are some deviations at the ends of the profiles that likely occur because the diffusing fluids reached the cell boundaries.

In summary, the validation tests demonstrate that the concentration profiles are self-consistent, follow the expected behavior with time, and are in good agreement with the literature data. There

was no evidence of disturbance at the interface, mixing, or convection, and the mass transfer process was dominated by molecular diffusion. Therefore, it is concluded that the concentration profiles obtained in this thesis can be used to determine diffusivities.
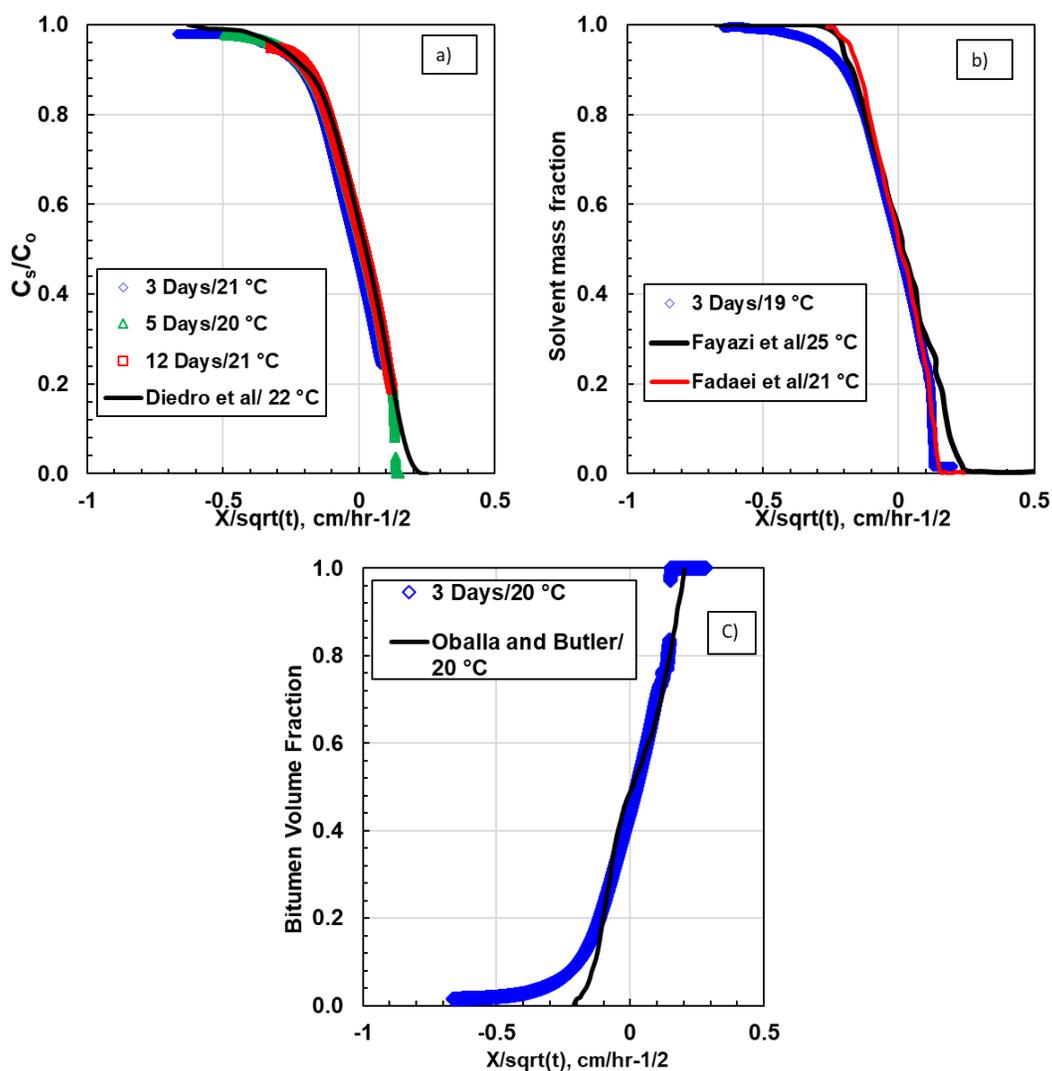
Figure 3.13. Concentration profile for toluene-bitumen system measured in this thesis compared with concentration profile reported in the literature. a) Diedro *et al.* (2015) b) Fayazi *et al (2017)* and Fayazi *et al.* (2017) c) Oballa and Butler (1989).
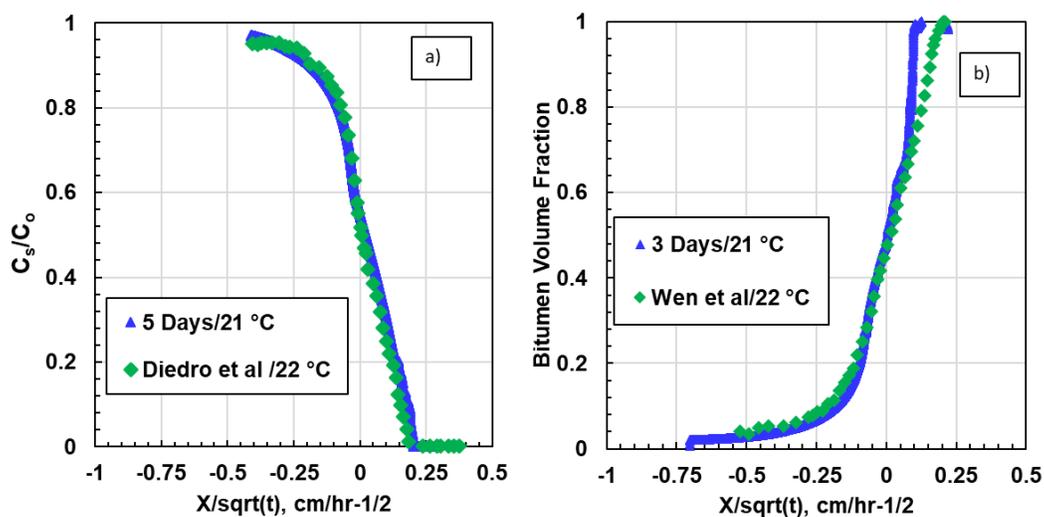
Figure 3.14. Concentration profile for a pentene bitumen system measured in this thesis compared with concentration profile reported in the literature. a) for *n*-pentane-bitumen system reported by Diedro et al. (2015) b) *n*-heptane-bitumen reported by Wen et al. (2004)

CHAPTER 4: MODELING DIFFUSITY EXPERIMENTS

In this chapter, a numerical model is developed for mass transfer in liquid-liquid systems with a concentration dependent mutual diffusivity. The key model assumptions and relevant boundary conditions are discussed. The density, viscosity, and diffusivity models used within the numerical mass transfer model are shown. Finally, procedures are presented to fit pressure decay data and density/concentration profiles to obtain gas-liquid and liquid-liquid mutual diffusivities, respectively. The proposed model is an extension of a numerical model developed by Richardson (2017) to fit pressure decay experiments and the chapter begins with a summary of this model.

4.1 Numerical Model for Gas-Bitumen Diffusion

Richardson (2017) developed a numerical model of gas-bitumen pressure decay experiments based on the continuity equation. The diffusivity of the gas in the bitumen was adjusted to fit the cumulative mass of solvent diffused into the bitumen over time. The model included the swelling of the liquid phase and the concentration dependence of the diffusivity. His numerical model and fitting procedure are the starting point of the liquid-liquid diffusion model developed in this thesis. It is also used to determine the diffusivity of gaseous toluene, *n*-heptane and *n*-pentene in bitumen and maltenes from the pressure decay data collected in this thesis. A detailed explanation of the model can be found in Richardson (2017) and a summary is provided below.

Recall that the pressure decay experiments are performed isothermally in a cylindrical cell with gas over a layer of bitumen. The experiments were conducted at conditions where only a single liquid phase could form; that is, no asphaltene precipitation or light solvent-rich phase formation. Richardson (2017) assumed that the bitumen could be represented as a single non-volatile pseudo-component. Hence, the pressure decay experiment could be modeled as a binary system with one-dimensional isothermal mass transfer from the gas to the liquid phase only. Additionally, he showed that natural convection, the velocity contribution to mass transfer, and chemical reactions could be neglected. With these assumptions, the continuity equation for the pressure decay experiment simplifies to:

$$\frac{\partial C_s}{\partial t} = \frac{\partial}{\partial x}\left(D_{sb}\frac{\partial C_s}{\partial x}\right) \tag{4.1}$$

where C_s is the concentration of solvent in bitumen in g/cm³, t is time in s, x is the distance along the oil column in cm, and D_{sb} is the mutual diffusivity in cm²/s. An initial condition and two boundary conditions are required to solve this equation. The relevant initial condition for this thesis is that there is no solvent in the bitumen it is given by:

$$C_s(x, t = 0) = 0 \tag{4.2}$$

The boundary conditions are applied at the gas-bitumen interface and at the bottom of the oil column. At the gas-bitumen interface ($x = 0$), it was assumed that the bitumen was immediately saturated with the solvent and the boundary condition is then given by:

$$C_s(x = 0, t) = C_{s,eq} \tag{4.3}$$

where $C_{s,eq}$ is the maximum solubility of solvent in bitumen in g/cm³. This value can be obtained from the end point of the pressure decay experiments or from independent measurements. At the bottom of the column ($x = hoil$), a finite acting boundary condition was applied, and it is given by:

$$\frac{dC_s}{dx}_{x=hoil} = 0 \tag{4.4}$$

where h_{oil} is the height of the oil column in cm. Equation 4.1 can be solved analytically with the given boundary conditions if the diffusivity is constant and there is no swelling of the liquid phase. Since swelling was significant for some experiments and the diffusivity depended on concentration (or viscosity), a numerical model was required.

A schematic of the model is provided in Figure 4.1. The oil phase was divided into layers of equal thickness and the gas phase was considered to be a homogeneous layer of pure gas. The height of the interface was set to $x = 0$ and the bottom to of the cell was set to $x = hoil$. The initial solvent concentration in each oil layer was set to zero, the solvent concentration at the interface was set to the solvent solubility limit, and the finite acting boundary condition was applied at the bottom of the column. The mass transfer in each layer other than the boundaries was determined from Eq. 4.1 discretized using a forward time centered space scheme as follows:

$$C_{sn}^{j+1} = C_{sn}^{j} + \frac{(t_{j+1} - t_j)}{\left(\Delta h_n^j\right)^2}\left(D_n^j\left(C_{sn-1}^{j} + C_{sn+1}^{j} - 2C_{sn}^{j}\right) + \frac{1}{4}(D_{n+1}^j\right.$$
$$\left. - D_{n-1}^j)(C_{sn+1}^{j} - C_{sn-1}^{j})\right)$$

(4.5)

where Δh_n^j is the height of the layer in cm, n and j are the indexes for vertical position and time.
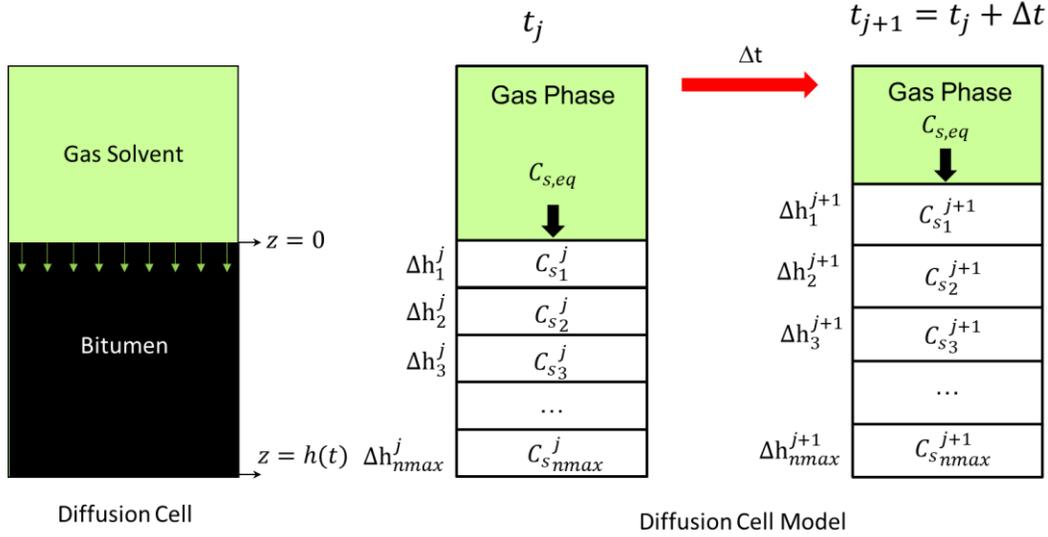
Figure 4.1. Numerical diffusion model for pressure decay experiments. Adapted from (Richardson, 2018a).

A schematic of the model algorithm is provided in Figure 4.2. The mass of bitumen in each layer was held constant. At each time step, the concentration of solvent in each layer is calculated from Eq. 4.5 and the updated mass of solvent and mass fraction of solvent in each layer is calculated from the solvent concentration and the mass of bitumen. The total mass of solvent diffused is determined from the sum of the solvent masses. The updated density of each layer is calculated from the solvent mass fraction using an excess volume mixing rule (Saryazdi et al., 2013). The updated height (accounting for swelling) of each layer is calculated from the mass of bitumen, updated mass of solvent, and updated density. The updated viscosity of each layer is calculated from the solvent mass fraction using the Expanded Fluid (EF) model (Yarranton and Satyro, 2009; Motahhari *et al*., 2013a-c Ramos-Pallares *et al*., 2015, 2016a). Finally, the diffusivity in each layer is updated either with a constant diffusivity, a fitting procedure, or using a correlation to viscosity.

The excess volume mixing rule, EF model parameters, and diffusivity correlations are discussed in Section 4.4. Equations for the height, mass diffused, and component mass fractions are discussed in more detail elsewhere (Richardson, 2017).
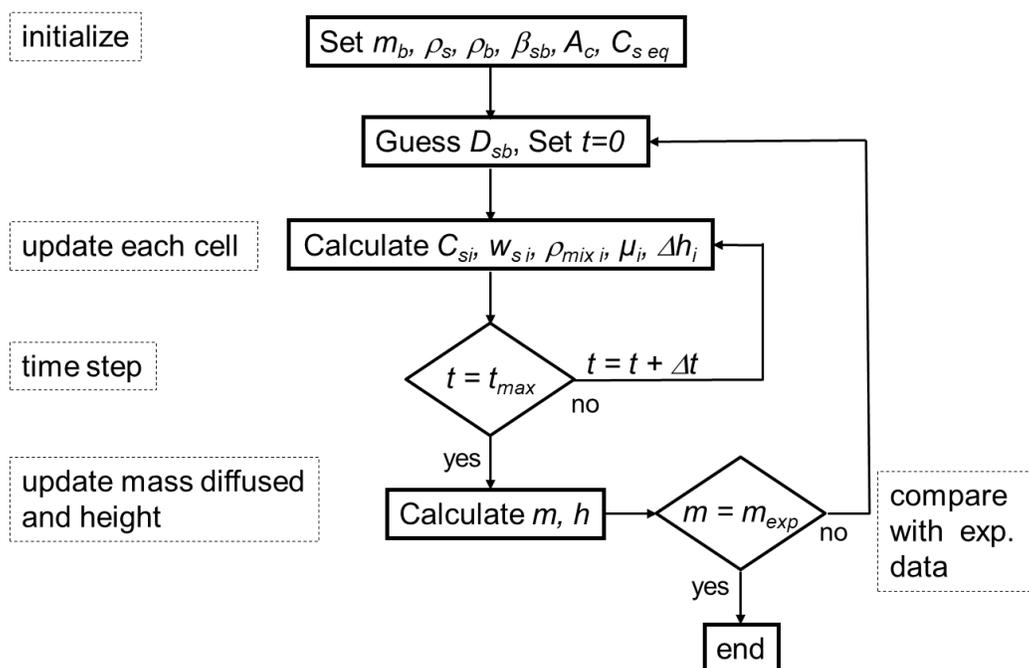
Figure 4.2. Algorithm for the diffusion model with constant diffusivity: m = mass in liquid phase, A_c = cross-sectional area, C = mass concentration, w = mass fraction, ρ = density, μ = viscosity, D = diffusivity, Δh = layer height, h = total liquid height, t = time, and Δt = time step; subscripts *b, s, mix, i, max*, and *exp* indicate bitumen, solvent, mixture, component *i*, maximum, and experimental, respectively. Adapted from (Richardson, 2017).

The model is initialized with the total mass of bitumen, the cross-sectional area of the diffusion cell, the solvent and oil densities, a binary interaction parameter for the density mixing rule, the solvent maximum solubility in the oil, and the Expanded Fluid model parameters for the oil and solvent. The only unknown at this point is the diffusivity. If the model is used in predictive mode, the parameters of the diffusivity correlation are specified and the model is run as is. If the model is used to fit data, an initial guess is required for either a constant diffusivity or the diffusivity correlation parameter to be fitted. The initial guess is updated iteratively until the calculated mass diffused over time matches the experimental data.

The initial guess of for a constant diffusivity is obtained from the slope in the linear region of an experimental plot of cumulative mass diffused versus square root of time:

$$D_{sb} = \left(\frac{S}{2A_{xo}c_{s,eq}}\right)^2 \pi \tag{4.6}$$

where S is the slope if the linear region in g/t$^{-0.5}$ and $c_{s,eq}$ the maximum solvent solubility in g/cm³. The initial guess of a diffusivity correlation parameter is chosen to approximately match the initial guess for the constant diffusivity.

Explicit numerical models do not necessarily converge and the solutions can become unstable. Richardson (2017) recommended the following constraint to ensure convergence:

$$\frac{(t_{j+1} - t_j)}{\left(\Delta h_n^j\right)^2} < 2100 \; min/cm^2 \tag{4.7}$$

where Δt is the time step and Δh is the layer thickness.

4.2 Numerical Model for Liquid Solvent-Bitumen Diffusion

The solvent-bitumen diffusion model is intended to determine the mutual diffusivities of toluene, n-pentane, and n-heptane with bitumen and maltenes based on measured concentration profiles. Figure 4.3 is a side view of the diffusion cell in a liquid solvent-bitumen diffusion experiment at two different diffusion times. Initially, the bitumen and solvent are in distinct layers (Figure 4.3a). In a gas-bitumen system, the two layers remain distinct although the interface may move over time. In the solvent-bitumen system, the solvent diffuses downwards into the bitumen and the bitumen diffuses upwards into the solvent over time (Figure 4.3b), and the initially distinct interface disappears. Hence, two significant differences from gas diffusion in bitumen are: 1) that there is diffusion of bitumen into the solvent phase as well as diffusion of solvent into bitumen; 2) the interface cannot be used as a boundary condition. Nonetheless, a similar numerical approach can be used to model the mass transfer process as discussed below.
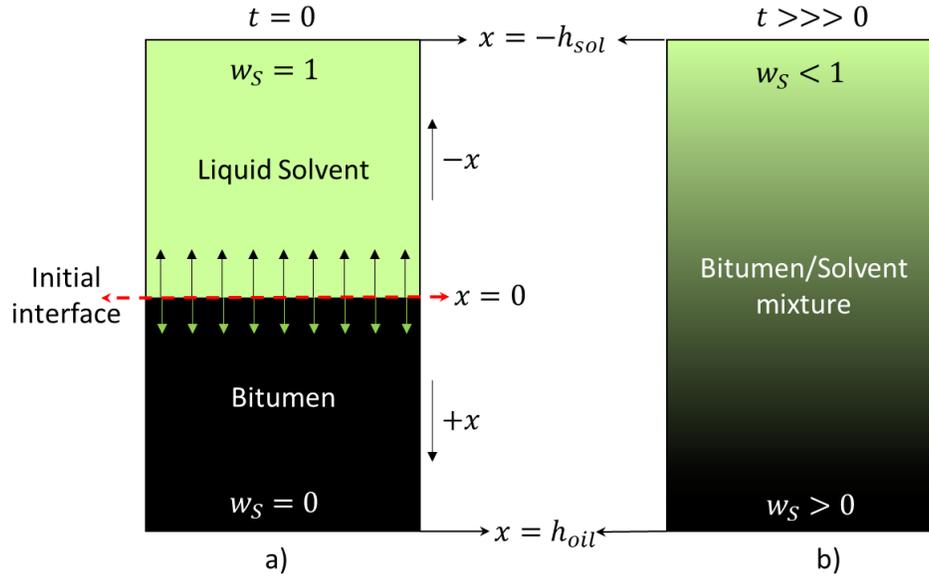
Figure 4.3. Side view of the diffusion cell: a) initial condition; b) after some time.

4.2.1 Applying the Continuity Equation

As shown in Chapter 2, a mass balance on a unit volume element inside the diffusion cell leads the general continuity equation, which for the solvent is given by:

$$\frac{D(\rho \cdot w_s)}{Dt} = -(\nabla \cdot \vec{J_s}) + r_s \tag{4.8}$$

where w_s is the solvent mass fraction, ρ is the density of the mixture in g/cm³, $\vec{J_s}$ is the mass flux of solvent in g/m²s, and r_s is the rate of mass addition per unit volume due to reaction in g/cm³s. Eq. 4.8 can be also be defined in terms of bitumen by changing the sub-index from s to b. The mass flux of the solvent and bitumen are given by:

$$\vec{J_s} = -\rho D_{sb} \nabla w_s \tag{4.9}$$

$$\vec{J_b} = -\rho D_{bs} \nabla w_b \tag{4.10}$$

where w_b is the mass fraction of bitumen and D_{sb} and D_{bs} are the diffusivities of solvent in bitumen and bitumen in solvent, respectively.

The following assumptions were made to simplify Eqs. 4.8 to 4.10:

One Dimensional Diffusion: It was assumed that radial diffusion was negligible compared to axial diffusion. The initial interface between the two fluid was flat and the diffusion fronts observed in glass tubes were always parallel to the initial interface. Hence, there is no evidence of axial diffusion. In addition, the diameter of the diffusion cell was large enough to avoid wall effects as shown in Appendix B. This assumption has been applied in all the available literature of liquid-liquid diffusion because it considerably simplifies the continuity and the mass flow equations. After applying this assumption, the grad operator (∇) becomes a partial derivate respect to direction of diffusion: in this case, ∇w_s becomes $\partial w_s / \partial x$.

Isothermal System: All the experiments performed in this thesis were done at ambient conditions at a stable, uniform temperature of 21 $\pm$2°C. Therefore, the system was considered to be isothermal and there was no need to couple heat and mass transfer equations.

No Natural Convection: In all of the experiments, the less dense liquid was always on top of the denser liquid. Therefore, there was no possibility of creating an inverse density gradient that could create natural convection within the diffusion cell. However, in systems of n-pentane-bitumen and n-heptane-bitumen it is possible for asphaltenes to precipitate during the experiment. Richardson (2017) found that asphaltenes precipitated from a Western Canadian bitumen (WC-B-B3) similar to the one used in this study at solvent contents above 42.6 wt% n-pentane and 54.6 wt% n-heptane. The precipitated asphaltene particles can settle and cause natural convection.

In gas-liquid diffusion the natural convection due to asphaltene precipitation can be avoided by performing the experiments at temperatures and pressures where the solubility of the solvent in the bitumen is below the threshold for precipitation. Unfortunately, in liquid-liquid systems, the solvent is partially miscible with the bitumen and this threshold cannot be avoided. However, including natural convection in the continuity equation is a complex problem that is outside the scope of this project. Therefore, natural convection was neglected in the model and only data collected prior to precipitation will be used to determine diffusivities. This assumption has been applied in all the available literature of liquid-liquid diffusion.

Pseudo-Binary System: Heavy oil and bitumen are mixtures of millions of molecules (McKenna *et al.*, 2013) and, strictly speaking, should be treated as a multi-component fluid. However, modeling a multi-component system is virtually impossible, since other phenomena such as reverse diffusion, osmotic diffusion, and diffusion barriers can occur (Bird *et al.*, 1960). Therefore, for the sake of simplicity, the bitumen was assumed to be a single pseudo-component and the solvent-bitumen system was treated as a pseudo-binary. This assumption has been made in all of the studies that involve diffusion in bitumen or heavy oil but to date no method has been found to test the assumption.

No Excess Volume of Mixing: In the experiments in this thesis, the diffusion cell is closed and therefore the diffusion process takes place in a fixed volume system. The effect of an excess volume of mixing would be to change the pressure of the system not the volume. The effect of pressure on diffusion in liquid systems is expected to be negligible (Bird *et al.*, 1960) and therefore the global effect of an excess volume of mixing is not an issue.

More significantly, it was necessary to assume that the total volume in either side of the initial interface did not change during the mass transfer process; that is, there was no change in volume upon mixing. As discussed in Chapter 2, if there is no volume change upon mixing on either side of the plane $x = 0$, it can be proved that (Crank, 1975):

$$D_{sb} = D_{bs} \tag{4.11}$$

Hence, the diffusion process can be modeled with a mutual diffusivity (which may vary with composition) rather than a coefficient for each component. In addition, if there is a volume change on either side of the interface, then a convection term must be introduced into the mass flux equations or a new frame of reference must be used (Crank, 1975).Therefore, in order to reduce the complexity of the model, the volume change upon mixing was neglected.

Most of the studies on the diffusion of liquid solvent in bitumen have assumed no excess volume of mixing. Nevertheless, Luo *et al.* (2007) evaluated the effect of the volume change of mixing on the diffusivity values for *n*-heptane and heavy oil systems. They concluded that including the excess volume of mixing in the model improved the trends for concentration dependency of the

diffusivity and eliminated the apparent time-dependence of the diffusivity. However, these issues appear to be related to the analysis technique (Modified Boltzmann-Transformation) rather than the mixing volume assumption. For example, Zhang and Shaw (2007) achieved the same improvements by including the density gradients in the analysis and using a different analysis technique. Furthermore, Richardson (2018a-b) evaluated the effect of the excess volume of mixing on modeling diffusion of gaseous hydrocarbons in bitumen. He found that excess volumes of mixing can be neglected in most cases. However, if the experimental method depends on the change in the height of the interface it can have an impact on the results. In this thesis, the Modified Boltzmann-Transformation was not used to analysis the data and the density gradients were included in the analysis. Therefore, it is expected that the error caused by assuming no volume change upon mixing will be small.

No Forced Convection: The diffusion cell is a closed fixed volume system and is immobile during the diffusion process. There are no external sources of mixing such as a stirrer. Additionally, since there is assumed to be no volume upon mixing, there is no mass velocity related to different diffusion rates between solvent and bitumen (Crank, 1975). Therefore, the velocity term in the continuity equation was assumed to be zero.

No Chemical Reactions: The solvents used in this are simple hydrocarbons and do not react with the oil at the temperature used in the mass transfer experiments ($< 250°C$, Gray (2015)). Therefore, the term r_s term in the continuity equation was neglected.

The above assumptions are applied and Eq. 4.8 is combined with either Eq. 4.9 or 4.10 to obtain the following expression for the mass transfer in the diffusion cell:

$$\frac{\partial(\rho \cdot w_s)}{\partial t} = \frac{\partial}{\partial x}(\rho D_{sb}\frac{\partial w_s}{\partial x}) \tag{4.12}$$

In gas-liquid systems, the density gradient of solvent in bitumen is low throughout the whole experiment. The density can then be treated as a constant over small time intervals and cancelled out from Eq. 4.12 when implemented in a numerical model. However, in liquid-liquid systems, the density gradient is very high at the initial liquid-liquid interface and the density cannot be

assumed to be constant. Therefore, the solution of Eq. 4.12 requires a relationship between solvent concentration and density and the numerical procedure would be complex and impractical. Therefore, in this thesis, the numerical model is based on discretized mass flow equations which do not include a density gradient.

To obtain the mass flow equations, mass flux equations (Eqs. 4.9 and 4.10) are multiplied by the cross-sectional area through which the diffusion process occurs. After applying the assumption of one-dimension diffusion process the mass flow of solvent and bitumen are given by:

$$\dot{m}_S = -A_{xo}\rho D_{sb}\frac{dw_s}{dx} \tag{4.13}$$

$$\dot{m}_b = -A_{xo}\rho D_{sb}\frac{dw_b}{dx} \tag{4.14}$$

where $\dot{m}_s$ and $\dot{m}_b$ are the mass flow of solvent and bitumen, respectively, in g/s and A_{xo} is the cross-sectional area in cm². Eqs 4.13 and 4.14 describe the mass flow of solvent or bitumen through a fixed plane such as $x = 0$ in Figure 4.3.

Initial and boundary conditions are required to solve the mass transfer equations. At time zero (Figure 4.3a), there are three apparent boundaries: 1) the initial interface between the fluids at $x = 0$; 2) the top of the cell (top of the solvent column) at $x = -h_{sol}$; 3) the bottom of the cell (bottom of the bitumen column) at $x = h_{oil}$. Recall that negative values of x are in the initial solvent phase while positive values are in the initial bitumen phase. As noted previously, the initially distinct interface between the two phases disappears over time and only the second and third boundaries persist. Therefore, the initial boundary is only used to set the reference height ($x = 0$) and the initial conditions. The boundary conditions used to solve the continuity equation are set at the top and bottom of the cell. The initial and boundary conditions used in this thesis are presented below.

Initial Conditions

An initial condition is defined for each of the solvent phase and the bitumen phase. If the initial solvent phase is pure solvent, then its initial condition is given by:

$$w_s(x < 0, t = 0) = 1 \tag{4.15}$$

If the solvent is not pure, for example, if there initially some bitumen in the solvent, then the initial condition is given by:

$$w_S(x < 0, t = 0) = w_{so} \tag{4.16}$$

where w_{so} is the initial solvent mass fraction in the solvent phase. Eq. 4.15 is used for most of the experiments. Similarly, the two initial conditions for the bitumen phase are given by:

$$w_s(x < 0, t = 0) = 0 \tag{4.17}$$

$$w_s(x < 0, t = 0) = w_{sbo} \tag{4.18}$$

where w_{sbo} is the initial solvent fraction in the bitumen phase. Eq. 4.17 is used for most of the experiments.

Boundary Conditions

As discussed previously, the two boundary conditions are applied at the top and bottom of the diffusion cell. At these two positions either a finite or an infinite condition may apply. An infinite condition applies at early times when neither the solvent has reached the bottom of the bitumen column nor the bitumen has reached the top of the solvent column. The finite condition applies at all times. Therefore, in this thesis the finite boundary conditions are applied at the top and bottom of the diffusion cell, and they are given by:

$$\frac{dw_s}{dx}\bigg|_{x=hoil} = 0 \tag{4.19}$$

$$\frac{dw_b}{dx}\bigg|_{x=-hsol} = 0 \tag{4.20}$$

4.2.2 Model Description

A schematic of the model is provided in Figure 4.4. The oil and solvent phases are divided into layers of equal thickness. The height of the interface is set to $x = 0$ and the bottom and top of the cell is set to h_{oil}. and $-h_{sol}$, respectively. The initial solvent concentration in each oil layer is set to zero or a specified value, and the finite acting boundary condition is applied at the top and bottom of the column. The density, viscosity, and diffusivity of each layer are initialized based on the composition of the layer.

At each time step, the mass transfer in each layer is determined from a mass balance based on the mass fluxes as shown in Figure 4.4. The highest concentration of bitumen is always at the bottom of the cell and the highest concentration of solvent is always at the top of the cell. Therefore, the solvent only diffuses downwards while the bitumen only diffuses upwards. At each time step in each layer, there is a mass flow of solvent entering the top of the layer and exiting the bottom of the layer. Similarly, there is a mass flow of bitumen entering the bottom of the layer and exiting the top of the layer. A mass balance is performed with the four fluxes and the mass fraction of each component in the layer is updated. A solvent concentration profile is calculated from the mass fractions of each layer. The density, viscosity, and diffusivity are updated for each layer using the updated composition and the height of the layer is recalculated. Then next time step is initiated. The discretized equations and fitting procedure are described below.
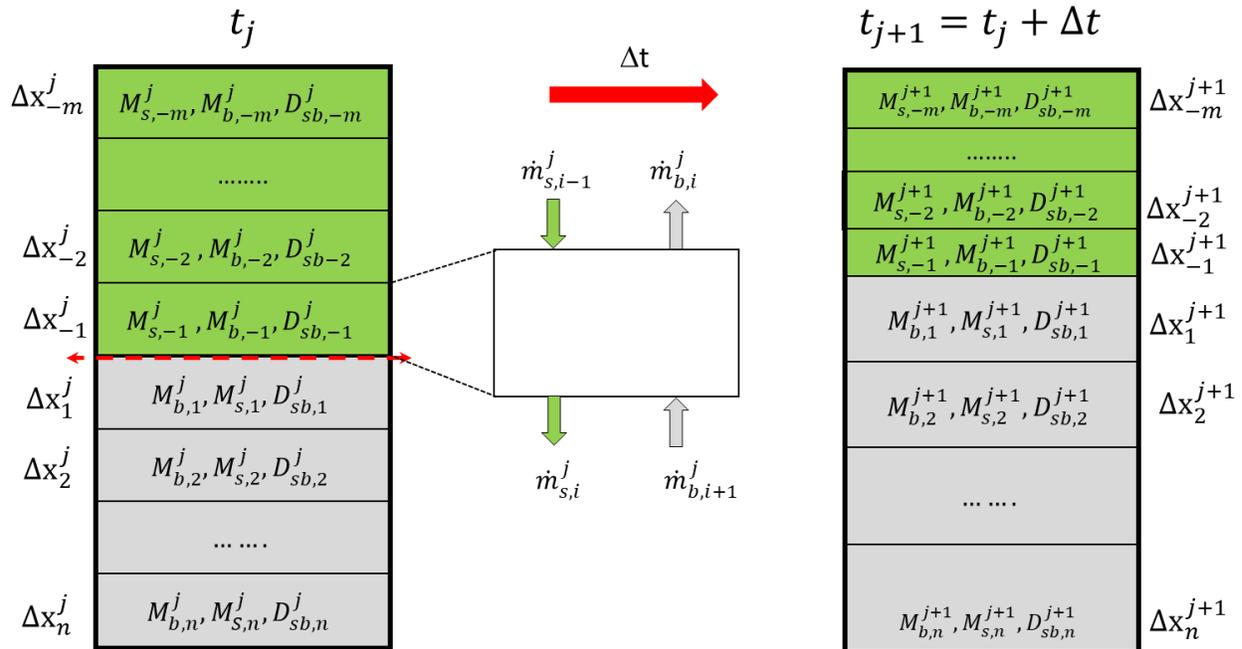
Figure 4.4. Numerical diffusion model for liquid-liquid experiments.

Discretized Mass Balance for Each Layer

The initial mass of each component in each layer is known. The mass fraction of each component is calculated at each layer the beginning of the time step:

$$w_s^j = \frac{M_s^j}{M_s^j + M_b^j} \tag{4.21}$$

$$w_b^j = 1 - w_{s,i}^j \tag{4.22}$$

where w and M are the mass and mass fraction, respectively, of a component in the layer, i is the spatial index, and j is the time index.

The mass balances for each component in a layer over a time step Δt are given by:

$$M_{b,i}^{j+1} = M_{b,i}^j + \dot{m}_{b,i+1}^j \Delta t - \dot{m}_{b,i}^j \Delta t \tag{4.23}$$

$$M_{s,i}^{j+1} = M_{s,i}^j + \dot{m}_{s,i-1}^j \Delta t - \dot{m}_{s,i}^j \Delta t \tag{4.24}$$

The mass flows of bitumen and solvent in these equations are expressed in g/min and are given by Eqs. 4.13 and 4.14 discretized using forward and backward space Taylor series for the derivatives (Fletcher, 1991):

$$\dot{m}_{b,i}^j = A_{xo} \overline{D}_{sb}^j \, \rho_{mix,i}^j \, \frac{(w_{b,i}^j - w_{b,i-1}^j)}{\overline{\Delta x}^j} \tag{4.25}$$

$$\dot{m}_{b,i+1}^j = A_{xo} \overline{D}_{sb}^j \, \rho_{mix,i+1}^j \, \frac{(w_{b,i+1}^j - w_{b,i}^j)}{\overline{\Delta x}^j} \tag{4.26}$$

$$\dot{m}_{s,i}^j = A_{xo} \overline{D}_{sb}^j \, \rho_{mix,i}^j \, \frac{(w_{s,i}^j - w_{s,i+1}^j)}{\overline{\Delta x}^j} \tag{4.27}$$

$$\dot{m}_{s,i-1}^j = A_{xo} \overline{D}_{sb}^j \, \rho_{mix,i-1}^j \, \frac{(w_{s,i-1}^j - w_{s,i}^j)}{\overline{\Delta x}^j} \tag{4.28}$$

where A_{xo} is the cross-sectional area in cm², w_S and w_b are the mass fraction of solvent and bitumen, ρ_{mix} is the initial density of the mixture of the layers where the fluid is moving from in g/cm³, $\overline{D_{sb}}$ is the average diffusivity between neighbor layers where the diffusion process occurs. The diffusivity and density calculations for each layer are discussed later. $\overline{\Delta x}$ is the average thickness between neighbor layers where the diffusion process occurs, in cm. The height of each layer is given by:

$$\Delta x_i^j = \frac{M_{b,i}^j + M_{s,i}^j}{\rho_{mix,i}^j A_{xo}} \tag{4.29}$$

And the average thickness $\overline{\Delta x}$ between the layers i and $i+1$ is calculated from:

$$\overline{\Delta x_i^j} = \frac{\Delta x_i^j + \Delta x_{i+1}^j}{2} \tag{4.30}$$

At the boundaries of the diffusion cell where the finite boundary conditions apply, Eqs. 4.23 and 4.24 are modified. At the bottom layer ($i = n$ in Figure 4.4) bitumen cannot enter nor solvent exit the bottom of the layer and the mass balance reduces to the following:

$$M_{b,n}^{j+1} = M_{b,n}^j - \dot{m}_{b,n}^j \Delta t \tag{4.31}$$

$$M_{s,n}^{j+1} = M_{s,n}^j + \dot{m}_{s,n-1}^j \Delta t \tag{4.32}$$

Similarly, at the top layer ($i = m$ in Figure 4.4), solvent cannot enter nor bitumen exit the top of the layer and the mass balance reduces to the following:

$$M_{b,-m}^{j+1} = M_{b,-m}^j + \dot{m}_{b,-m+1}^j \Delta t \tag{4.33}$$

$$M_{s,-m}^{j+1} = M_{s,-m}^j - \dot{m}_{s,-m}^j \Delta t \tag{4.34}$$

Model Initialization

Model initialization includes setting the layer thickness, number of layers, mass of each layer, the properties (density, viscosity, and diffusivity) for each layer, and the time step. Each are discussed below.

The initial layer thicknesses (Δx) are calculated from:

$$\Delta x = \frac{M_s}{m \rho_S A_{xo}} \quad for \ j < 0 \tag{4.35}$$

$$\Delta x = \frac{M_b}{n \rho_b A_{xo}} \quad for \ j > 0 \tag{4.36}$$

where m and n are input parameters, which refer to the number of layers in the initial solvent and bitumen phase, respectively, ρ is the density in g/cm³, A_{xo} is the cross-sectional area of the diffusion cylinder in cm² and M is the initial mass in g. The initial mass M is the total initial mass of the combined solvent and bitumen used in the liquid-liquid diffusion experiments, while, the initial mass of each layer is given by:

$$M_{s,i}^j = \frac{M_s}{m} \tag{4.37}$$

$$M_{b,i}^{j} = \frac{M_b}{n} \tag{4.38}$$

The density, viscosity, and diffusivity for each layer are set from the known properties of the bitumen and the solvent. More details on the properties are provided in Section 4.4.

The numerical solution becomes more exact with smaller time steps (Δt) and smaller layer thicknesses (Δx) until numerical dispersion becomes significant. However, if the steps are too small the computation time for the model becomes too large for practical applications. In addition, if the layer thickness is too small compared to the time step, the initial masses on each layer could be smaller than the mass flows of each component and the numerical model will not converge. Similarly, at early times when the concentration gradients are large, if the time step is too big, the mass flow of each component could be higher than the mass of the layer. Therefore, the time step and the number of solvent and bitumen layers must be defined based on the mass flows and the initial mass on each layer.

It was found that the maximum mass flow at time j must be less than the 10% of the initial mass in each layer to guarantee a stable solution. In addition, if the maximum mass flow at time j is less than $1 \cdot 10^{-3}$ g/s, the computation time for the model becomes too large. Therefore, at early times when the concentration gradients are large (*i.e.* large mass flows), the time step must be small enough to meet the mass flow constraint. At late times when the concentration gradients are small (*i.e.* small mass flows), the time step can be increased. It was found that for the 10 first hours of each experiment, a time step of 5 seconds led to a stable solution. Then, the time step was increased to 0.4 minutes until the mass flows were less than $1 \cdot 10^{-3}$ g/s and subsequently to 0.8 minutes. The solution was stable and the total run time was maximum 120 seconds.

4.2.3 Algorithm for Fitting Experimental Data

The algorithm for fitting measured concentration profiles is shown in Figure 4.5. The model is initialized with the duration of the experiment, the total masses of solvent and bitumen, and the density of bitumen and solvent at the temperature and pressure of the experiment. An initial guess is provided for a constant diffusivity or for the diffusion correlation parameter of interest. For the

constant diffusivity model, the initial value for diffusivity can be obtained from literature or any number with the expected order of magnitude can be used. For a concentration dependent diffusivity model, the correlation parameter is initialized to match a diffusivity from the literature or provide a diffusivity value with the expected order of magnitude. The recommended order of magnitude for both cases is between 10^{-5} and 10^{-7} cm²/s.

There are two loops in the model. In the inner loop, at each time step, the mass flows are calculated, and the new masses of solvent and bitumen are updated in each layer of the model. Then, the mass fraction of solvent in each layer is calculated and the densities, viscosities, and diffusivities (except for the constant diffusivity case) in each layer are updated. The same procedure is repeated until the time in the model reaches the time of the experiment. The output of the inner loop is a concentration profile at a specified time (usually the end of the experiment).

The outer loop is used to update the diffusivity or diffusivity parameter. First, the average ARD and the maximum ARD between the calculated profile and the target measured profile are calculated. If the calculated profile is less developed than the experimental data, the diffusivity is increased and *vise versa*. In this study, the diffusivity was adjusted manually until the average ARD was minimized. An example of the model fitted to a concentration profile using a constant diffusity and a concentration dependent diffusivity correlation is provided in Figure 4.6
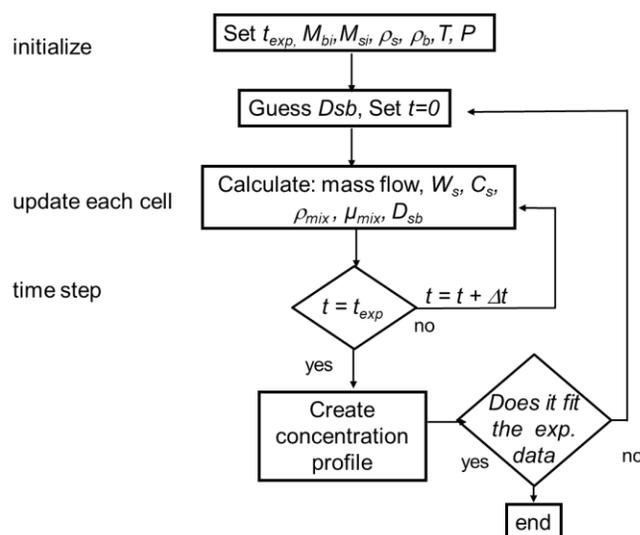
Figure 4.5. Algorithm for fitting the liquid-liquid diffusion model to a measured concentration profile.
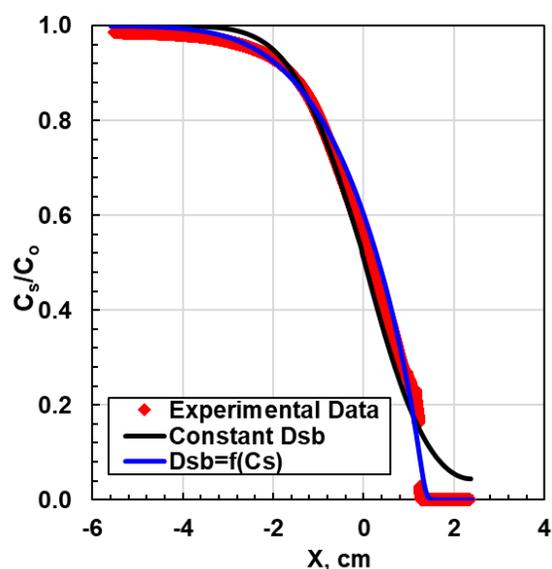
Figure 4.6. Measured and modeled concentrations profile for a n-heptane/maltenes system after 3 days of diffusion at 21°C and 0.1 MPa.

4.3 Configuring the Model for Gas-Liquid Diffusion

The solvent-bitumen diffusion model explained above can be adjusted for gas-liquid experiments, this configuration is intended to determine the diffusivities of gaseous solvents in bitumen and also to validate the proposed model.

To set up the numerical model for the gas-liquid experiments, the bitumen column is divided into layers of equal thickness, while the solvent is kept as one homogenous layer, Figure 4.5. Eqs. 4.2, 4.3, and 4.4 provide the initial and the two boundary conditions, respectively. The mass of bitumen in each layer is initialized and the initial mass fractions, density, viscosity, and diffusivity are calculated for each layer.

At each time step in each layer, the mass flux of solvent entering the top of each layer and exiting the bottom of the layer is calculated from Eqs. 4.27 and 4.28. The mass flux of bitumen into all layers is assumed to be zero; that is, zero flux into the solvent and no explicit flux between bitumen layers. Bitumen diffusion is accounted for indirectly in the swelling of each layer. Hence, the mass of bitumen in each layer is constant while the mass of solvent is determined at each time step from the mass balance (Eqs. 4.24 and 4.32). The mass fraction of each component in each layer is updated and the density, viscosity, and diffusivity for each layer using the updated composition. Finally, the height of the layer is recalculated and the next time step is initiated.
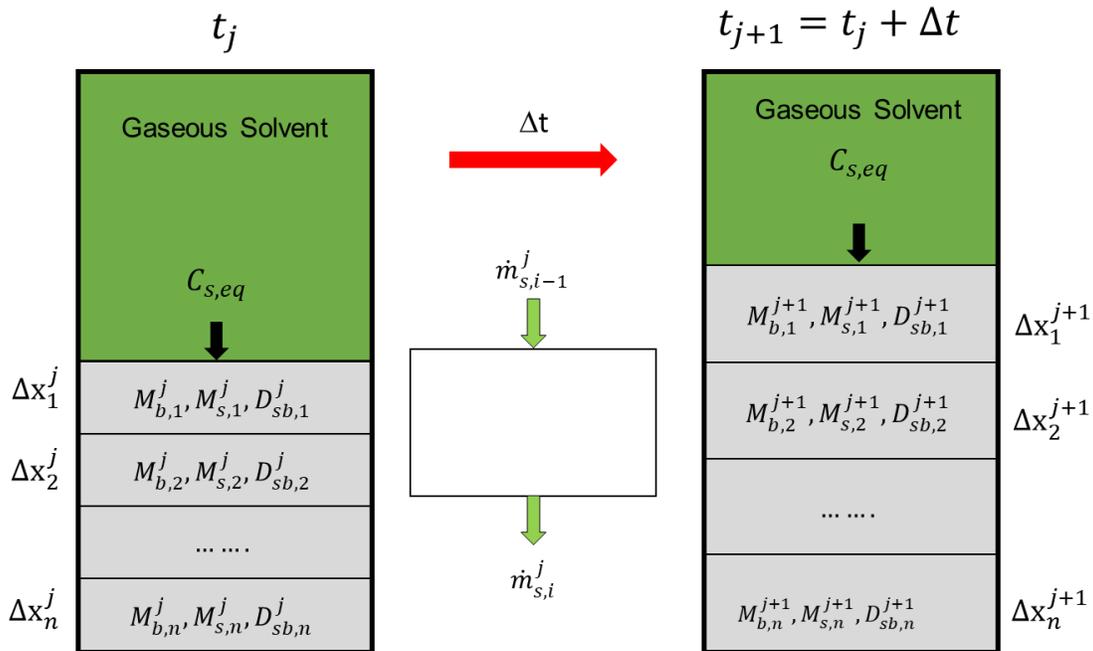
Figure 4.7. Numerical diffusion model for pressure decay experiments.

The swelling of the bitumen is accounted for by the change in height of the bitumen layers. The total height of the oil at any time step is calculated from the layer thicknesses as follows:

$$h_{total} = \sum_{i=1}^{nmax} \Delta x_i^{j+1}$$

(4.39)

The total amount of solvent diffused is given by:

$$m_{total}^j = \sum_{i=1}^{nmax} M_{s,i}^j$$

(4.40)

The output of the inner loop is the cumulative solvent mass diffused with time. The diffusivity or diffusivity correlation parameter is adjusted in the outer loop to fit the measured solvent mass transferred over time. The algorithm for fitting the experimental data is the same as the one used by Richardson, (2017) and shown in Figure 4.2.

One test of the proposed model was to compare it with the gas-bitumen mass transfer model presented by Richardson, (2017). The Richardson model was based on the solution of the continuity equation (Eq. 4.1) while the proposed model is based on the mass fluxes at the layer boundaries (Eqs. 4.13 and 4.14). Therefore, the models are equivalent as long as the bitumen mass fluxes in the proposed model are set to zero and the upper boundary condition is reset to the gas-bitumen interface boundary condition. The comparison of the two models is then a validation that the diffusion process can be represented either by mass balances and mass flows or a solution of the continuity equation. Figure 4.8 confirms that the two diffusion models give identical results.
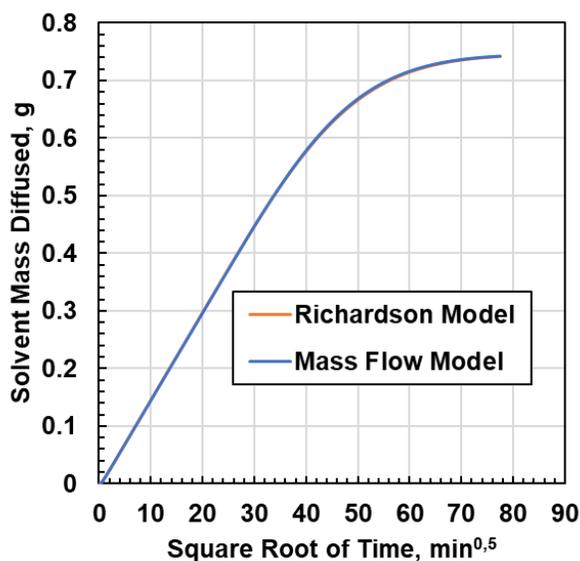
Figure 4.8. Comparison between the proposed model and the gas-bitumen mass transfer model presented by Richardson, (2017).

4.4 Property Models

4.4.1 Density

Densities of pure components and mixture are needed in the modeling process to calculate the initial height of the fluids, viscosities and diffusivities. Therefore, accurate density predictions are required.

Bitumen Density

The density and viscosity of Athabasca bitumen (WC-B-A3) were measured from 50 to 175°C and 0.1 to 10 MPa with the in house capillary viscometer. These data were measured by Florian Schoeggl at the University of Calgary). The density and viscosity of WC-B-A3 maltenes were measured with a cone and plate rheometer and a glass oscillating u-tube Aton Paar density meter, respectively, from 15 to 80°C and atmospheric pressure. These data were measured as part of this thesis.

The measured densities were fitted with the following empirical equation (Saryazdi *et al*., 2013):

$$\rho_b = (A^* - B^*T) \exp\{[F^* \exp(D^*T)](P - 0.1)\} \tag{4.41}$$

where ρ_b is the density of the bitumen/maltenes in kg/m³, P is the pressure in MPa, T is the temperature in K, and A^*, B^* F^* and D^* are fitting parameters. The fitted parameters for WC-B-A3 and maltenes are provided in Table 4.1. Eq. 4.41 fit the density of bitumen with a maximum absolute deviation of $3\cdot10^{-4}$ gr/cm³.

Table 4.1. Parameters for the bitumen density equation.

Component	A^*	B^*	F^*	D^*
	kg/m³	kg/(m³K)	1/MPa	1/K
WC-B-A3	1196.2	0.63743	0.00014	0.00433
Maltenes	1168.5	0.63806	0.00014	0.00433

Solvent Density

The densities of liquid toluene, *n*-heptane, and *n*-pentane from 15 to 200°C and from 0.1 to 0.5 MPA were obtained from the NIST Chemistry Book (2018). These data were fitted using the effective density correlations from Saryazdi *et al*. (2013) (where the effective density is the density of a gas dissolved in a liquid), given by:

$$\rho_s = (a_1^* + a_2^*T) + (b_1^* + b_2^*T)P \tag{4.42}$$

where ρ_s is the effective density of a gas in liquid in kg/m³, P is the pressure in MPa, T is temperature in K, and a_1^*, a_2^*, b_1^*, and b_2^* are fluid specific parameters. The effective density parameters for *n*-heptane, and *n*-pentane and were taken from Saryazdi *et al.* (2013). The parameters for toluene were determined following the procedure presented by Saryazdi *et al*. (2013). The parameters are provided in Table 4.2. Eq. 4.42 fits the liquid density of the solvent to within an absolute deviation of $7\cdot10^{-4}$ gr/cm³ for the range of temperatures and pressures used in this thesis.

Table 4.2. Parameters for the effective liquid density correlation from Saryazdi *et al*. (2013).

Component	a_1^*	a_2^*	b_1^*	b_2^*
	kg/m³	kg/(m³·K)	kg/(m³·MPa)	kg/(m³·MPa·K)
n-heptane	918.603	-0.79155	-0.17738	0.002692
n-pentane	878.006	−0.82817	−0.09229	0.002648
toluene	1150.778	-0.96697	-1.08866	0.006169

Density Mixing Rule

The mixing rule developed by Saryazdi et al. (2013) is used to calculated the density of the mixture in each layer of the model. For a binary system of bitumen and solvent, the mixing rule is given by:

$$\rho_{mix_i}^{\ j} = \left(\left(\frac{w_{s_i}^{\ j}}{\rho_s} + \frac{1 - w_{s_i}^{\ j}}{\rho_b} \right) - \left(w_{s_i}^{\ j} \left(1 - w_{s_i}^{\ j}\right) \left(\frac{1}{\rho_s} + \frac{1}{\rho_b} \right) \beta_{sb} \right) \right)^{-1} \tag{4.43}$$

where $\rho_{mix_i}^{\ j}$ is the mixture density in kg/m³, $w_{s_i}^{\ j}$ is the weight fraction of solvent, and ρ_s is the effective density of the solvent in kg/m³, ρ_b is the density of the bitumen in kg/m³, both at the experimental pressure and temperature and β_{sb} is the binary interaction parameter between solvent and bitumen. The interaction parameter can be obtained either by fitting experimental data or calculated from a correlation. For the gas-liquid diffusion model, the binary interaction parameter is given by Saryazdi et al. (2013):

$$\beta_{sb} = \beta_{sb}^{298} + 8.74 * 10^{-5}(T - 298) \tag{4.44}$$

$$\beta_{sb}^{298} = -0.092 \left| 0.435 - 2 \left(\frac{\left| v_s^{298} - v_b^{298} \right|}{(v_s^{298} + v_b^{298})} \right) \right| + 0.022 \tag{4.45}$$

where β_{sb}^{298} is the binary interaction parameter between components at 298 K, and v_s^{298} and v_b^{298} are the specific volume of solvent and bitumen at 298 K. For the liquid-liquid model, the volume of the system was fixed and it was necessary to neglect the excess volume of mixing; therefore, β was set to zero.

4.4.2 Diffusivity

Five diffusivity correlations were evaluated:

1) Constant diffusivity

$$D_{sb}{}_i^{\,j} = Constant \tag{4.46}$$

2) Linear model

$$D_{sb}{}_i^{\,j} = \left[D_{sb}^{\infty} x_b{}_i^{\,j} + D_{bs}^{\infty} x_s{}_i^{\,j} \right] \alpha_i^{\,j} \tag{4.47}$$

3) Vignes equation

$$D_{sb}{}_i^{\,j} = \left[(D_{sb}^{\infty})^{x_b{}_i^{\,j}} (D_{Bbs}^{\infty})^{x_s{}_i^{\,j}} \right] \alpha_i^{\,j} \tag{4.48}$$

4) Leffler equation

$$D_{sb}{}_i^{\,j} \mu_{mix}{}_i^{\,j} = \left[(D_{sb}^{\infty} \mu_b)^{x_b{}_i^{\,j}} (D_{bs}^{\infty} \mu_s)^{x_s{}_i^{\,j}} \right] \alpha_i^{\,j} \tag{4.49}$$

5) Modified Hayduk and Cheng equation

$$D_{sb}{}_i^{\,j} = \frac{A_p T}{\mu_{mix}{}_i^{\,j}{}^{n}} \tag{4.50}$$

where $x_s{}_i^{\,j}$ and $x_b{}_i^{\,j}$ are the molar fraction of solvent and bitumen, $\mu_{mix}{}_i^{\,j}$ is the mixture viscosity, D_{sb}^{∞} and D_{bs}^{∞} are the infinite dilution diffusivity of solvent in bitumen and bitumen in solvent respectively, μ_s and μ_b are the viscosity of the solvent and bitumen at the experimental pressure and temperature, $\alpha_i^{\,j}$ activity coefficient, and A_p and n are fluid specific parameters. The diffusivity is the fitting parameter for the numerical mass transfer model. For Eq. 4.46, the constant diffusivity was iterated to best fit the measured diffusion data. For Eqs. 4.47 to 4.49, the infinite dilution diffusivities were adjusted to fit the data. For Eq. 4.50, the A_p and n parameters were adjusted.

Properties such as mole concentration, activity coefficient and viscosity of the mixture are required to calculate the diffusivity. Guerrero-Aconcha et al. (2008) used Vignes equation to model diffusivity data by using the activity coefficient as fitting parameter. They found that activity coefficients for *n*-alkane-bitumen systems differ only slightly from unity at experimental times greater than 20 hours. The experiments in this thesis are greater than 48 hours, therefore, the

activity coefficient was assumed to be unity. The molar fraction of solvent and bitumen are obtained from the following equations:

$$x_{s_i}^{j} = \frac{\dfrac{w_{s_i}^{j}}{MW_s}}{\dfrac{w_{s_i}^{j}}{MW_s} + \dfrac{1 - w_{s_i}^{j}}{MW_b}} \tag{4.51}$$

$$x_{b_i}^{j} = 1 - x_{s_i}^{j} \tag{4.52}$$

where $w_{s_i}^{j}$ is the mass fraction of solvent in the layer and MW_s and MW_b are the molar mass of solvent and bitumen respectively in g/mol. Viscosity is discussed in the next section.

4.4.3 Viscosity

In this thesis, the viscosity of bitumen, solvent and mixtures are determined using the Expanded Fluid Viscosity Model (Yarranton and Satyro, 2009; Motahhari *et al*., 2013a-c Ramos-Pallares *et al*., 2015, 2016a). In this model, the viscosity of a single fluid is calculated as a density dependent departure function from a dilute gas viscosity, as follows:

$$\mu - \mu_D = 0.165(exp(c_2\beta) - 1) \tag{4.53}$$

where μ_D is the dilute gas viscosity in mPa·s, c_2 is a fluid specific parameter and the parameter β is given by:

$$\beta = \frac{1}{exp\left(\left(\dfrac{\rho_s^*}{\rho}\right)^{0.65} - 1\right) - 1} \tag{4.54}$$

ρ_s^* is defined as compressed state density in kg/m³ given by:

$$\rho_s^* = \frac{\rho_s^0}{exp(-c_3 P)} \tag{4.55}$$

where P is pressure in MPa, ρ_s^0 and c_3 are fluid specific parameters. The parameters ρ_s^0, c_2 and c_3 for bitumen and maltenes were obtained by fitting Eq. 4.53 to experimental data minimizing the relative absolute deviation between the calculated and measured values. The parameters for the solvents were taken from Ramos-Pallares *et al.* (2016b). The correlation fit the maltene viscosities from 15 to 80°C and at atmospheric pressure to within ±4.5% with an AARD (average absolute relative deviation) of 2.3%. It fit the bitumen viscosities from 50 and 175°C at pressures from 0.1 to 10 MPa to within ±2.8% with an AARD of 1.1%.

Table 4.3. Expanded Fluid model fluid specific parameters for the used fluids.

Component	$\rho_s{}^0$ kg/m³	c_2	c_3 10^{-3} MPa^{-1}
n-pentene	837.0	0.1980	0.18
n-heptane	857.8	0.2130	0.17
toluene	1049.6	0.2155	0.14
Maltenes	1041.8	0.4528	0.34
WC-B-A3	1061.2	0.4905	0.34

The dilute gas viscosity of the components was determined from the following empirical correlation:

$$\mu_D = A_0 + B_0 T + E_0 T^2 + F_0 T^3 \tag{4.56}$$

where T is the temperature in K, A_0, B_0, C_0 and D_0 are fitting parameters specific for each pure component. The parameters were obtained from Yaws (2018).

To calculate the viscosity of mixtures, the parameters ρ_s^0, c_3 and c_2 in the viscosity model (Eqs.4.53 to 4.55) are calculated with the following mixing rules (Motahari *et al.*, 2011):

$$\rho_{s,mix}^0 = \left[\sum_{i=1}^{nc} \sum_{j=1}^{nc} \frac{w_i w_j}{2} \left(\frac{1}{\rho_{s,i}^0} + \frac{1}{\rho_{s,j}^0} \right) (1 - \theta_{ij}) \right]^{-1} \tag{4.57}$$

$$\frac{c_{2,mix}}{\rho_{s,mix}^0} = \sum_{i=1}^{nc} \sum_{j-1}^{nc} \frac{w_i w_j}{2} \left(\frac{c_{2,i}}{\rho_{s,i}^0} + \frac{c_{2,j}}{\rho_{s,j}^0} \right) (1 - \theta_{ij}) \tag{4.58}$$

$$c_{3,mix} = \left[\sum_{i=1}^{nc} \frac{w_i}{c_{3,i}} \right]^{-1} \tag{4.59}$$

$$\mu_{D,mix} = \sum_i \frac{x_i \mu_{D,i}}{\sum_j x_j \delta_{ij}} \tag{4.60}$$

$$\delta_{ij} = \frac{\left[1 + \left(\mu_{D,i}/\mu_{D,j}\right)^{0.5}\left(MW_j/MW_i\right)^{0.25}\right]^2}{\left[8\left(1 + MW_i/MW_j\right)\right]^{0.5}} \tag{4.61}$$

where nc is the number of components in the system and, θ_{ij} is a binary interaction parameter that can be adjusted with experimental data or can be calculated using the procedure and equations presented by (Ramos-Pallares *et al*., 2015, 2016a).

In this thesis, for the liquid-liquid diffusion experiments, the binary interaction parameters were determined by fitting the measured viscosities of solvent-bitumen mixtures. The adjusted expanded fluid model fit the viscosities of mixtures of *n*-pentane, *n*-heptane, and toluene with bitumen or maltenes at 15 to 25°C and atmospheric pressure with an AARD of 10%. For gas-liquid diffusion experiments, the binary interaction parameter was calculated and the viscosity was predicted. The error when using predicted binary interaction parameters is expected to be within ±14% (Ramos-Pallares *et al*., 2016a).

CHAPTER 5: RESULTS AND DISCUSSION: LIQUID-LIQUID DIFFUSION

This chapter presents the results from the liquid-liquid diffusivity experiments. First, the concentration profiles obtained for *n*-alkanes/bitumen, n-alkanes/maltenes, toluene/bitumen, and toluene/maltenes are presented. Then, the effects of the initial masses, diffusion time, type of solvent, initial oil viscosity, and asphaltene precipitation are on the mass transfer rate is discussed. The mutual diffusivity is determined for each of the systems fitting the numerical model developed in Chapter 4 to the experimental data. Concentration dependent diffusivity tendency is discussed and a comparison between the collected data and literature data is presented. Finally, three density profiles for liquid-liquid diffusion of toluene and Peace River bitumen were fitted and predicted with the model.

5.1 Data Collected in this Thesis

Density profiles for six different liquid-liquid systems were measured at ambient conditions for the systems listed in Table 5.1. The density profiles were converted into concentration profiles as discussed in Chapter 3. The effects of the initial masses, diffusion time, type of solvent, initial oil viscosity, and asphaltene precipitation are each discussed below.

Table 5.1. Experimental matrix for liquid-liquid diffusion experiments.

Oil	Solvent	Initial mass of oil, g	Initial mass of solvent, g	Diffusion times, Days
Bitumen 357,000 mPa·s @ 20°C	toluene *n*-pentane *n*-heptane	10 to 40	10 to 80	3 to 15
Maltenes 12,670 mPa·s @ 20°C	toluene *n*-pentane *n*-heptane	10 to 40	20 to 80	3 to 10

5.1.1 Effect of Diffusion Time

Figure 5.1 shows how the concentration profiles for toluene/bitumen systems evolve over time. The four concentration profiles were measured in four separate experiments, each with the same

initial masses of solvent and bitumen (56 and 28 g, respectively). Each concentration profile is normalized to C_o, the concentration of pure solvent in g/cm³. The concentration profiles each have two regions: 1) the initial solvent side at $x < 0$; 2) the initial bitumen side at $x > 0$. On the solvent side, the solvent concentration decreases progressively over time as the bitumen diffuses into the solvent. On the bitumen side, the solvent concentration increases progressively over time as the solvent diffuses into the bitumen. Given enough time, the solvent concentration would become uniform at the average solvent concentration of the system.
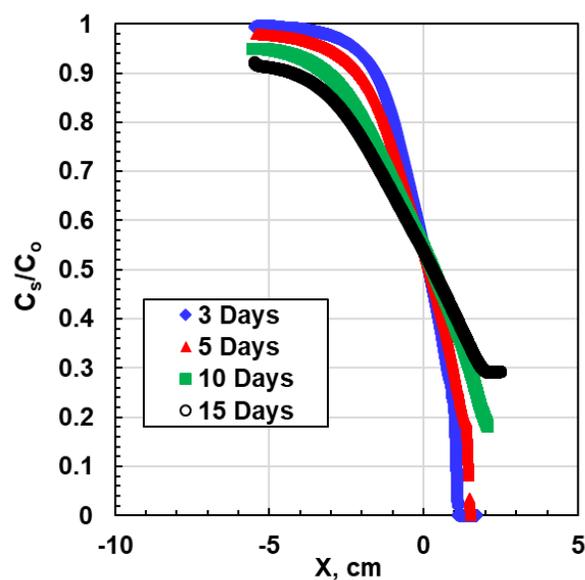
Figure 5.1. Evolution over time of the concentration profiles for toluene/bitumen systems at ambient conditions. Note, when the solvent or bitumen reach the boundary, the end points are no longer one or zero.

Figure 5.1 also shows that the solvent concentration at the top of the cell (the smallest value of X) is no longer equal to one after 3 days of diffusion time. In other words, the bitumen has reached the top of the solvent column. In this case, the bitumen traveled 5.2 cm in 3 days. However, the solvent only reaches the bottom the oil column after 5 days; that is, it travelled less than 1 cm in 5 days. Although the bitumen molecules are larger than the solvent molecules, they diffuse faster because they are passing through a much less viscous medium.

For semi-infinite Fickian diffusion in a binary mixture, the concentration profile at any time collapses onto the same curve when plotted versus the Boltzmann parameter, $X/\sqrt{t}$ (Oballa and Butler, 1989). Figures 5.2a-c show the concentration profiles versus $X/\sqrt{t}$ for toluene/bitumen, *n*-heptane/bitumen, and *n*-pentane/maltene systems, respectively. Plots for the other systems are provided in Appendix C. The concentration profiles all follow the same "master" curve with the following exceptions. Small deviations occur at the ends the profiles when the semi-infinite assumption is not valid; that is, when the solvent reaches the bottom of the bitumen column and the bitumen reaches the top of the solvent column. In addition, the concentration profiles deviate from the master curve when asphaltenes precipitate, as will be discussed later.

For systems with no boundary effects and with no precipitation, all of the concentration profiles fall onto the master curve. As shown in Appendix D, the master curve only formed when the data were plotted against the Boltzmann parameter ($X/\sqrt{t}$) and not, for example, against $X/\sqrt[3]{t}$ and $X/\sqrt[4]{t}$. Hence, the mass transfer is molecular diffusion dominated (no convection) and for each system there exists a unique form of the diffusivity. Consequently, the diffusivity can be determined from any concentration profile for a given system.
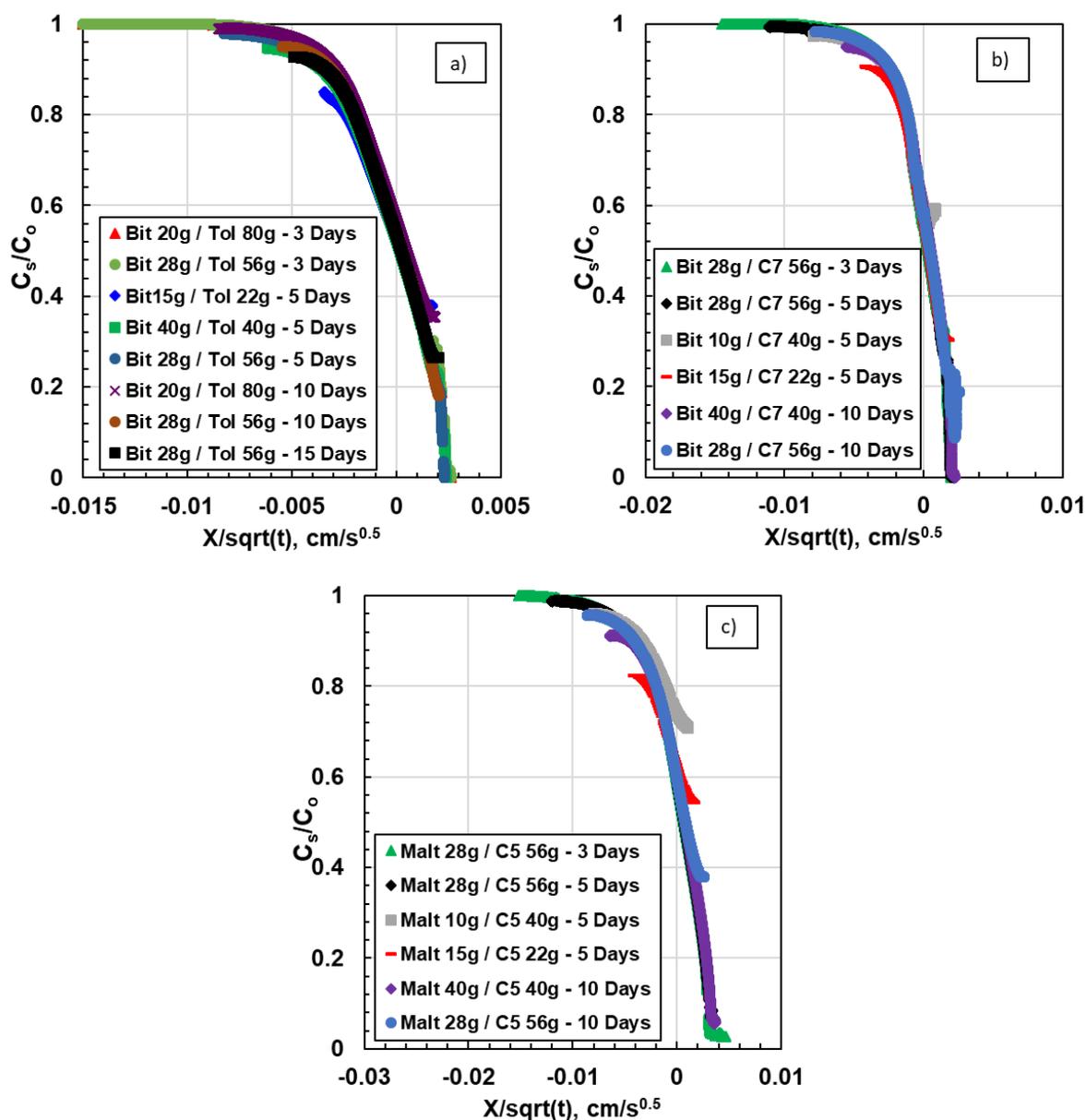
Figure 5.2. Concentration profiles plotted against $X/\sqrt{t}$ for: a) toluene/bitumen systems; b) *n*-heptane/bitumen systems; c) *n*-pentane/maltenes systems.

5.1.2 Effect of Initial Masses

Figures 5. 2a-c also show the effect of the initial masses of solvent and bitumen. As expected, if the initial mass of bitumen is reduced (lower height), the solvent reaches the top of the bitumen column sooner and *vice versa*. However, other than reaching the boundary sooner, the initial

masses have no effect on the concentration profile when plotted against Boltzmann parameter. Therefore, the initial masses do not have an effect on the diffusivity measurement.

5.1.3 Effect of Solvent Type

Two paraffinic solvents (*n*-pentane and *n*-heptane) and one aromatic solvent were investigated in this thesis. Table 5.2 shows the molecular weight, viscosity, and density of these solvents at ambient conditions (NIST, 2018). The effect of each solvent on the concentration profiles was evaluated in solvent/maltene systems because no asphaltenes precipitation occurs in these mixtures. For the sake of the visual analysis performed in this section, the concentration profiles are shown as mass fraction profiles; this is, the mass fraction of solvent, w_s, versus X.

Table 5.2. Physical properties for the solvent used in this thesis. NIST (2018).

Solvent	Molecular Weight g/mol	Density g/cm³@ 20°C	Viscosity mPa·s @ 20°C
toluene	92.14	0.8668	0.6023
***n*-heptane**	100.20	0.6838	0.4114
***n*-pentane**	72.15	0.6257	0.2275

Figure 5.3 shows three mass fraction profiles for systems of maltenes and toluene, *n*-heptane, and *n*-pentane (40 g of maltenes and 40 g of solvent) after 10 days of diffusion at ambient conditions. On the maltenes side (Figure 5.3b), the mass fraction profiles of toluene and *n*-heptane are similar and the *n*-pentane profile has a higher solvent mass fraction than the others at the same location. The *n*-pentane diffuses faster than *n*-heptane or toluene because it is a smaller molecule. Toluene and *n*-heptane are similar in size and diffuse at a comparable rate. On the solvent side (Figure 5.3a), the toluene and *n*-heptane profiles are again similar but the *n*-pentane profile has lower solvent mass fractions than the others. The maltene molecules diffuse more rapidly in *n*-pentane because it is the less viscous medium. Toluene and *n*-heptane are similar in viscosity and the maltenes diffuse through them at a comparable rate. The solvent side end points for the toluene/maltenes and *n*-heptane/maltenes systems look different in Figure 5.3a because the initial

solvent heights were different. Toluene is denser and has less height for the same mass. Similar behavior was observed at all diffusion times and all initial masses of solvent and maltenes.
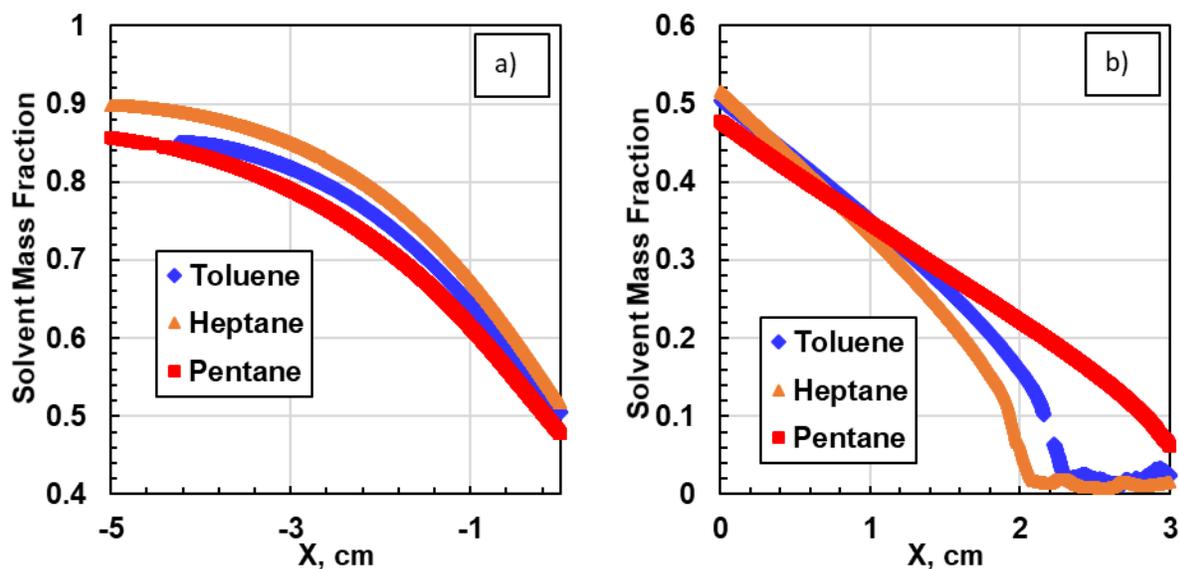
Figure 5.3. Concentration profiles for systems of maltenes and toluene, *n*-heptane, or *n*-pentane (40 g of maltenes and 40 g of solvent) after 10 days of diffusion at ambient conditions: a) solvent side; b) bitumen side.

5.1.4 Effect of Initial Oil Viscosity

The effect of the initial oil viscosity on the concentration profiles was evaluated in toluene/bitumen and toluene/maltenes systems because no asphaltenes precipitation occurs in these mixtures. Figure 5.4 compares the mass fraction profiles for a toluene/bitumen system and a toluene/maltene system (56 g of toluene and 28 grams of maltenes or bitumen) after 3 days of diffusion at ambient conditions. In this case, the solvent and oil have barely or not at all reached their respective boundaries. There is little or no difference in the mass transfer rate even though the bitumen is far more viscous than the maltenes. Figure 5.5 compares the mass fraction profiles for the same systems and conditions except with 40 g of toluene and 10 g of maltenes or bitumen and the experiment last 5 days. In this case, both the solvent and oil have reached the boundaries and a difference in the mass transfer rate becomes apparent. The difference in mass transfer rate is nonetheless small considering the difference in the bitumen and maltene viscosities but is

consistent with Cussler's (2009) observation that, in highly viscous systems such as maltenes or bitumen, the diffusion becomes independent of viscosity.
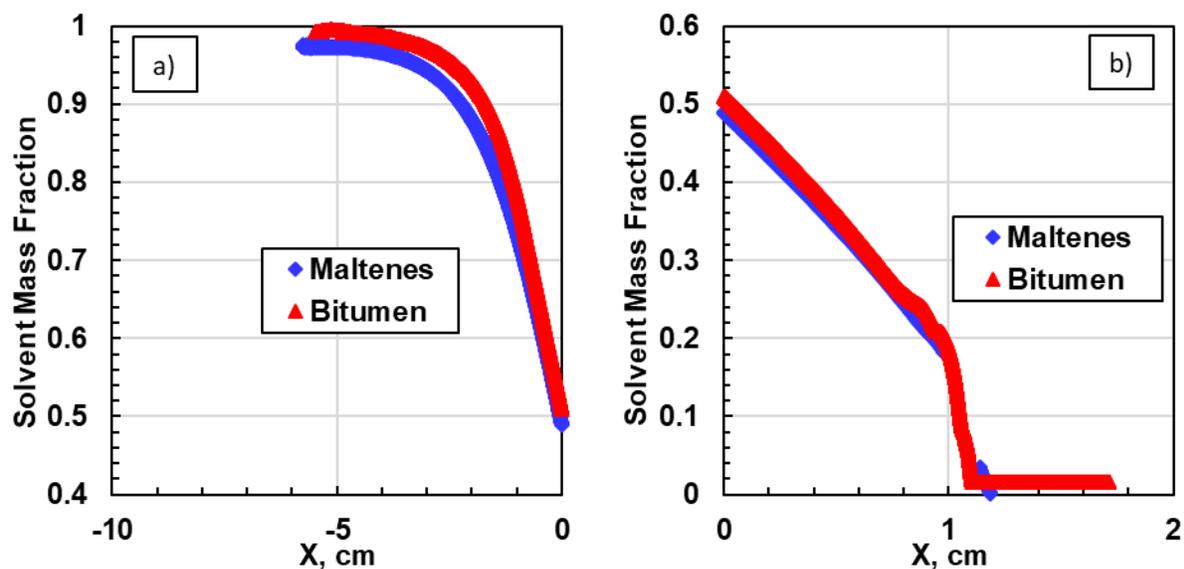
Figure 5.4. Effect of initial oil viscosity on the concentration profiles for systems of toluene/maltenes and toluene/bitumen (28 g of maltenes or bitumen and 56 g of toluene) after 3 days of diffusion at ambient conditions: a) solvent side; b) bitumen side.
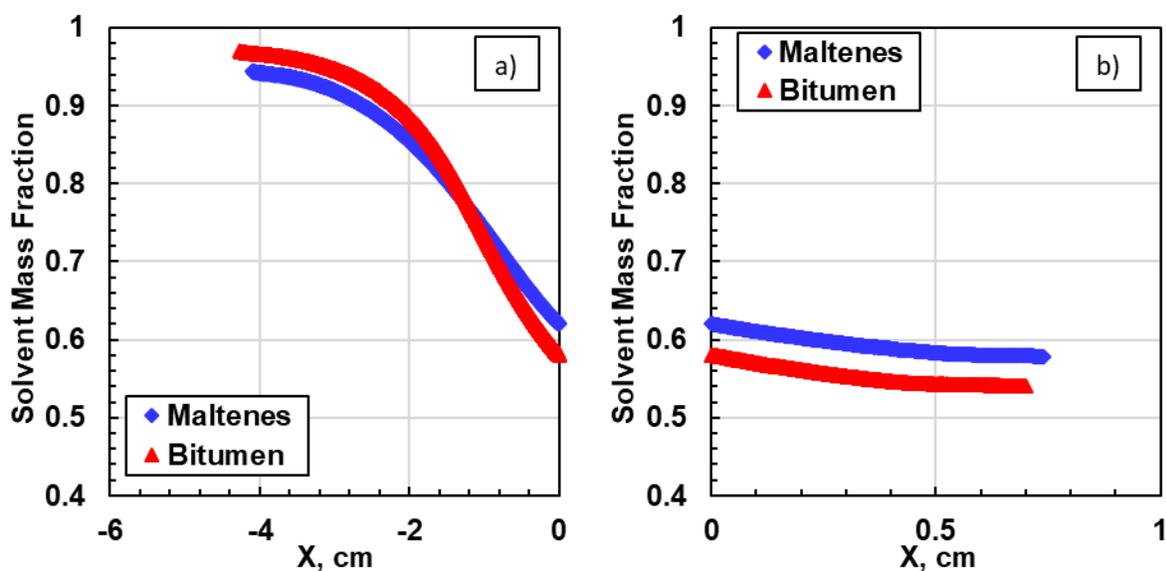
Figure 5.5. Effect of initial oil viscosity on the concentration profiles for systems of toluene/maltenes and toluene/bitumen (10 g of maltenes or bitumen and 40 g of toluene) after 5 days of diffusion at ambient conditions: a) solvent side; b) bitumen side.

5.1.5 Effect of Asphaltene Precipitation

The solvent content at which asphaltenes first precipitate from a diluted bitumen is termed the onset of precipitation. Asphaltenes will precipitate during the mass transfer process wherever the solvent content exceeds the onset condition. The precipitated asphaltene particles can affect the mass transfer rate if they settle and cause convection or if they accumulate and create a barrier. The onsets of precipitation for the bitumen used in this thesis were 42.6 wt% n-pentane and 54.6 wt% n-heptane at ambient conditions. The effect of the asphaltenes precipitation on the mass transfer rate was assessed by comparing concentration profiles from systems where asphaltenes precipitation occurs (n-alkanes/bitumen) with those where it does not (toluene/bitumen, toluene/maltenes and n-alkanes/maltenes).

Figure 5.6 compares the mass fraction profiles for a toluene/bitumen system, a toluene/maltene system, an n-pentane/maltene system and an n-pentane/bitumen system (56 g of toluene or pentane and 28 grams of maltenes or bitumen) after 3 days of diffusion at ambient conditions. In this case, the solvent and oil have barely or not at all reached their respective boundaries. Note, the end points for the toluene/maltenes or bitumen and n-pentane/maltenes or bitumen systems look different in Figure 5.6a because the initial solvent heights were different (same mass, different densities). On the solvent side (Figure 5.6a), no obvious effect of asphaltene precipitation is observed. Diffusion is faster (lower solvent content at the same location) in n-pentane, the less viscous medium. Diffusion is also faster with the smaller molecules (maltenes versus bitumen). However, on the maltenes/bitumen side (Figure 5.6b), the mass fraction profile in the system with precipitation (n-pentane) has lower solvent contents than the systems with no precipitation (all the others); that is, less mass transfer. If all else were equal, the mass transfer rate with n-pentane would be higher than with toluene because it is a smaller molecule. Therefore, in this case, it appears that precipitated asphaltenes have reduced the mass transfer rate.
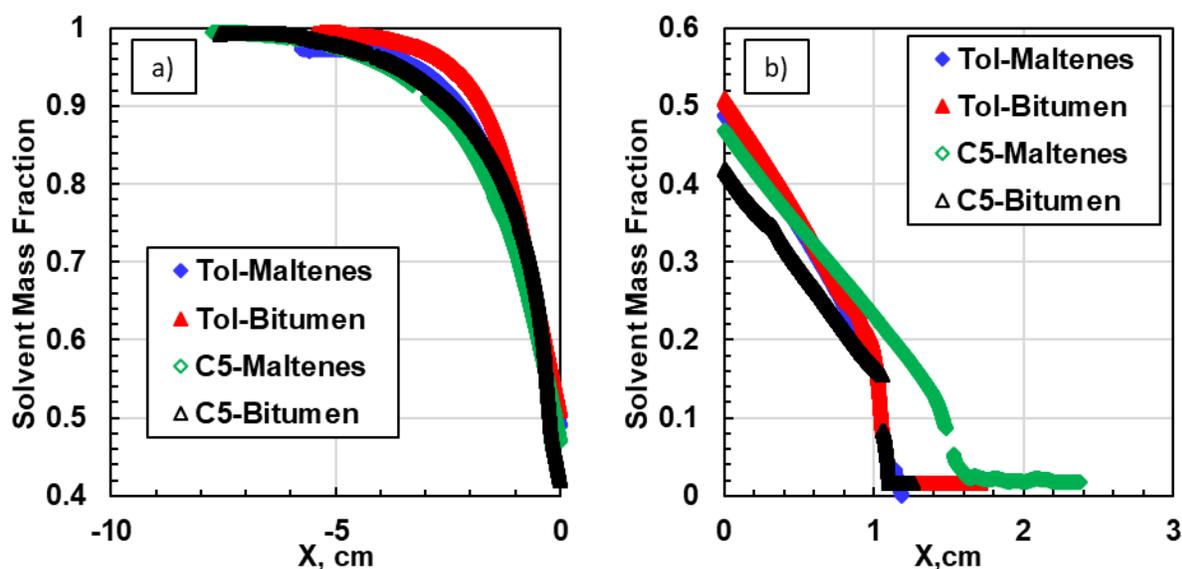
Figure 5.6. Concentration profiles for toluene/maltenes, *n*-pentane/maltenes, and *n*-pentane/bitumen systems (28 g of maltenes or bitumen and 40 g of toluene or *n*-pentane) after 5 days of diffusion at ambient conditions: a) solvent side; b) bitumen side.

Figure 5.7 compares the mass fraction profiles for the same systems and conditions except with 40 g of solvent and 10 g of maltenes or bitumen and the experiment lasted 5 days. In this case, the solvent and oil have reached the cell boundaries. On the solvent side (Figure 5.7a), the trends are as expected: faster diffusion (lower solvent content) in *n*-pentane versus toluene and with maltenes versus bitumen. On the maltenes/bitumen side (Figure 5.7b), there is faster diffusion (higher solvent content) with *n*-pentane/bitumen than the others. In this case, it appears that asphaltene precipitation has increased the mass transfer rate.
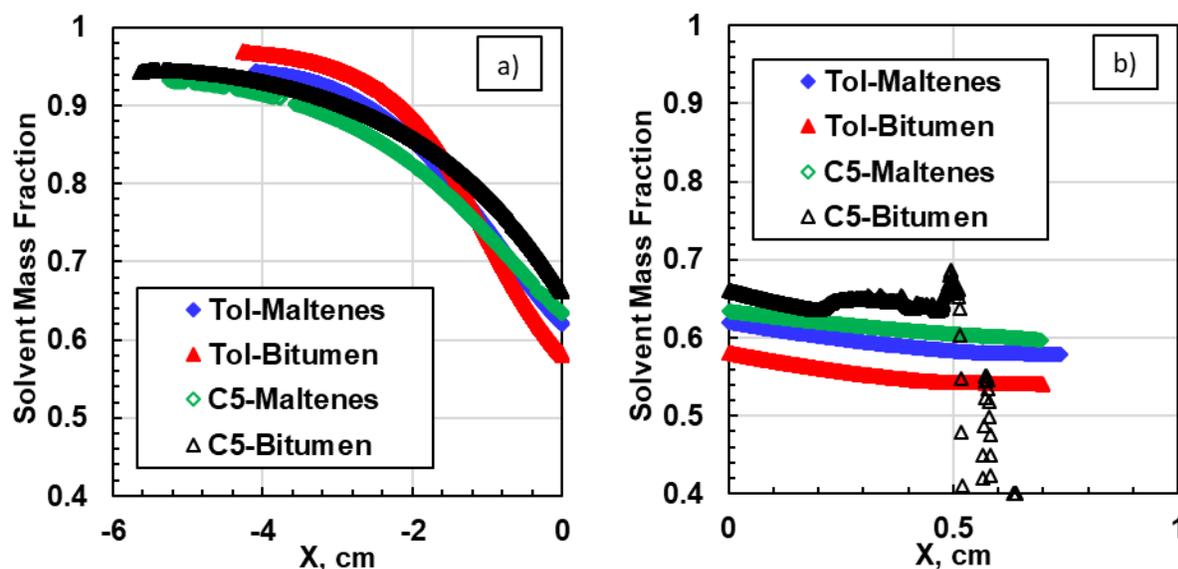
Figure 5.7. Concentration profiles for toluene/maltenes, *n*-pentane/maltenes, and *n*-pentane/bitumen systems (10 g of maltenes or bitumen and 40 g of toluene or *n*-pentane) after 5 days of diffusion at ambient conditions: a) solvent side; b) bitumen side.

Table 5.3 summarizes the observations for all of the systems where asphaltenes precipitated. In most cases, asphaltene precipitation reduced the mass transfer rate. Enhanced mass transfer was observed when the initial average solvent content (initial mass of solvent divided by mass of solvent + bitumen) was 80 wt%. One hypothesis is that precipitated asphaltenes form a barrier to mass transfer when there is limited settling (low solvent content) but enhance mass transfer when there is significant settling (high solvent content). To test this hypothesis, settling rate profiles were calculated from Stoke's law (Bird *et al*., 1960). The settling rate depends on the asphaltene particle size and density and on the viscosity and density of the medium which in turn depend on the solvent content. Asphaltene particle sizes and densities were assumed to be the same for all systems and were obtained from Duran (2018). The property profiles of the medium were calculated with the numerical model from Chapter 4. The effect of asphaltene precipitation on the solvent mass fraction and viscosity was neglected for this qualitative analysis. Details for these calculations are found in Appendix E.

Figure 5.8a shows calculated mass fraction profiles for n-pentane/bitumen systems with different masses of solvent and bitumen after 5 and 10 days of contact time. The corresponding settling rate profiles starting from just above the interface $(X = -1)$ to the bottom of the oil column are shown in Figure 5.8b. At the lower solvent contents (50% to 67%), the asphaltene settling rate drops to low values (0 to 0.2 cm/s) at the bottom of the oil column. In this case, the asphaltenes are likely to accumulate somewhere between the original interface and the bottom of the cell. The accumulation could explain the reduced mass transfer observed in these systems. At 80 wt% average solvent content, the settling rate stays above 1 cm/s throughout the bitumen-phase column. In this case, the precipitated asphaltenes could settle to the bottom of the column rapidly relative to diffusion. The settling likely causes convection and enhances the mass transfer rate. More data and a more detailed model would be required to predict at what conditions asphaltene precipitation increases or reduces the mass transfer rate.

Table 5.3. Effect of asphaltene precipitation on mass transfer rate for n-pentane/bitumen and n-heptane/bitumen systems at ambient conditions.

System	Time d	Bitumen Mass g	Solvent Mass g	Average Solvent Content wt%	Effect on Mass Transfer
n- pentane/bitumen	10	40	40	50	lower
	5	15	22	59	lower
	3,5,10	28	56	67	lower
	5	10	40	80	higher
n-heptane bitumen	10	40	40	50	lower
	5	15	21	59	lower
	3,5,10	28	56	67	lower
	5	10	41	80	higher
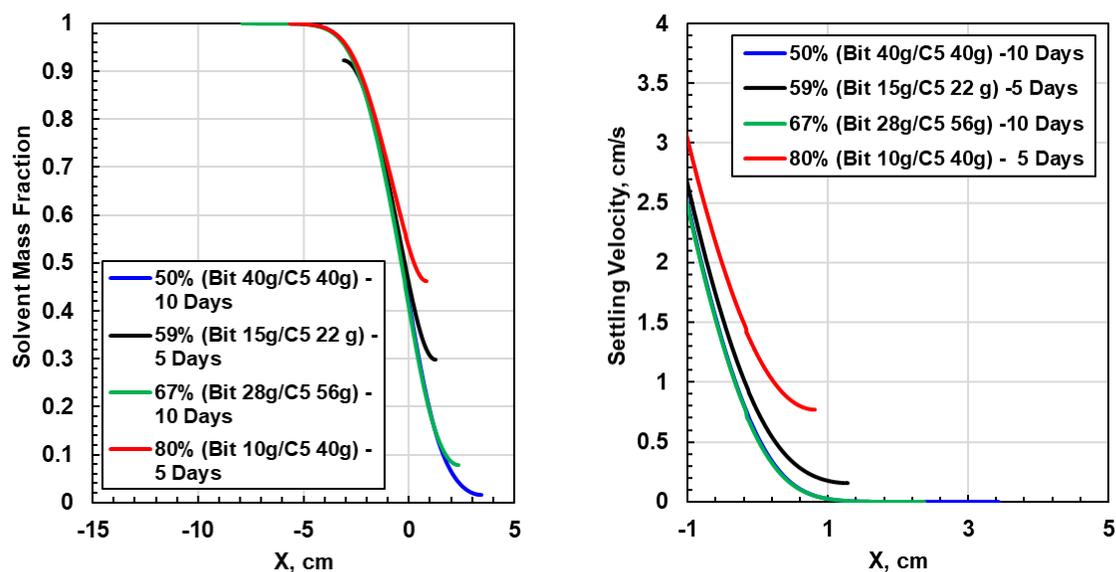
Figure 5.8. Calculated mass fraction (a) and settling rate (b) profiles for *n*-pentane/bitumen systems at ambient conditions with average *n*-pentane contents from 50 to 80 wt% and diffusion times of 5 and 10 days.

5.2 Modeling Concentration Profiles

All the measured concentration profiles were fitted using the numerical model from Chapter 4. The diffusivity (constant or as a function of solvent content or viscosity) was the fitting parameter. First, the results with a constant diffusivity are examined. Then, different correlations for the solvent or viscosity dependent diffusivity are assessed. Finally, the model with the selected diffusivity equation is tested against literature data.

5.2.1 Constant Diffusivity

Figures 5.9 a and b show concentration profile for a toluene/bitumen system after 3 and 15 days of diffusion, respectively. The data were fitted with the mass transfer model with a constant diffusivity. Two values of diffusivity were used in each case: one tuned to match the solvent end of the liquid column and one to match the bitumen end. A single constant diffusivity could not fit both ends of the concentration profiles nor could a single value fit the profiles at different times. The main issue is that the bitumen diffuses faster through the solvent than the solvent through the

bitumen. Hence, a diffusivity dependent on the solvent concentration or mixture viscosity is required.
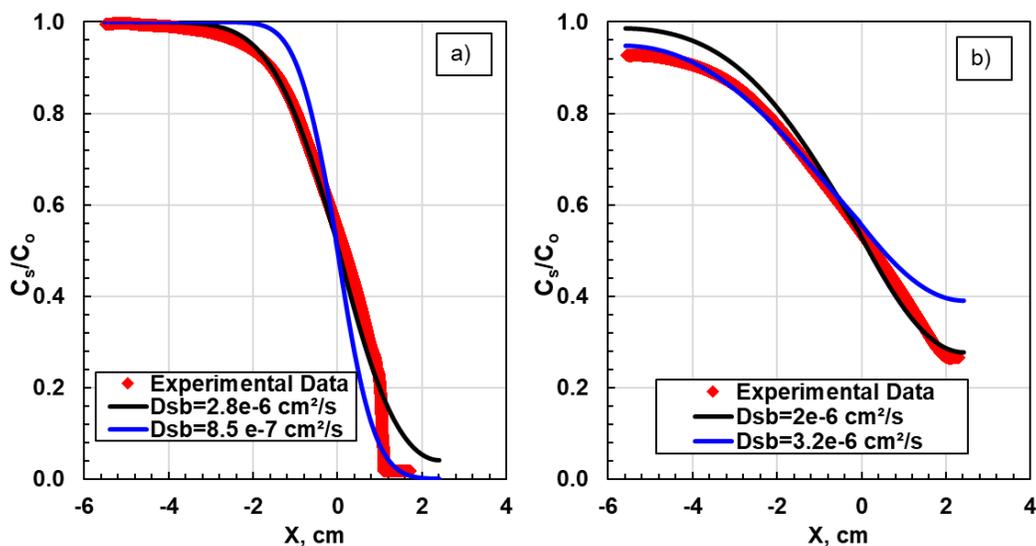
Figure 5.9. Concentration profile for toluene/bitumen system (28g of bitumen and 56g of toluene at ambient conditions) modeled with constant diffusivity at diffusion times of: a) 3 days; b) 15 days.

5.2.2 Variable Diffusivity

In this thesis, "variable" diffusivity indicates that the diffusivity depends on the solvent concentration or mixture viscosity. Figure 5.10 shows the same data as Figure 5.9, but this time fitted with a constant diffusivity and one of the variable diffusivity correlations to be discussed later (see Eq. 5.4). The numerical model with one consistent relationship for the variable diffusivity fitted the entire concentration profile at any diffusion time. Therefore, a solvent concentration or viscosity dependent diffusivity is sufficient to model mass transfer in solvent/bitumen systems.
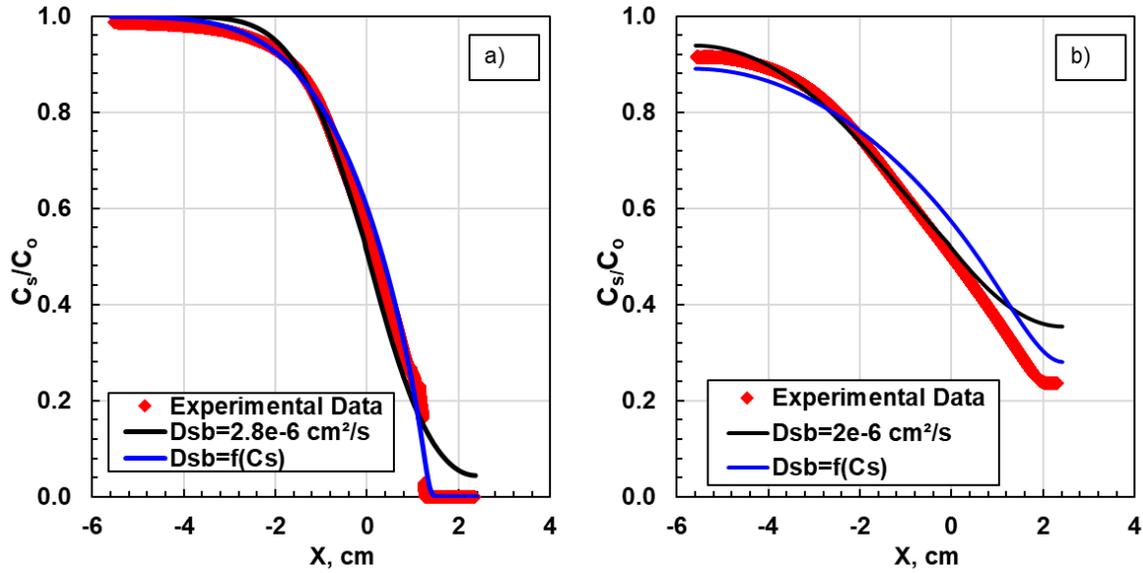
Figure 5.10. Concentration profile for toluene/bitumen system (28g of bitumen and 56g of toluene at ambient conditions) modeled with constant diffusivity and a viscosity dependent diffusivity (Eq 5.4) at diffusion times of: a) 3 days; b) 15 days.

Correlations for Variable Diffusivity

Since there is not a clear relationship between concentration and diffusivity (Poling *et al*., 2001) the performance of four concentration dependent diffusivity models was tested. The correlations were listed in Chapter 4 and are repeated here for the reader's convenience:

Linear $$D_{sb} = (D_{sb}^{\infty}x_b + D_{bs}^{\infty}x_s)\alpha \qquad \textbf{(5.1)}$$

Vignes (1966) $$D_{sb} = (D_{sb}^{\infty})^{x_b}(D_{bs}^{\infty})^{x_s}\alpha \qquad (5.2)$$

Leffler (1970) $$D_{sb}\mu_{mix} = (D_{sb}^{\infty}\mu_b)^{x_b}(D_{bs}^{\infty}\mu_s)^{x_s}\alpha \qquad (5.3)$$

Modified Hayduk and Cheng (1971) $$D_{sb} = \frac{A_pT}{\mu_{mix}{}^n} \qquad (5.4)$$

Eqs. 5.1 to 5.3 are fitted to the experimental data using the infinite dilution diffusion coefficients (D_{sb}^{∞} and D_{bs}^{∞}) as fitting parameters, while Eq. 5.4 is fitted to the experimental data by adjusting A_p and n parameters. In this thesis, the activity coefficient (α) is assumed to be one. More details about the methodology to fit the data in each of these equations and the implications of the assumption made are presented in Chapter 4.

Figure 5.11 shows a concentration profile for the toluene/bitumen system after 5 days of diffusion time at ambient conditions. The Vignes, Leffler and Hayduk-Cheng correlations all matched the measured concentration profile but the linear model deviated at low solvent concentrations. Therefore, the linear model will not be used any further. Figure 5.12 shows the diffusivity from the Vignes, Leffler and Hayduk-Cheng correlations versus mole fraction of solvent. The concentration is presented here in terms of mole fraction to match the input of most of the correlations. All the correlations are very similar and all are below the self-diffusion coefficient of toluene. Hence, all three correlations fit the data with physically plausible diffusivity values. In this thesis, the modified Hayduk and Cheng correlation was selected because it does not require an activity coefficient and in order to be consistent with the gas-liquid diffusion model from Richardson (2017).
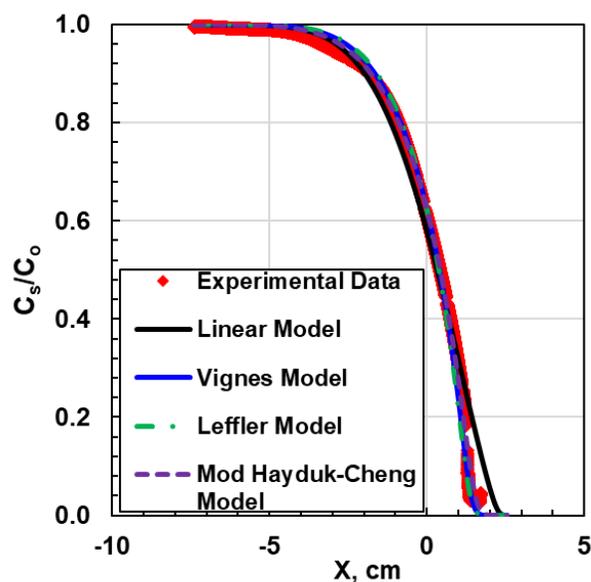
Figure 5.11. Concentration profile for a toluene/bitumen system (28 g of bitumen and 56 g of toluene at ambient conditions, 5 days of diffusion) modeled with four diffusivity correlations. The AARD was 12% for the linear model was 1% for the other models.
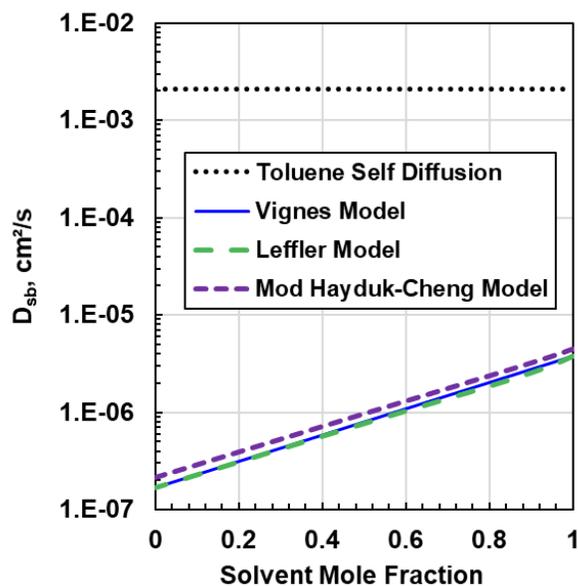
Figure 5.12. Dependence of diffusivity on solvent mole fraction for the fitted Vignes, Leffler, and modified Hayduk-Cheng variable diffusivity correlations compared with self-diffusion coefficient of toluene.

Constraining the Modified Hayduk-Cheng Correlation

One issue with the Modified Hayduk-Cheng equation is that there are multiple solutions when fitting a single concentration profile. For instance, Figure 5.13 shows several combinations of the *A* and *n* parameters that satisfactorily fit the concentration profile for the same toluene/bitumen system presented in Figure 5.11. However, each set of parameters leads to very different diffusivity profiles as shown in Figure 5.14. The diffusivity at a given solvent concentration can vary by almost an order of magnitude depending on the choice of A_p and *n*. Therefore, a method to constrain the model is required.
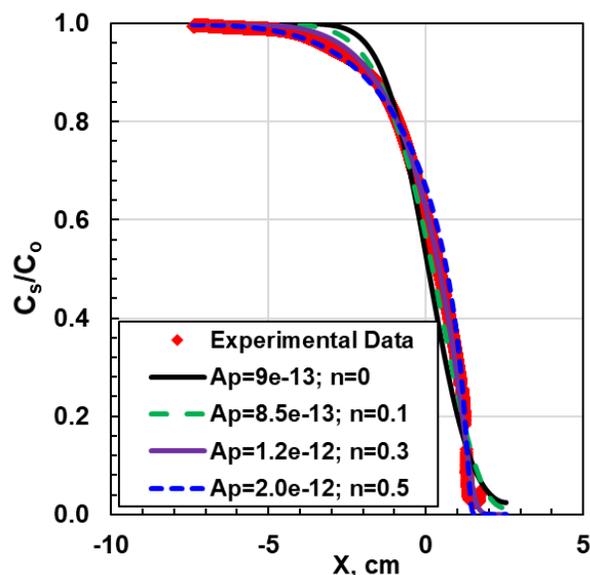
Figure 5.13. Concentration profile for a toluene/bitumen system (28 g of bitumen and 56 g of toluene at ambient conditions, 5 days of diffusion) modeled with the Modified Hayduk-Cheng equation using 4 different sets of fitting parameters. The AARD was 8, 6, 2, and 1% for n of 0, 0.1, 0.3, and 0.5, respectively.
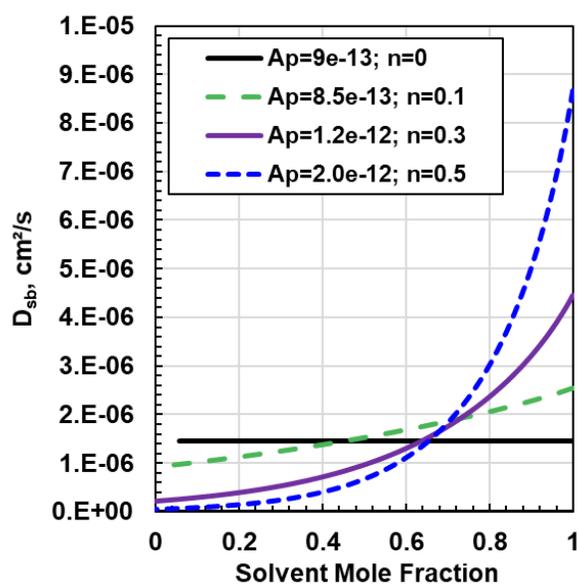
Figure 5.14. Dependence of diffusivity on solvent mole fraction dependence using different combinations of the fitting parameters for Hayduk and Cheng equation.

The correlation was constrained following the approach used by Richardson (2017) for gas-liquid diffusion. First, the parameters A and n were related to the infinite dilution diffusivities (endpoints) as follows:

$$n = \frac{\log \frac{D_{bs}^{\infty}}{D_{sb}^{\infty}}}{\log \frac{\mu_s}{\mu_b}} \tag{5.5}$$

$$A_p = \frac{D_{bs}^{\infty}}{T} {\mu_s}^n \tag{5.6}$$

where D_{bs}^{∞} is the infinite diffusivity of bitumen in a medium of almost pure solvent, D_{sb}^{∞} is the infinite dilution diffusivity of solvent in bitumen, μ_s is the viscosity of the liquid solvent, and μ_b is the viscosity of the bitumen. The values of D_{bs}^{∞} were determined from existing correlations and the values of D_{sb}^{∞} were calculated by fitting the experimental data. Then, a correlation was developed for D_{sb}^{∞}. Existing correlations were used for D_{bs}^{∞} rather than D_{sb}^{∞} because these correlations are suitable for diffusion through a low viscosity medium; that is, bitumen through solvent rather than solvent through bitumen.

Infinite Dilution Diffusivity of Bitumen in Solvent, D_{bs}^{∞}

This infinite dilution diffusivity of bitumen in solvent was calculated using the Hayduk-Minhas (1982) equation or the Wilke-Chang (1955) equation, depending on the solvent. The Hayduk-Minhas equation was developed for normal paraffinic solvents and in this thesis is used to calculate the endpoint for the *n*-alkanes/bitumen and *n*-alkanes/maltenes systems. It is given by:

$$D_{bs}^{\infty} = \frac{13.3 \cdot 10^{-8} T^{1.47} \mu_s^{\left(10.2/\check{v}_b - 0.791\right)}}{\check{v}_b^{0.71}} \tag{5.7}$$

where T is the temperature in K and $\check{v}_b$ is the molar volume of the bitumen at its normal boiling temperature in cm³/mol. The Wilke-Chang equation is used for the toluene end points because toluene was in the dataset used to develop this correlation. For unassociated solutes like toluene, it is given by:

$$D_{bs}^{\infty} = \frac{7.4 \cdot 10^{-8} \sqrt{MW_s} \, T}{\mu_s \check{v}_b^{0.6}} \tag{5.8}$$

where MW_s is the molecular weight of the solvent. In fact, both correlations give a similar value for the toluene endpoints.

Both equations require the viscosity and molecular weight of the solvent and the molar volume of the bitumen at its normal boiling point. The properties of the medium were obtained from NIST (2018) and the bitumen normal boiling point was estimated using the Soreide Correlation (Riazi 2005) given by:

$$T_b = 1071.28 - 9.417 \cdot 10^4 \ \exp[Z] \ MW_b{}^{-0.03522} SG^{3.266}$$
$$Z = -4.922 \cdot 10^{-3} WM_b - 4.7685 \ SG + 3.462 \cdot 10^{-3} WM_b SG$$

(5.19)

where T_b is the normal boiling point of the bitumen in K, MW_b is its molecular weight, and SG is its specific gravity. The calculated normal boiling point and molar volume are 519°C and 827 cm³/mol, respectively, for the WC-B-A3 bitumen and 406°C and 476 cm³/mol, respectively, for the maltenes.

Infinite Dilution Diffusivity of Solvent in Bitumen, D_{sb}^{∞}

Once the infinite dilution of bitumen endpoint was calculated, D_{sb}^{∞} was determined by fitting the numerical model to the experimental concentration profile. The infinite dilution diffusion coefficient of solvent in bitumen was manually adjusted to minimize the average ARD between the predicted and measured concentration profiles. At each iteration, new A_p and n values were calculated from Eqs. 5.5 and 5.6 and the known oil viscosity and temperature of the experiment. As discussed in Chapter 4, the model matched the concentration profiles where there was no asphaltene precipitation to within the experimental error. However, the model could not exactly match the profiles where there was precipitation, as shown in Figure 5.15. The fitted infinite dilution end points are nonetheless reported below as qualitative indicators of the mass transfer rate in these systems.
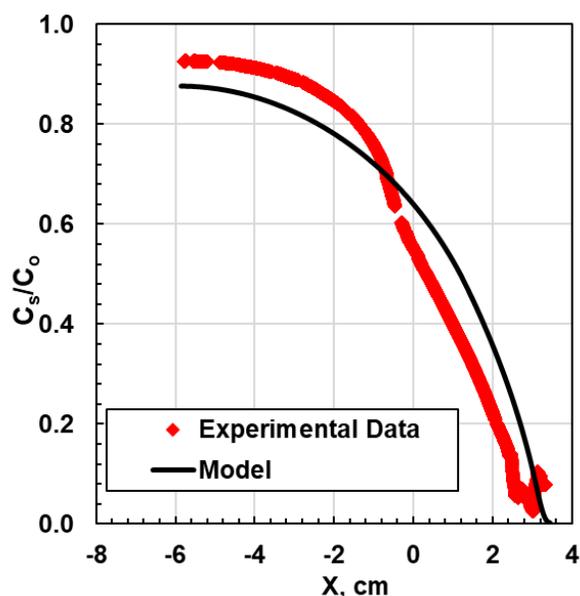
Figure 5.15. Concentration profile for a *n*-pentane/bitumen system (40g of bitumen and 40g of toluene at ambient conditions, 10 days of diffusion) modeled with the Modified Hayduk-Cheng equation. The gap in the data was caused by the removal of a density outlier.

5.3 Fitted Variable Diffusivities

Table 5.4 presents average values of the constrained A and n parameters for each of the systems studied in this thesis, and the average and maximum ARD between the modeled and measured concentration profiles. The average deviations were less than 3% and the maximum deviations were less than 8%. The error with *n*-pentane and *n*-heptane was more than double the error with toluene. For the solvent/maltene systems, the error may arise because the model did not consider the volume change of mixing. Saryazdi *et al*. (2013) calculated the excess volumes of mixing for solvent/bitumen systems at 20°C. At a solvent content of 50 wt%, the excess volume mixing of bitumen with *n*-heptane or *n*-pentane is approximately double in magnitude that with toluene (approximately $-10 \cdot 10^{-6}$ versus $+4 \cdot 10^{-6}$ cm³/g). For the solvent/bitumen systems, the error is compounded because the model did not consider the effects of asphaltene precipitation and settling. In fact, the results for the *n*-alkane/bitumen systems are used just as a qualitative indicator.

Table 5.4. Parameters of the modified Hayduk and Cheng equation fit to the measured concentration profiles for each solvent. Units are m²/s for diffusivity and mPa·s for viscosity.

Oil	Solvent	Temperature °C	A_P (x 10^{12})	n	MARD %	AARD %
Maltenes	toluene	20.0	2.36	0.42	2.10	0.40
	n-pentane	20.8	3.06	0.51	5.30	1.67
	n-heptane	19.8	2.72	0.51	4.40	1.14
Bitumen	toluene	20.3	1.80	0.31	1.70	0.39
	n-pentane	20.8	2.74	0.35	7.40	2.56
	n-heptane	20.4	2.35	0.35	6.30	1.57

Table 5.5 presents the average infinite dilution diffusivities for the systems studied in this thesis, and the 95% confidence interval of the average. Recall that the values of D_{sb}^{∞} for the n-alkane/bitumen systems are not the true molecular diffusivities but rather approximate the total effect of molecular diffusion and convection and/or mass transfer barriers caused by asphaltene precipitation and settling. Except where asphaltene precipitation occurred, the results are consistent with the physical properties of the systems as outlined below:

- The infinite dilution diffusivity of bitumen in solvent is approximately 100 times greater than the diffusivity of the infinite dilution solvent in bitumen. The high viscosity of the bitumen significantly reduces the mass transfer rate of the solvent. A consequence is that in any mass transfer process between bitumen and solvent, the movement of bitumen into the solvent is expected to dominate.

- The infinite dilution diffusivity of toluene in maltenes is approximately 20% higher than that of toluene in bitumen. The difference is to be expected behavior because the viscosity of the maltenes is approximately 35 times lower than that of the bitumen. Interestingly, the infinite dilution diffusivity of n-alkanes in bitumen is higher than in maltenes even though in most cases the concentration profiles suggested reduced mass transfer rates when asphaltenes precipitate (see Section 5.1). The end point diffusivity with the n-alkanes were likely skewed because the model could not match the concentration profiles when there was asphaltene precipitation.

- The infinite dilution diffusivity of maltenes in *n*-pentane is higher than in *n*-heptane or toluene. The viscosity of *n*-pentane is lower than that of the other two solvents and a higher mass transfer rate is expected.

- The infinite dilution diffusivity of both *n*-alkanes in maltenes is lower than that of toluene. As was discussed previously, the excess volume change of mixing in *n*-alkanes is relative large and positive (while in toluene it is relatively small and negative), indicating stronger repulsive forces with *n*-alkanes. Hence, it may be more difficult for a maltene molecule to diffuse through an alkane medium giving a lower than expected infinite dilution diffusivity.

Table 5.5. Infinite dilution diffusivity solvents in bitumen and maltenes fit to the experimental data with the modified Hayduk-Cheng equation using the infinite dilution diffusivity as the constraint.

Oil	Solvent	D_{sb}^{∞} 10^{-8} cm²/s	CI 10^{-8} cm²/s	D_{bs}^{∞} 10^{-6} cm²/s	CI 10^{-6} cm²/s
Bitumen	toluene	10.8	±0.5	6.2	±0.03
	n-pentane*	9.7	±0.5	13.1	±0.1
	n-heptane*	8.1	±0.3	8.7	±0.08
Maltenes	toluene	13.6	±1.3	8.6	±0.1
	n-pentane	7.8	±1.1	18.2	±0.08
	n-heptane	6.2	±0.2	12.0	±0.1

Figure 5.16 show the mutual diffusivity of maltenes and the three solvents calculated from Eq. 5.4 versus solvent mole fraction. The diffusivity increases significantly as the solvent content increases because the mixture viscosity decreases dramatically with increasing solvent content. The diffusivity increases from toluene to *n*-heptane to *n*-pentane because the diffusion of bitumen into the solvent is the dominant mechanism; that is, the mass transfer rate follows the trend of the D_{sb}^{∞} values. Similarly, the mutual diffusivity in maltenes in higher than in bitumen as shown in Figure 5.17.
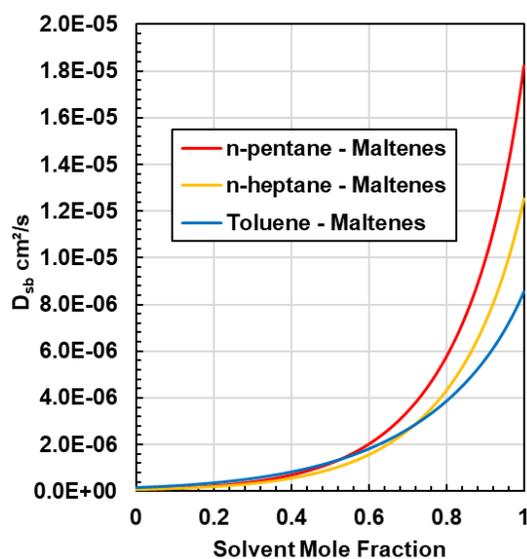
Figure 5.16. Comparison between diffusivity as function of solvent mole fraction for *n*-pentane/maltenes, *n*-heptane/maltenes, and toluene/maltenes systems.
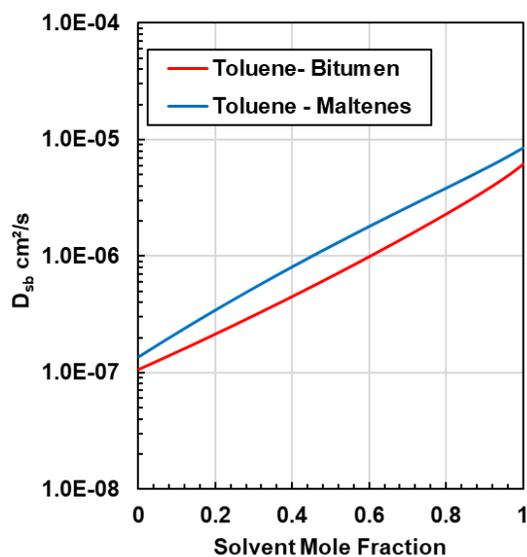
Figure 5.17. Comparison between diffusivity as function of concentration for toluene/bitumen and toluene/maltenes systems.

5.4 Comparison with Literature Data

Since the data of the diffusivities of solvent and bitumen are presented in different ways, the values of diffusivity obtained in this thesis are compared with the literature values in four distinct categories: 1) the value of the infinite dilution diffusivity of solvent in bitumen; 2) the average mutual diffusivity; 3) the mutual (solvent concentration dependent) diffusivity; 4) concentration profile modeling. The concentration in some of the plots presented here is in terms of solvent mass fraction and solvent volume fraction to match the data as it was reported in the literature.

5.4.1 Infinite Dilution Diffusivity of Solvent in Bitumen

The data points available from the literature for the infinite dilution diffusivity of solvent in bitumen are listed in the Table 5.6. To compare with the results from this thesis, the value of D_{sb}^{∞} was predicted from the bitumen viscosity and temperature of the sample reported in the literature as follows:

$$(D_{sb}^{\infty})^* = A_p \frac{T}{\mu_b^n} \tag{5.11}$$

where $(D_{sb}^{\infty})^*$ is the predicted infinite dilution diffusivity, μ_b is the viscosity of the literature sample, T is the temperature of the literature experiment, and A_p and n are the correlation coefficients previously found by fitting the data from this thesis (Table 5.4). Table 5.6 shows that the infinite dilution diffusivities predicted with Eq 5.11 are in the same order of magnitude as the reported values: absolute relative deviations of 56 and 23% for the toluene/bitumen and *n*-heptane/bitumen systems, respectively. One potential source of error is that the composition of the oils is different (for example a different asphaltenes content) but Eq. 5.11 only accounts for the effect of viscosity. For the toluene/bitumen system, the difference could also arise from the use of the Boltzmann-Transformation technique for the literature value (Oballa and Butler, 1989). This technique fails to predict diffusivities at concentration extremes (Sarafianos, 1986).

Table 5.6. Comparison of measured, D_{sb}^{∞}, and predicted, $(D_{sb}^{\infty})^*$, infinite diffusivities of solvent in bitumen. Ref. 1 is Oballa and Butler (1989) and Ref. 2 is Guerrero-Aconcha *et al*. (2008).

Solvent	Source	Oil Viscosity Pa. s	Temperature °C	D_{sb}^{∞} 10^{-8} cm²/s	$(D_{sb}^{\infty})^*$ 10^{-8} cm²/s
toluene	Ref. 1	31.1	20	50	22
***n*-heptane**	Ref. 2	6.0	24	43	33

5.4.2 Average Mutual Diffusivity for Solvent and Bitumen

Since most of the studies performed in this area have reported an average mutual diffusivity, the diffusivities obtained in this thesis were averaged to compare with the literature data. The average mutual diffusivities were calculated by dividing the entire solvent concentration range (0 to 100 wt%) into 100 points of equal mole fraction. For each point, the viscosity of the mixture was obtained with the Expanded Fluid model (Yarranton and Satyro, 2009; Motahhari *et al*., 2013a-c Ramos-Pallares *et al*., 2015, 2016a). The diffusivity was calculated from Eq.5.24 with the fluid parameters reported in Table 5.4 and the 100 diffusivity points were averaged. These average values are compared with the literature data in Table 5.6 along with the temperature and the original viscosity of the oil. The average values from this thesis are within the scatter of the literature values. Note that the diffusivities for the *n*-alkane/oil systems are larger than for the toluene/oil systems, again consistent with asphaltene precipitation enhancing the mass transfer process.

Table 5.7. Comparison between average diffusivity of solvent in bitumen estimated in this thesis and literature values.

Solvent	Source	Temperature °C	Original oil Viscosity Pa. s	$\overline{D_{sb}}$, $\times 10^6$ cm²/s
Toluene	Wen *et al*. (2004, 2005)	22	130	9.26
	Fadaei *et al*. (2013)	21	2	2.00
	Diedro *et al*. (2015)	22	55	1.71
	Diedro *et al*. (2015)	22	12000	1.85
	This Thesis	**20**	**357**	**3.02**
n-pentane	Wen *et al*. (2004, 2005)	22	130	8.89
	Salama and Kantzas (2005)	22	21.4	5.46
	Zhang and Shaw (2007)	22	18	1.70
	Diedro *et al*. (2015)	22	55	2.93
	Diedro *et al*. (2015)	22	12000	1.20
	This Thesis	**21**	**357**	**6.18**
n-heptane	Wen *et al*. (2004, 2005)	22	130	5.06
	Wen *et al*. (2004, 2005)	22	6	7.81
	Wen *et al*. (2004, 2005)	22	671	4.95
	Salama and Kantzas (2005)	22	21.4	1.58
	Zhang and Shaw (2007)	22	130	1.60
	This Thesis	**20**	**357**	**4.02**

5.4.3 Concentration Dependent Mutual Diffusivity of Solvent and Bitumen.

No literature data were found the mutual diffusivities of solvent and maltenes and therefore only *n*-alkane/bitumen and toluene/bitumen systems are discussed here.

Toluene/Bitumen Systems

Figure 5.18 shows the mutual diffusivities for toluene and heavy oil or bitumen reported in the literature. Oballa and Butler (1989) determined the mutual diffusivities using the Boltzmann-Transformation approach (Eq. 2.30) and found a maximum at volume concentrations of bitumen of approximately 50%. Fadaei *et al*. (2013) used a special solution of the continuity equation for systems with variable density and also found a maximum. Diedro *et al*. (2015) used the slope and intercept technique (Eqs. 2.45 to 2.47) and reported a monotonic increase in the diffusivity with toluene concentration. Fayazi *et al.* (2017) also used the slope and intercept method but again observed a maximum in the concentration dependence. Finally, Babak *et al.*, (2018) reevaluated

the data reported by Diedro *et al*. (2015) for toluene/Peace River bitumen with a modified slope and intercept method and found a monotonic increase in diffusivity with all data below the self-diffusion coefficient of toluene. Although most of the studies reported a maximum in the mutual diffusivity, there is no physical reason to expect one because the viscosity of the mixture increases monotonically with increasing toluene concentration. It is likely that analysis methods such as the Boltzmann-Transformation create an artificial maximum in systems with a highly concentration dependent diffusivity.

Figures 5.18 also compares the mutual diffusivities from this thesis with the literature data and with the self-diffusion coefficient of toluene reported by Reimschussel and Hawlicka (1977) at 20°C. The mutual diffusivity must be less than the self-diffusion coefficient of toluene because bitumen consists of larger molecules than toluene and is more viscous. All of the data except for the high toluene concentration data from Diedro *et al*. (2015) meet this criterion. All of the data are in good agreement (generally within the expected error of ±15%) at toluene contents up to approximately 50 vol%. At higher toluene contents, only the data from this thesis and the data reported by Babak *et al*, (2018) do not show maximum and remain below the toluene self-diffusion coefficient.
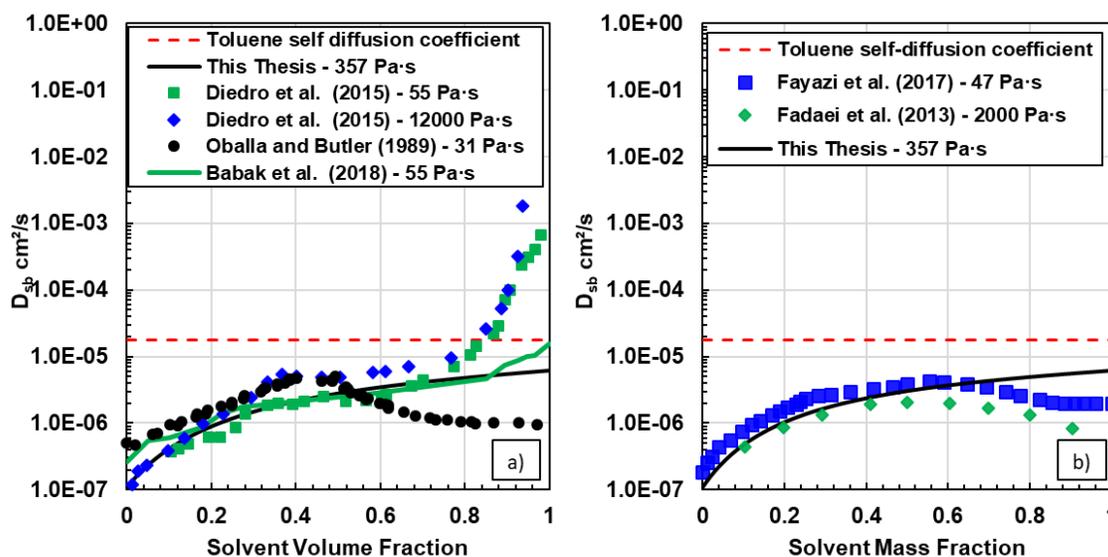
Figure 5.18. Comparison of the concentration dependent mutual diffusion of toluene and bitumen from this thesis with the self-diffusion coefficient of toluene and literature mutual diffusivities

reported by: a) Oballa and Butler (1989), Diedro *et al*. (2015) and Babak et al, (2018) ; b) Fadaei *et al*. (2013) and Fayazi *et al*. (2017). The viscosities refer to the original oil viscosities

n-Heptane/Bitumen Systems

Figure 5.19 shows the mutual diffusivities for *n*-heptane and heavy oil or bitumen reported in the literature. Wen and Kantzas (2005) used the Boltzmann-Transformation approach to determine the mutual diffusivity of n-heptane and Peace River bitumen. This method shows a maximum in the mutual diffusivity. Luo *et al*. (2007) used a modified Boltzmann-Transformation technique which accounted for the volume change of mixing to determine the mutual diffusivity of *n*-heptane and a heavy oil. Their analysis shows a monotonic increase in the diffusivity with increasing *n*-heptane concentration. Guerrero-Aconcha *et al*. (2008) used slope and intercept technique for another *n*-heptane and a heavy oil system and also reported a monotonic increase in the mutual diffusivity.

Figure 5.19 also compares the mutual diffusivities from this thesis with the literature data. All of the data from the literature and the thesis are below the *n*-heptane self-diffusion coefficient reported by Geet and Adamson, (1965) at 20°C. The diffusivities from this thesis are in good agreement (generally with the expected error of ±15%) with the data reported by Luo et al. (2007) and Guerrero-Aconcha et al. (2008) at solvent contents above 30 vol%. It is possible that the data at lower solvent contents are affected by asphaltene settling. The oil used by Luo *et al*. (2007) and Guerrero-Aconcha *et al*. (2008) are much less viscous that the bitumen used in this thesis. Therefore, the precipitated asphaltenes can settle more easily, enhancing the mass transfer process and making the apparent diffusivity larger.
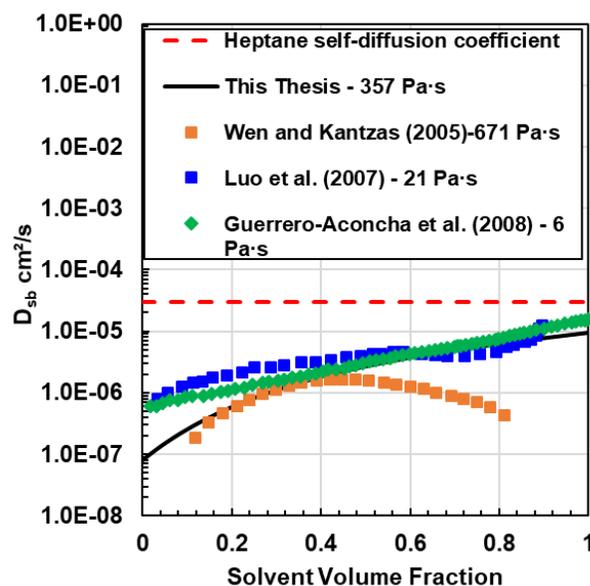
Figure 5.19. Comparison of the concentration dependent mutual diffusion of *n*-heptane and bitumen from this thesis with the self-diffusion coefficient of *n*-heptane and literature mutual diffusivities reported by Wen and Kantzas (2005), Luo *et al*. (2007) and Guerrero-Aconcha *et al*. (2008). The viscosities refer to the original oil viscosities.

n-Pentane/Bitumen Systems

Figure 5.20 shows the mutual diffusivities for *n*-pentane and heavy oil or bitumen reported in the literature. Salama and Kantzas (2005) used the Boltzmann-Transformation approach to determine the mutual diffusivities for *n*-pentane in a heavy oil. Their diffusivity profiles exhibited a small local maximum. Sadighian *et al.* (2011) evaluated the mutual diffusivity of *n*-pentane and two different oils. They reported the diffusivity as a monotonically increasing quadratic function of the *n*-pentane content. Diedro *et al*. (2015) determined the mutual diffusivity of n-pentane and a heavy oil two different viscosities using the slope and intercept method. Their diffusivity profiles were irregular and exhibited a local maximum.

Figure 5.20 also compares the mutual diffusivities from this thesis with the literature data. All of the data from the literature and the thesis are below the *n*-pentane self-diffusion coefficient reported by Geet and Adamson, (1965) at 20°C except for the high *n*-pentane concentration data from Diedro *et al*. (2015). The data from Diedro *et al*. (and likely all of the data for *n*-pentane and

heavy oil) are almost certainly affected by asphaltene precipitation. Nonetheless, the mutual diffusivities from this thesis are in qualitative agreement with the literature data. The biggest difference occurs at *n*-pentane contents below 20 vol%. This difference is again attributed to more rapid asphaltene settling in the less viscous oils used in the studies from the literature.
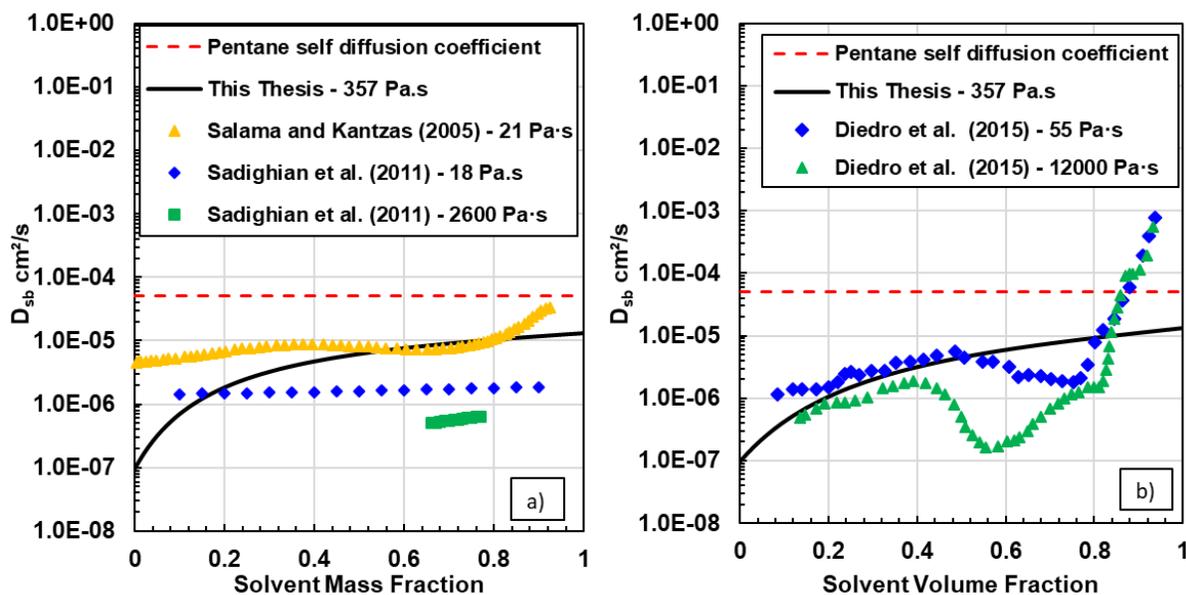
Figure 5.20. Comparison of the concentration dependent mutual diffusion of *n*-pentane and bitumen from this thesis with the self-diffusion coefficient of *n*-pentane and literature mutual diffusivities reported by: a) Salama and Kantzas (2005) and Sadighian *et al.* (2011); b) Diedro et al. (2015). The viscosities refer to the original oil viscosities.

5.4.4 Modeled Concentration Profiles

Three density profiles for liquid-liquid diffusion of toluene and Peace River bitumen were obtained at 22°C and atmospheric pressure (Kantzas, 2018). Details of the measurement method and oil properties are provided elsewhere (Diedro *et al.*, 2015). This bitumen had a viscosity of 55,000 mPa·s compared with a viscosity of 357,000 mPa·s for the bitumen used in this thesis. The profiles were first fitted with the model to test the ability of the model to match measured concentration profiles. They were then predicted to evaluate the consistency of the model when applied to other oils.

Figure 5.21 shows the density profiles fitted with the numerical model. The infinite dilution diffusivity of the Peace River bitumen in toluene was calculated from Eq. 5.8 and was $5.66 \cdot 10^{-6}$ cm²/s. The infinite dilution diffusivity of toluene in bitumen was fitted and found to be $1.68 \cdot 10^{-7}$ cm²/s. The constrained A_p and n parameters were $1.63 \cdot 10^{-12}$ and 0.307, respectively. The maximum ARD and the average ARD between the fitted and experimental density profiles were 1.5% and 0.5%, respectively.

The profiles were then predicted using the A and n parameters determined in this thesis ($1.80 \cdot 10^{-12}$ and 0.307, respectively from Table 5.4). The infinite dilution diffusivity of toluene in the Peace River bitumen was calculated as described above. The infinite dilution diffusivity of toluene in bitumen was calculated from Eqs. 5.11 and was $1.86 \cdot 10^{-7}$ cm²/s; that is, 10% higher than the fitted value. Figure 5.21b compares the measured and predicted density profiles. The predicted density profiles are slightly less accurate than the fitted profiles with a maximum and average ARD of 2% and of 0.7%, respectively. Hence, the model with the A and n parameters used in this thesis can be used to predict the concentration profiles for solvent diffusion in other bitumens with relatively little error.
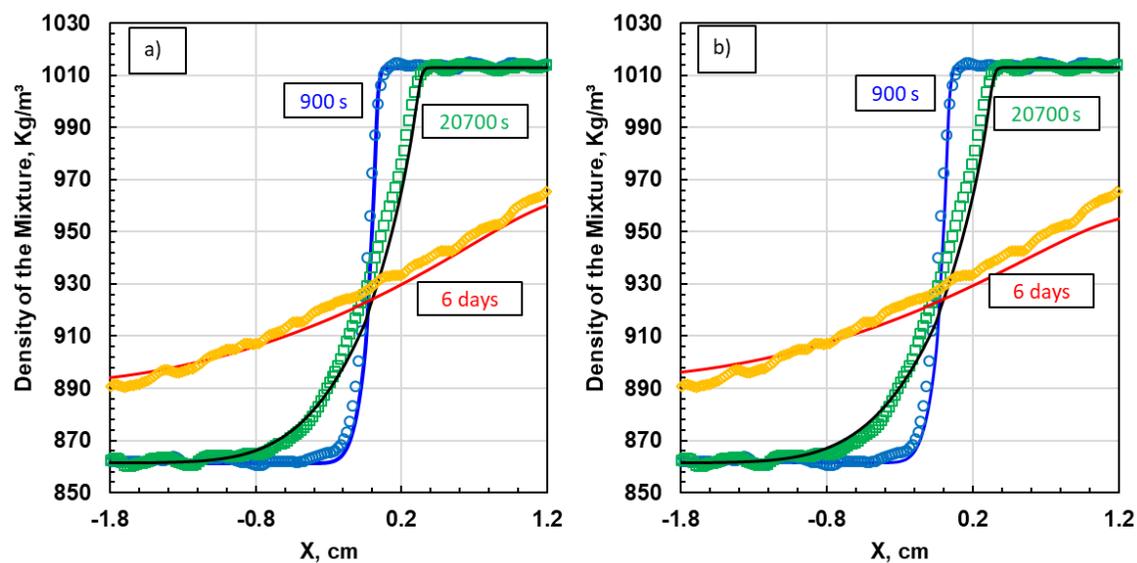
Figure 5.21. Measured and modeled density profiles for diffusion in a toluene/Peace River bitumen system at 22°C and atmospheric pressure at 3 different diffusion times: a) fitted profiles; b) predicted profiles. Symbols are measured data and lines are the model fits or predictions.

CHAPTER 6: RESULTS AND DISCUSSION: GAS-LIQUID DIFFUSION

Once a gas molecule enters a liquid medium, it becomes part of a liquid phase and is expected to diffuse through the media just as if it had entered from a liquid phase. Therefore, the diffusivity determined from gas-liquid experiments should be equivalent to the diffusivity determined from liquid-liquid experiments if all other factors were equal. To confirm this deduction, pressure decay (gas-liquid diffusion) experiments were performed for toluene, *n*-pentane, and *n*-heptane gas phases over bitumen or maltenes. First, constant "average" diffusivities were determined from the measured mass transferred over time using the methodology proposed by Richardson (2017) and presented in Chapter 4. These diffusivities were used to compare with data from the literature. Then, the mass transfer data were fitted with a viscosity dependent diffusivity correlation to obtain the infinite dilution diffusivity of solvent in bitumen for the gas-liquid experiments. The infinite dilution diffusivities were compared with those obtained from the liquid-liquid diffusion experiments.

6.1 Constant Diffusivity from Pressure Decay Measurements

Table 6.1 provides the constant diffusivities determined from the pressure decay data for toluene, *n*-pentene, and *n*-heptane in bitumen and maltenes. The solubilities determined from the end point of the pressure decay experiments are also provided in Table 6.1 but are not discussed further. The constant diffusivity represents an "average" diffusivity from the initial to the final conditions of the experiment. A constant value of diffusivity is sufficient to represent the mass transfer process for gas-liquid systems because the solubility of the hydrocarbon gases in bitumen are low (less than 20%, Richardson *et al.*, 2018a-b)**.** As observed for liquid-liquid systems, the diffusivity of gaseous toluene in maltenes is slightly higher than in bitumen at the same conditions due to the differences in their viscosity. The diffusivity of the gaseous *n*-alkanes in maltenes is also higher than in bitumen for the same reason. Unlike the liquid *n*-alkane/bitumen systems, the physically expected trend was observed because the gas-liquid diffusion experiments were conducted below the onset of asphaltene precipitation and therefore were unaffected by precipitation. The error of the measured diffusivities with pressure decay experiment is ±15% Richardson *et al.* (2018a-b)**.**

Table 6.1. Diffusivity of toluene, n-pentane, and n-heptane gas in WC-B-A3 bitumen and maltenes.

Oil	Solvent	Temperature ^{o}C	Saturation Pressure kPa	Solubility wt%	Viscosity mPa.s	Diffusivity 10^{-9} m^2/s
	toluene	180	206	10.6	12.5	4.5
	toluene	153	141	8.43	24.4	3.2
Bitumen	*n*-pentane	153	898	14.3	24.7	2.9
	n-heptane	153	207	7.58	24.3	3.5
	n-heptane	148	231	6.14	27.3	3.0
	toluene	153	161	9.31	10.8	4.6
Maltenes	*n*-pentane	153	982	17.4	11.0	4.3
	n-heptane	153	242	11.8	10.9	4.5

6.1.1 Comparison with Literature Data

No data were found in the literature for gas diffusion of toluene, *n*-pentene and *n*-heptane in bitumen. Therefore, to evaluate the reliability of the gas/bitumen diffusivities obtained in this thesis, the constant diffusivities from Table 6.1 were compared with the constant diffusivity data reported by Richardson *et al.* (2018a-b) for ethane, propane, and *n*-butane in bitumen. Richardson found the following relationship for constant diffusivity of *n*-alkanes in bitumen:

$$\frac{D_{sb}}{T} = \frac{A_p}{\mu_b^{0.36}} \exp(B_p P_N) \tag{6.1}$$

where P_N is the ratio of the pressure to the vapor pressure of the solvent at the system temperature, A_p and B_p are parameters that depend on the molecular weight of the solvent. Richardson *et al.* (2018a-b) reported that the correlation matched their own data with a maximum average relative deviation (MARD) of 50% and literature data with a MARD of 110%. Eq. 6.1 predicted the constant diffusivity measured in this thesis with a MARD of 66% for toluene/bitumen or maltenes systems and 50% for *n*-alkanes/bitumen or maltenes. The slightly higher deviation in toluene systems may occur because Eq. 6.1 was developed for *n*-alkanes. Since the MARD are within the expected range, it is concluded that the measurements in this thesis are consistent with Richardson's measurements.

6.1.2 Comparison of Gas-Liquid and Liquid-Liquid Diffusivity

Although a constant diffusivity does not accurately represent liquid-liquid diffusion, the constant gas-liquid diffusivities from Table 6.1 were compared with the average liquid-liquid diffusivities from Table 5.6 as a qualitative consistency check. Figure 6.1a plots the gas-liquid and liquid-liquid diffusivities versus viscosity for toluene/bitumen and toluene/maltenes systems. The data follow a consistent trend; however, there are too few data points at intermediate viscosities to draw a firm conclusion. The average absolute relative deviation (AARD) and MARD from the linear trend (solid line) are 16% and 38%, respectively. Figure 6.1b shows the same comparison for n-alkanes in bitumen and maltenes and a similar but more scattered trend is observed. In this case the AARD is 17%, and the MARD is 62%. It is likely that asphaltene precipitation and settling in the liquid n-alkane-bitumen systems contributes to the scatter.
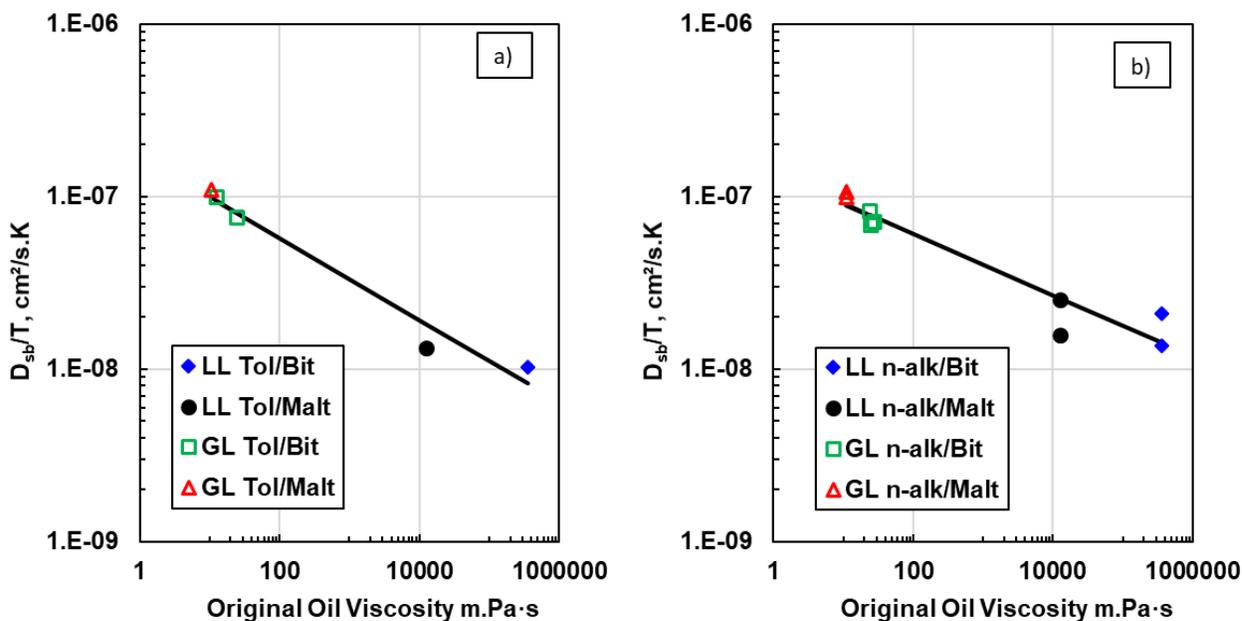
Figure 6.1. Comparison between gas-liquid and liquid-liquid average diffusivity for: a) toluene/bitumen and toluene/maltenes systems; b) n-heptane/bitumen and n-heptane/maltenes systems. GL and LL indicate gas-liquid and liquid-liquid, respectively.

6.2 Viscosity Dependent Diffusivity from Pressure Decay Measurements

6.2.1 Determining Viscosity Dependent Diffusivities

As discussed in Chapter 4, the pressure decay data from Richardson (2017) were previously fit with a numerical model using the Modified Hayduk and Cheng equation to represent the viscosity dependent diffusivity. As observed for the liquid-liquid systems, there were many combinations of the fitting parameters (A and n) that could fit the experimental data and a constrained solution was required. As a first pass, the infinite dilution diffusivity of bitumen in solvent, D_{bs}^{∞}, was fixed using the Wilke-Chang equation for toluene/oil systems and the Hayduk-Minhas equation for the n-alkane/oil systems. The infinite dilution diffusivity of solvent in bitumen, D_{sb}^{∞}, was iterated to fit the data where, at each iteration, new A and n values were calculated from Eqs. 5.5 and 5.6 and the known oil viscosity and temperature of the experiment.

Figure 6.2 shows the performance of the constrained solutions for an n-pentane/bitumen system at 153°C and 898 kPa. The D_{bs}^{∞} values were constrained below a maximum D_{sb}^{∞} set equal to D_{bs}^{∞}; D_{sb}^{∞} must be lower than D_{bs}^{∞} because bitumen diffuses faster in the solvent than the solvent does in bitumen. Even with the maximum D_{sb}^{∞}, the model could not fit the data. The same behavior was observed for all of the systems. The only way to match the data with this model is to increase the magnitude of the infinite dilution diffusivity of bitumen in solvent. Hence, it appears that the Wilke-Chang and Hayduk-Minhas under-predict this endpoint diffusivity.

The source of error is likely the viscosity of the solvent which is an input parameter for either of the two endpoint diffusivity equations. The pure solvent is a gas at the experimental conditions but the dissolved solvent is part of a liquid. In this thesis, the density of the dissolved solvent was taken as it effective liquid density from Eq. 4.43. The viscosity was determined from the EF model (Eq. 4.53) using the effective density as an input. It appears that this method overestimates the viscosity at high temperature (>150°C) and low pressure (< 1MPa). It is possible that the effective density is too high at high temperature and low pressure (Tharanivasan, 2012) resulting in an overestimation of the viscosity.
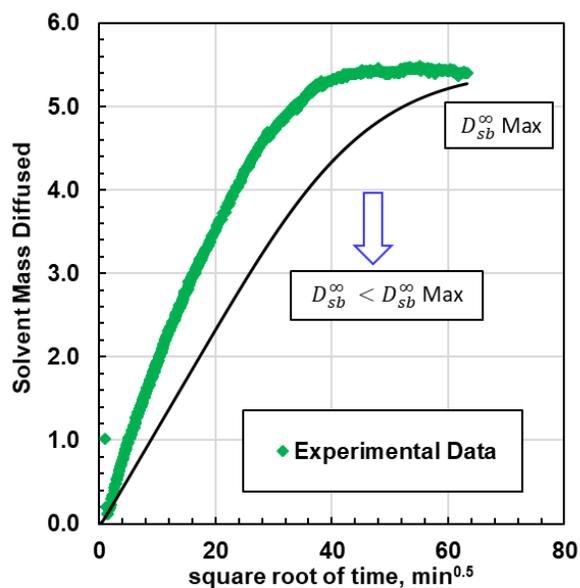
Figure 6.2. Measured and modeled mass transfer for a pressure decay experiment with n-pentane-bitumen system at 153 °C and 898 kPa. The model was constrained with the Hayduk-Minhas equation for the infinite dilution diffusivity of bitumen in solvent.

Since there was no initial known value for the infinite dilution diffusivity of bitumen in solvent, the model was instead constrained by the n parameter. The value of n for a given system was set equal the value determined with the liquid-liquid experiments for that system (Table 5.3). Then, the infinite dilution diffusivity of bitumen in solvent was adjusted to fit the mass transfer data. The A_p parameter and infinite dilution diffusivity of solvent in bitumen were calculated from Eqs. 5.5. and 5.6. Figure 6.3 shows that the model is now capable of fitting the mass transfer data from the same n-pentane-bitumen system at 153°C and 898 kPa. The solvent viscosity that corresponds to the updated D_{sb}^{∞} value is 0.039 mPa·s compared with a gas viscosity of 0.010 mPa·s and an effective density-based viscosity of 0.108 mPa·s.
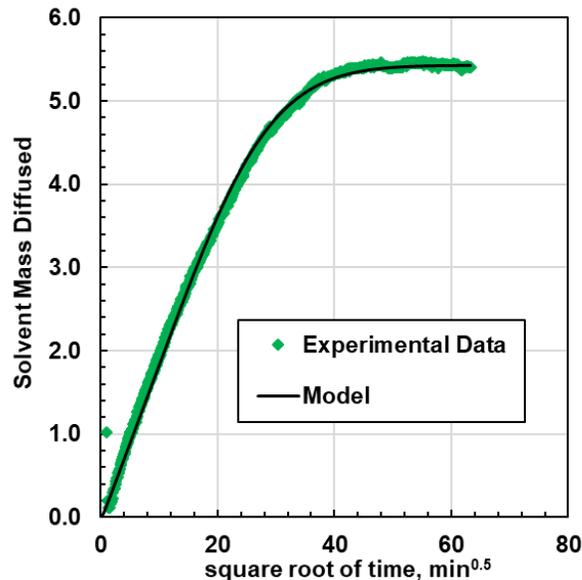
Figure 6.3. Modified Hayduk and Cheng constrained model using Hayduk-Minhas equation plus the correction factor for a gas-liquid diffusivity experiment with n-pentane-bitumen system at 153 °C and 898 kPa.

Table 6.2 provides the fitted infinite dilution diffusivities of bitumen in solvent and the calculated infinite dilution diffusivity of solvent in bitumen for all of the systems considered in this study. The fitted D_{bs}^{∞} was 2.5 to 5 times larger than the value from the original correlations. The fitted D_{bs}^{∞} and D_{sb}^{∞} were both higher in the lower viscosity medium (maltenes versus bitumen) at the same conditions. Recall that the opposite trend was observed for liquid-liquid systems likely because the measurements were affected by asphaltenes precipitation and settling which was not accounted for in the model. There was no asphaltenes precipitation in the gas-liquid systems. The variation of the endpoints for each system were within the experimental error of 15%. Nonetheless, the D_{sb}^{∞} with *n*-pentane was slightly lower than with *n*-heptane and toluene, suggesting that diffusion is slower with the less compatible solvent.

Table 6.2. Infinite dilution diffusivity gaseous solvents in bitumen and maltenes fit to the experimental data with the modified Hayduk-Cheng using the infinite dilution diffusivity with the correction factor as the constraint.

Oil	Solvent	Temperature °C	Pressure kPa	Viscosity mPa.s	D_{BS}^{∞} 10^{-8} m²/s	D_{SB}^{∞} 10^{-9} m²/s
Bitumen	toluene	180	206	12.5	1.4	3.6
	toluene	153	141	24.4	1.1	2.5
	n-pentane	153	898	24.7	1.1	1.9
	n-heptane	153	207	24.3	1.5	2.9
	n-heptane	148	231	27.3	1.5	2.7
Maltenes	toluene	153	161	10.8	2.0	4.7
	n-pentane	153	982	11.0	2.2	3.4
	n-heptane	153	242	10.9	2.5	4.4

6.2.2 Comparison with Literature

As it was mentioned before, no data was found in the literature for the diffusion of gaseous toluene, *n*-pentene, and *n*-heptane in bitumen. Therefore, the infinite dilution diffusivity of solvent in bitumen from this thesis were compared with the values reported for by Richardson (2017) for methane, ethane, propane and *n*-butane in bitumen. Since the measurements in this study were not performed with the same solvents and the same conditions as Richardson (2017), the datasets could not be compared directly. Instead, the data sets were plotted versus the initial oil viscosity to qualitatively assess their consistency. The infinite dilution diffusivity is expected to follow a power law relationship to the viscosity of the medium, in this case, the viscosity of the bitumen (Richardson *et al.*, 2018a-b). Figure 6.4 shows that the D_{sb}^{∞}/T from this thesis and from Richardson do follow an approximately power law relationship to μ_b. Hence, the data from the two sources are consistent with each other. The average absolute relative deviation (AARD) from the linear tend (solid line) for both data sets is 33% while, AARD for the data collected in this study is 14%.
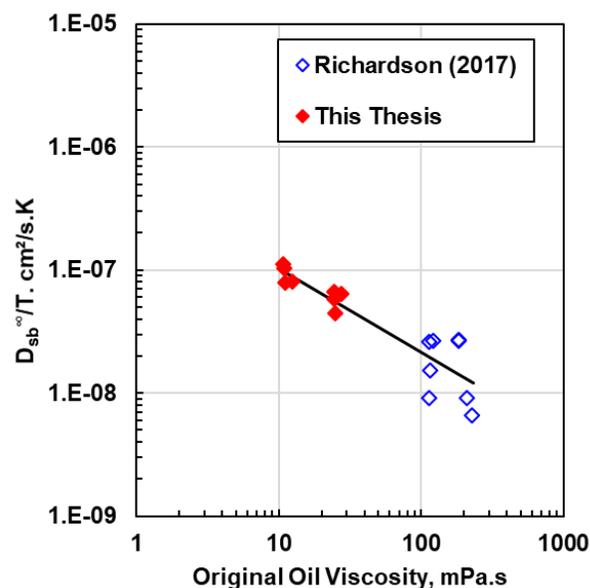
Figure 6.4. Comparison of the solvent infinite dilution diffusion diffusivity in bitumen/maltenes obtained in this thesis for gas-liquid diffusion with the data reported by Richardson (2017).

6.2.3 Comparison of Gas-Liquid and Liquid-Liquid Infinite Dilution Diffusivity of Solvent in Bitumen

Figure 6.5 compares the gas-liquid and liquid-liquid infinite dilution diffusivities (D_{sb}^{∞}) of toluene and n-alkanes in bitumen. The data are from this thesis plus the data point determined from the concentration profiles provided by Kantzas (2018). The liquid-liquid results for the n-alkane/bitumen systems are included only for a qualitative comparison but are not included in error estimates or correlation development. All of the data follow a power law relationship with the bitumen viscosity. The AARD and MARD from the linear trend (solid line) are 16 and 44%, respectively. Hence, D_{sb}^{∞} is consistent for at least two bitumens and is insensitive to the type of solvent at least within the range of solvents tested in this work.

Figure 6.6 compares the gas-liquid and liquid-liquid diffusivities infinite dilution diffusivities of solvent in oil for the solvent/bitumen and solvent/maltene systems. While the D_{sb}^{∞} for each system appear to follow a power law relationship to viscosity, the relationship is different for each oil. Hence, while D_{sb}^{∞} depends mainly on viscosity it also depends on the composition of the oil.
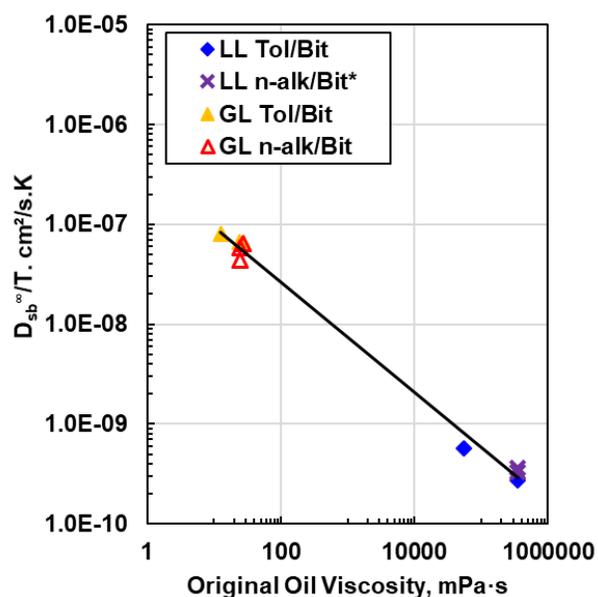
Figure2 6.5. Comparison between gas-liquid and liquid-liquid infinite dilution diffusivity of solvent in bitumen, $D_{sb}{}^{\infty}$, for toluene/bitumen and *n*-alkane/bitumen systems. GL and LL indicate gas-liquid and liquid-liquid, respectively. *LL n-*alk/bitumen systems are used only as a qualitative indicator.
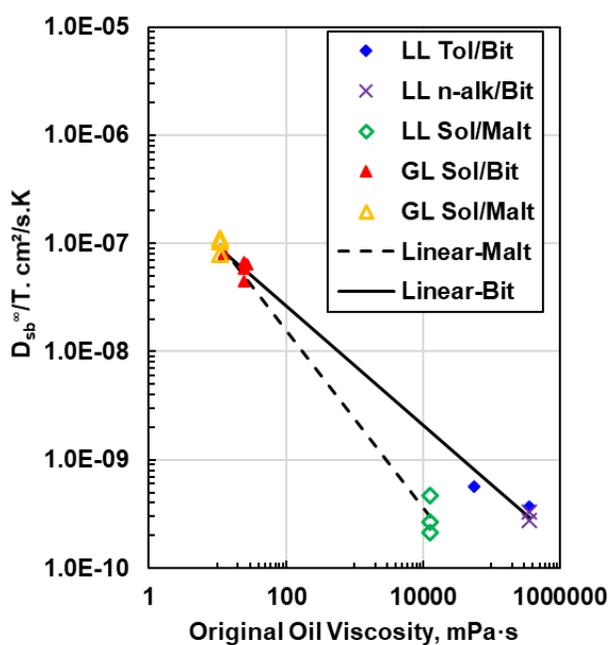
Figure 6.6. Comparison between gas-liquid and liquid-liquid infinite dilution diffusivity of solvent in bitumen, $D_{sb}{}^{\infty}$, for solvent/bitumen and solvent/maltene systems. GL and LL indicate gas-liquid and liquid-liquid, respectively. *LL n-*alk/bitumen systems are used only as a qualitative indicator.

6.3 Developing a Correlation for Infinite Dilution Diffusivity of Solvent in Bitumen

Figure 6.7 shows all the data points D_{sb}^{∞} for gaseous solvent in bitumen reported by Richardson *et al*. (2018a-b), the D_{sb}^{∞} points obtained in this thesis from gas-bitumen and liquid solvent-bitumen experiments (plus the data point determined from the concentration profiles provided by Kantzas (2018)). Since the data points of liquid-liquid for the *n*-alkane/bitumen systems are a qualitative indicator they are shown but excluded from this analysis. All of the data follow a power law relationship with the bitumen viscosity (dotted line), suggesting that the diffusivity determined from gas-liquid experiments is equivalent to the diffusivity determined from liquid-liquid experiments. Additionally, it seems that relationship between D_{sb}^{∞} and viscosity is consistent for at least three bitumens and is insensitive to the type of solvent at least within the range of solvents tested in Richardson et al. (2018a-b) and this work.

Richardson *et al.* (2018a-b) developed a correlation for infinite dilution diffusivity of solvent in bitumen base on the data obtained from gas-liquid diffusivity of methane, ethane, propane, and *n*-butane in Athabasca bitumen. Their correlation is given by:

$$\frac{D_{sb}^{\infty}}{T} = \frac{A^{\infty}}{\mu_b^{0.39}} \tag{6.2}$$

where A^{∞} is a $16.7 \cdot 10^{-12}$ (m²/sK)(mPa·s)$^{0.39}$ for methane and $8.40 \cdot 10^{-12}$ (m²/sK)(mPa·s)$^{0.39}$ for higher carbon number *n*-alkanes. Figure 6.7 also shows the predictions from Eq. 6.2 (solid line). The error for each system is reported in Table 6.3. Eq. 6.2 matched the Richardson *et al.* (2018a-b) data with an AARD of 20%. However, the AARD was 60% for the gas-liquid diffusivity of toluene, *n*-pentane, and *n*-heptane in bitumen, and 83% and for liquid-liquid diffusivity data of toluene/bitumen. Hence, the Richardson *et al.* (2018a-b) correlation required an update to better match the diffusivities at higher carbon number solvents.
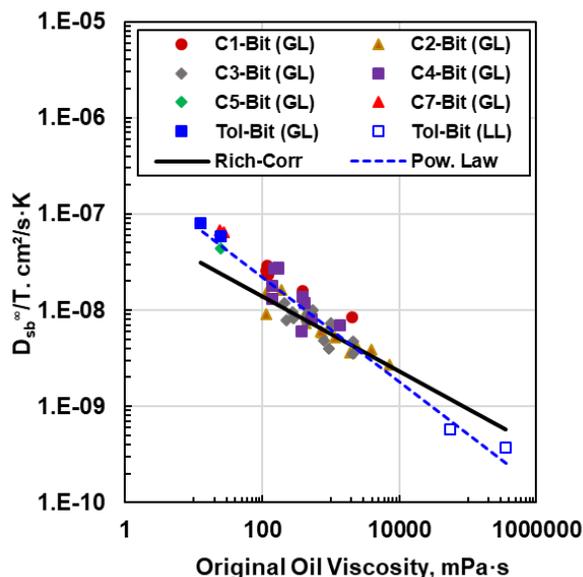
Figure 6.7. Infinite dilution diffusivity of solvent in bitumen, D_{sb}^{∞}, for toluene/bitumen and *n*-alkane/bitumen systems (this thesis) and for methane, ethane, propane, and *n*-butane (Richardson *et al*., 2018a-b). GL and LL indicate gas-liquid and liquid-liquid, respectively.

Based on a power law relationship with bitumen viscosity (dotted line in Figure 6.7), the following correlation is proposed to calculate the infinite dilution diffusivity of solvent in bitumen for solvents from methane to *n*-heptane and toluene in bitumen:

$$\frac{D_{sb}^{\infty}}{T} = \frac{2.696 \cdot 10^{-7}}{\mu_b^{0.544}} \qquad (6.3)$$

where D_{sb}^{∞} infinite dilution diffusivity of solvent in bitumen in cm²/s, μ_b is the viscosity of the oil in mPa·s, and T is the temperature in K. The AARD of this equation for each of the system are presented in Table 6.3. Eq. 6.3 considerably reduced the error for the systems studied in this thesis (40 to 80% AARD improvement); however, it slightly increased the error (10% AARD increase) for the systems studied by Richardson *et al*. (2018a-b).

Figure 6.8a shows that the developed correlation is also consistent with Cussler's (2009) observation that, in highly viscous systems such as maltenes or bitumen, the diffusion becomes nearly independent of viscosity. For instance, when the viscosity increases from 1 to 100 mPa·s,

the diffusivity decreases by almost two orders of magnitude. However, from 10^6 to 10^8 mPa·s, the diffusivity decreases only by a factor of approximately 2, Figure 6.8b.

Table 6.3. Average absolute relative deviation of Richardson *et al*. (2018a-b) and proposed new correlation for the infinite dilution diffusivity of solvent in bitumen. Data from Richardson *et al*. and this thesis.

System	Richardson *et al.* (2018a-b)	Proposed Eq. 6.3
	AARD %	**AARD %**
C1-Bit (GL)	5	29
C2-Bit (GL)	15	27
C3-Bit (GL)	18	33
C4-Bit (GL)	36	31
C5-Bit (GL)	46	6
C7-Bit (GL)	64	30
Tol-Bit (GL)	60	17
Tol-Bit (LL)	56	30
Tol-Bit (LL)*	109	25
Overall	**29**	**29**

* Kantzas (2018) data point.
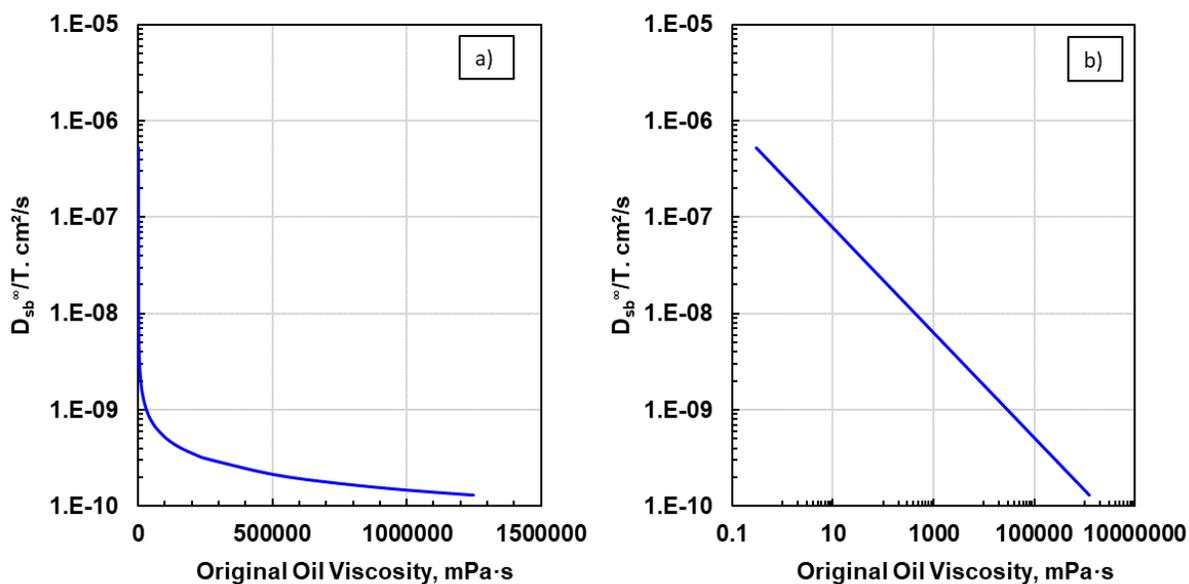
Figure 6.8. Change in the correlated infinite dilution diffusivity of solvent in bitumen with increased oil viscosity.

6.3.2 Testing the Correlation for Infinite Dilution Diffusivity of Solvent in Bitumen

Literature Data

Eq. 6.3 was used to predict the data points available from the literature for the infinite dilution diffusivity of solvent in bitumen and the comparison is shown in Table 6.4. The proposed correlation can predict the diffusivities of systems similar to those studied in this thesis with a maximum ARD of 64%.

Table 6.4. Average deviation of the correlation for the infinite dilution diffusivity of solvent in bitumen: literature data. Ref. 1 is Oballa and Butler (1989) and Ref. 2 is Guerrero-Aconcha *et al.* (2008).

Solvent	Source	Oil Viscosity Pa. s	Temp. °C	Reported D_{sb}^{∞} 10^{-8} cm²/s	Correlated D_{sb}^{∞} 10^{-8} cm²/s	ARD %
toluene	Ref. 1	31.1	20	50	28	43
n-heptane	Ref. 2	6.0	24	43	70	64

n-Alkanes/Bitumen from this Thesis

Table 6.5 shows that Eq. 6.3 predicted the infinite dilution diffusivities of liquid *n*-heptane and *n*-pentane in bitumen from this thesis with a maximum ARD of 22%. Recall that these data points were not used to develop the correlation because they were affected by asphaltene precipitation and settling. It appears that the effect of asphaltene precipitation was modest and that Eq 6.3 applies to these systems as well as it does to the systems without precipitation.

Table 6.5. Average deviation of the correlation for the infinite dilution diffusivity of solvent in bitumen: *n*-heptane/bitumen and *n*-pentane/bitumen systems.

Solvent	Oil Viscosity Pa. s	Temperature °C	Fitted D_{sb}^{∞} 10^{-8} cm²/s	Correlated D_{sb}^{∞} 10^{-8} cm²/s	ARD %
n-pentane	357	20	9.7	7.6	22
n-heptane	357	21	8.1	7.5	7

n-Alkanes/Maltenes from this Thesis

Eq. 6.3 was also compared with the fitted infinite dilution diffusivities from this thesis for of *n*-heptane, *n*-pentane, and toluene in maltenes at 20°C (liquid-liquid) and 153°C (gas-liquid) plus those of methane in maltenes reported by Richardson *et al.* (2018a-b). Table 6.6 shows that the equation predicted the infinite dilution diffusivity of gaseous *n*-heptane, *n*-pentane, and toluene in maltenes with a maximum ARD of 34%. The error for methane/maltenes systems increased to a maximum ARD of 69%. However, for liquid *n*-heptane, *n*-pentane, and toluene in maltenes the maximum ARD was 650%. The errors indicate that a correlation to viscosity alone does not fully account for the differences in the oil composition. In fact, the infinite dilution diffusivities of solvents in maltenes follow a different power law relationship to viscosity than in bitumen. Hence, an additional parameter related to the oil composition would be required for a more accurate correlation.

Table 6.6. Average deviation of the correlation for the infinite dilution diffusivity of solvent in bitumen: *n*-heptane, *n*-pentane, and toluene in maltenes.

System	Fitted D_{sb}^{∞} 10^{-8} cm²/s	Correlated D_{sb}^{∞} 10^{-8} cm²/s	ARD %
Malt-C1 (GL)	318	100	69
Malt-C5 (GL)	3388	3113	8
Malt-C7 (GL)	4382	3127	29
Malt-Tol (GL)	4759	3154	34
Malt-C5 (LL)	7.8	46.4	496
Malt-C7 (LL)	6.2	46.2	650
Malt-Tol (LL)	13.6	46.3	240
Overall			185

Since data were lacking to develop a complete correlation, a separate correlation was developed for the maltene systems. Figure 6.9 shows the available data for the infinite dilution diffusivity of solvents in maltenes. There are just nine data points and they are at very different experimental

conditions (solvents, oils, pressure, and temperature) and are scattered. Nonetheless, the data were fitted to obtain the following preliminary correlation:

$$\frac{D_{sb}^{\infty}}{T} = \frac{1.477 \cdot 10^{-6}}{\mu_{malt}^{0.876}} \tag{6.4}$$

where D_{sb}^{∞} infinite dilution diffusivity of solvent in maltenes in cm^2/s, μ_{malt} is the viscosity of maltenes in mPa·s and T is the temperature of the system in K. Table 6.7 provides the AARD for each of the systems. The average AARD is 64% for Eq.6.4 compared to 185% for Eq 6.3.
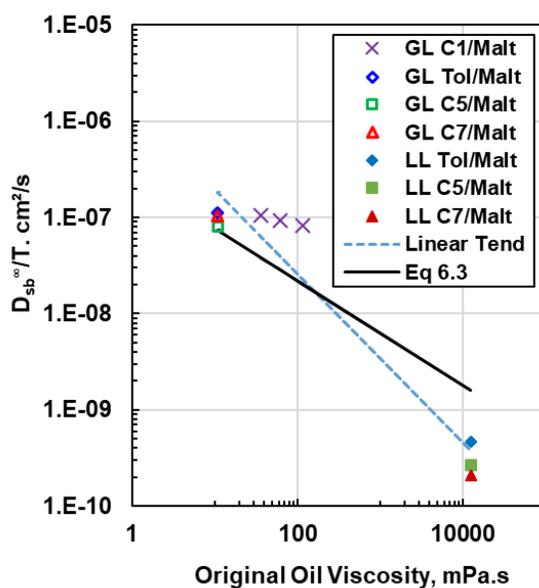
Figure 6.9. Infinite dilution diffusivity of solvent in maltenes, D_{sb}^{∞}, for toluene/maltenes and *n*-alkane/maltenes systems (this thesis) and methane/maltenes (Richardson *et al*., 2018a-b). GL and LL indicate gas-liquid and liquid-liquid, respectively.

Table 6.7. Average deviation of the correlation for the infinite dilution diffusivity of solvent in maltenes: *n*-heptane, *n*-pentane, and toluene in maltenes.

System	Fitted D_{sb}^{∞} 10^{-8} cm²/s	Correlated D_{sb}^{∞} 10^{-8} cm²/s	ARD %
Malt-C1 (GL)	318	145	56
Malt-C5 (GL)	3388	7689	127
Malt-C7 (GL)	4382	7745	77
Malt-Tol (GL)	4759	7852	65
Malt-C5 (LL)	7.8	11.0	42
Malt-C7 (LL)	6.2	11.0	78
Malt-Tol (LL)	13.6	11.0	19
Overall			**64**

Predicting Concentration Profiles

Recall that for systems with no boundary effects and with no precipitation, all of the concentration profiles fall onto a master curve. Therefore, in this section, only the concentration profiles for the shortest and the longest diffusion times for each system are examined. The shortest time corresponds to the infinite acting boundary condition and the longest time to the finite boundary conditions. The model with the proposed correlations can then be tested with both boundary conditions.

Figure 6.10 shows, as an example, the predicted concentration profiles for the toluene/bitumen system from Kantzas (2018). Table 6.8 summarizes the error of the concentration profiles predicted by the mass transfer model with Eqs 6.3 or 6.4 for this system and the data collected in the thesis. The errors are the average of the absolute deviations from each measured concentration point along the profile. The average deviations are 3% or less and the maximum deviation is 7.6%, compared to an average deviation of 2.5% and maximum deviation of 7.4% for the fitted concentration profiles. Hence, the correlations only increased the error by 0.5% over the fitted model. The relatively small errors are to be expected because the correlations were based on diffusivities determined from these concentration profiles.
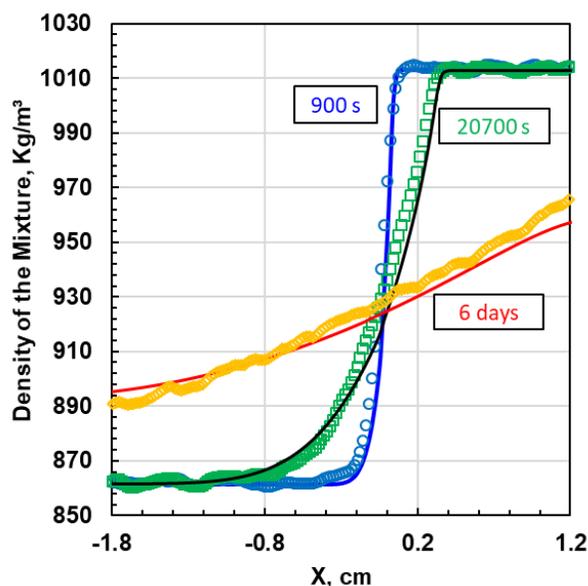
Figure 6.10. Measured and modeled density profiles for diffusion in a toluene/Peace River bitumen system at 22°C and atmospheric pressure at 3 different diffusion times. Symbols are measured data from Kantzas (2018) and lines are the correlation predictions. The oil viscosity was 55 Pa·s.

Table 6.8. Average and maximum deviation of the concentration profiles predicted by the mass transfer model with the proposed infinite dilution diffusivity correlations.

Oil	Solvent	Eq. 6.3		Eq. 6.4	
		MARD	AARD	MARD	AARD
		%	%	%	%
Maltenes	toluene	-	-	2.5	0.6
	n-pentane	-	-	6.1	2.1
	n-heptane	-	-	5.2	2.1
Bitumen	toluene	2.0	0.5	-	-
	n-pentane	7.6	3.0	-	-
	n-heptane	6.6	2.1	-	-

Figure 6.11 compares the predicted concentration profiles with the mass fraction profiles reported by Fayazi *et al.* (2017) for toluene heavy oil system at 35°C. These data were not used to develop the correlations. To avoid dividing by small numbers, the deviations were calculated based on

solvent mass fractions for $w_s > 0.5$ and on bitumen mass fractions for $w_s > 0.5$. The average and maximum ARD were 3 and 6%, respectively.
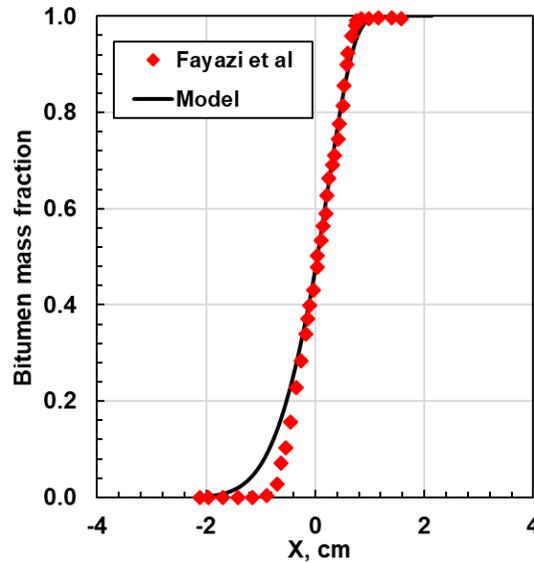
Figure 6.11. Measured and modeled density profiles for diffusion in a toluene/heavy oil system at 35°C and atmospheric pressure after 10 hr of diffusion. Symbols are measured data from Fayazi *et al.* (2017) and lines are the correlation predictions. The oil viscosity was 46.6 Pa·s.

6.4 Summary of Correlations

Since the correlations were presented piecemeal as they were developed, the final set of correlations is provided here for the reader's convenience. The viscosity dependent diffusivity is given by:

$$D_{sb} = \frac{AT}{\mu_{mix}{}^n}$$ (6.5)

where D_{sb} is the diffusivity of solvent in bitumen in cm²/s, T is the temperature in K, μ_{mix} is the viscosity of the solvent and bitumen mixture in mPa·s, and the parameters n and A are given by:

$$n = \frac{\log \frac{D_{bs}{}^\infty}{D_{sb}{}^\infty}}{\log \frac{\mu_s}{\mu_b}}$$ (6.6)

$$A = \frac{D_{sb}{}^\infty}{T} \mu_b{}^n$$

$$(6.7)$$

where μ_s is the predicted viscosity of the liquid solvent in mPa.s, μ_b is the viscosity of the bitumen, $D_{bs}{}^\infty$ and $D_{sb}{}^\infty$ are the infinite dilution diffusivities of bitumen in solvent and solvent in bitumen, respectively. Here, bitumen can also refer to maltenes.

$D_{bs}{}^\infty$ can be calculated either with Hayduk-Minhas equation, given by:

$$D_{bs}^\infty = \frac{13.3 \cdot 10^{-8} T^{1.47} \mu_s^{\left(10.2/\breve{v}_b - 0.791\right)}}{\breve{v}_b^{0.71}}$$

$$(6.8)$$

or the Wilke-Chang equation, given by:

$$D_{bs}^\infty = \frac{7.4 \cdot 10^{-8}\sqrt{MW_s}\,T}{\mu_s \breve{v}_b^{0.6}}$$

$$(6.9)$$

where T is the temperature in K and $\breve{v}_b$ is the molar volume of the bitumen at its normal boiling temperature in cm³/mol and MW_s is the molecular weight of the solvent. Eqs. 6.8 and 6.9 are not recommended for systems with n-pentane, n-heptane, or toluene at 150°C and low pressure (gas-liquid diffusivity experiments), unless an accurate estimation of the effective solvent density and viscosity are available.

$D_{sb}{}^\infty$ is given by:

$$\frac{D_{sb}^\infty}{T} = \frac{A_p^\infty}{\mu_b{}^m}$$

$$(6.10)$$

where A_p^∞ and m are constants. Recommended values for the constants are provided in Table 6.9.

Table 6.9. Recommended constants for infinite dilution diffusivity of solvent in bitumen, $\boldsymbol{D}_{sb}^\infty$. $\boldsymbol{D}_{sb}^\infty$ is in cm²/s, $\boldsymbol{\mu_b}$ in mPa·s, and T in K.

Oil	A_p^∞ (x 10^7)	m
Bitumen	2.70	0.544
Maltenes	14.8	0.876

CHAPTER SEVEN: CONCLUSIONS AND RECOMMENDATIONS

The goals of this thesis were to: 1) develop a straightforward method to experimentally determine the mass transfer rate of liquid hydrocarbons in bitumen from concentration profiles measurements, and; 2) develop a model for this mass transfer process with which to determine the mutual diffusivity. In addition, a consistent relationship was sought between diffusivity and solvent concentration (using the mixture viscosity) for both gas-liquid and liquid-liquid diffusion. This chapter lists the major contributions of this thesis and the recommendations for future work in the same area.

7.1 Contributions and Conclusions

The main contributions from this thesis are:

1. The development of a new practical and straightforward apparatus and procedure to measure concentration profiles in liquid hydrocarbon and bitumen/maltenes systems at ambient conditions.

2. The development of a one dimensional numerical model based on Fick's First Law of diffusion and a fitting procedure to determine the diffusivity from the concentration profiles measurements.

3. The measurement of concentration dependent liquid-liquid diffusivities of toluene, *n*-pentane and *n*-heptane in a Western Canadian bitumen and maltenes at ambient conditions.

4. The measurement of constant and concentration dependent gas-liquid diffusivities of toluene, *n*-pentane and *n*-heptane in a Western Canadian bitumen at 153 °C using the pressure decay technique.

5. A preliminary confirmation that the diffusivity determined from gas-liquid experiments is equivalent to the diffusivity determined from liquid-liquid experiments and that they can be correlated based on the original oil viscosity.

6. The modification of an existing correlation to predict either gas or liquid concentration dependent diffusivity of toluene, *n*-pentane and *n*-heptane in a Western Canadian and maltenes.

7. The qualitative assessment of the impact of asphaltene precipitation on the mass transfer rates.

The contributions and main conclusions from this thesis are presented in more detail below.

Liquid-Liquid Diffusivity Equipment, Method, and Numerical Model

The new apparatus consists of a cylindrical diffusion cell where a column of solvent is placed on a column of bitumen and left to diffuse for a specified time. The combined fluid column is displaced through a density meter and a concentration profile is obtained from the measured densities. The apparatus and procedure are straightforward and provide a direct measurement of the density profile.

To determine the diffusivity from a concentration profile, a one-dimensional numerical model based on Fick's First Law of diffusion was developed. The model accounted for the dependence of diffusivity on viscosity with the Hayduk and Cheng (1971) equation and the infinite dilution diffusivities of the solvent and the oil. The measured diffusivities were physically plausible; they increased as the solvent concentration increased and were below the solvent self-diffusion coefficient. In contrast, most of the literature report only a constant diffusivity or the reported data are scattered and have physically implausible trends with the solvent concentration.

Diffusivity Measurements

This thesis contributes to the data available in literature with concentration dependent diffusivities for liquid toluene, *n*-pentane and *n*-heptane in a Western Canadian and maltenes at ambient condition. In addition, to the author's knowledge, this thesis provides the only data available in the literature for the constant and concentration dependent diffusivities of toluene, *n*-pentane, and *n*-heptane gases in bitumen and maltenes at 153°C. The data were required to establish a preliminary correlation for the mutual diffusivity of liquid hydrocarbons and bitumen.

Relationship between Liquid-Liquid and Gas-Liquid Diffusivity

A common linear relationship was observed between the original oil viscosity and both the liquid-liquid and gas-liquid diffusivity. The common trend suggests that the diffusivity determined from

gas-liquid experiments is equivalent to the diffusivity determined from liquid-liquid experiments. The diffusivities are expected to be equivalent because once a gas molecule enters the liquid, it is expected to behave as a liquid.

Relationship between Diffusivity and Viscosity in Different Oils and Solvents

The relationship between diffusivity and viscosity was consistent for at least three bitumens and was insensitive to the type of solvent at least within the range of solvents tested in Richardson *et al*. (2018a-b) and this work. However, the relationship for maltene systems was different. It appears that the diffusivity also depends on the composition of the oil in way that is not completely accounted for with the oil viscosity.

Concentration Dependent Diffusivity Correlation

A correlation was developed for the gas-liquid diffusivities of *n*-alkanes from methane to *n*-heptane plus toluene in bitumen, as well as the liquid-liquid mutual diffusivities of toluene, *n*-pentane and *n*-heptane and bitumen. The correlation is a function of the mixture viscosity and the inputs are the temperature, the infinite dilution diffusivity of bitumen in solvent, and the infinite dilution diffusivity of solvent in bitumen. The infinite dilution diffusivity of bitumen in solvent is calculated either with Hayduk and Minhas (1982) or Wilke-Chang (1955) equations. The infinite dilution diffusivity of solvent in bitumen is calculated a modified Richardson, et al. (2018a-b) correlation, based on the initial oil viscosity and the temperature. The model with the proposed correlations can match the measured concentration profiles to within ±2% for bitumen and ±7% for maltenes. It predicts toluene-bitumen concentration profiles (on the same dataset) with a maximum absolute relative deviation of 3%.

Qualitatively Assessment of the Impact of Asphaltene Precipitation

A qualitative analysis was performed on the concentration profiles for all of the systems where asphaltenes precipitated. In viscous systems (average solvent content in bitumen of less than 80 wt%), asphaltene precipitation reduced the mass transfer rate. In less viscous systems (lower viscosity oil or higher average solvent content), asphaltene precipitation increased the mass transfer rate. It appears that precipitated asphaltenes form a barrier to mass transfer when there is

limited settling (low solvent content) but enhance mass transfer when there is significant settling (high solvent content). At low solvent contents, the asphaltenes are likely to accumulate somewhere between the original interface and the bottom of the cell. The accumulation could explain the reduced mass transfer observed in these systems. At high solvent contents, the precipitated asphaltenes could settle to the bottom of the column rapidly relative to diffusion. The settling could cause convection and enhance the mass transfer rate.

7.2 Recommendations

Recommendations for future studies are as follows:

1. Use the Taylor dispersion technique to measure the infinite dilution diffusivity of bitumen in toluene systems because this method is suitable for dilute conditions. The end point values can then be used to update the Hayduk and Minhas (1982) or Wilke-Chang (1955) equations for the infinite dilution diffusivity of bitumen in liquid hydrocarbons.

2. Modify the liquid-liquid apparatus developed in this thesis to measure the diffusivities of liquid hydrocarbons at higher temperatures and pressures. To make this modification, it will be necessary to be figure out how to: 1) bring the fluid in contact without causing mixing, and; 2) deal with heat loss and prevent fluid convection arising from temperature gradients.

3. Collect liquid-liquid diffusivities of liquid hydrocarbons at higher temperatures and pressures to determine diffusivities closer to reservoir conditions.

4. Include the volume change of mixing in the numerical model. To make this modification, the excess volume of mixing must be determined; for example, using the mixing rule from Saryazdi *et al*. (2013). Since the volume is fixed, the pressure (and component densities) must be iterated until the volume calculated from the known component masses and mixture density matches the fixed volume. This update will provide a more accurate relationship between the density and the solvent concentration at each point along the concentration profile for asymmetric mixtures such as hydrocarbon/bitumen mixtures.

5. Perform more liquid-liquid mass transfer experiments in systems with asphaltene precipitation to a better assess the effect of asphaltenes precipitation on the mass transfer process.

References

Afsahi, B., Kantzas, A. (2006). Advances in Diffusivity Measurement of Solvents in Oil Sands. *Petroleum Society of Canada*. Paper PETSOC-2006-130. Canadian International Petroleum Conference, Calgary, Alberta, Canada, 13-15 June 2006.

Alboudwarej, H. (2003). Asphaltene Deposition in Flowing Systems. Ph.D. Dissertation, University of Calgary.

Ahmed, T., Belova, I. V., Murch, G. E. (2015a). Finite Difference Solution of the Diffusion Equation and Calculation of the Interdiffusion Coefficient using the Sauer-Freise and Hall Methods in Binary Systems. *Procedia Engineering*, 105, 570-575.

Ahmed, T., Belova, I. V., Evteev, A. V., Levchenko, E. V., Murch, G. E. (2015b). Comparison of the Sauer-Freise and Hall Methods for Obtaining Interdiffusion Coefficients in Binary Alloys. J. *Phas. Equ. & Diff.*, 36, 366-374.

Arnold, J. H. (1930). Studies In Diffusion. Ii. A Kinetic Theory Of Diffusion In Liquid Systems. *J. Amer. Chem. Soc.*, 52, 3937-3955

Agrawal, P., Schoeggl, F.F., Satyro, M.A., Taylor, S.D., Yarranton, H.W., "Measurement and Modeling of the Phase Behavior of Solvent Diluted Bitumens" *Fluid Phase Equilibria* (334) pg. 51-64 (2012)

Bayestehparvin, B., Farouq Ali, S. M., Abedi, J. (2018). Solvent-Based and Solvent-Assisted Recovery Processes: State of the Art. *Society of Petroleum Engineers*. SPE-EOR Conference at Oil and Gas West Asia; Muscat, Oman, 21–23 March 2016.

Bayestehparvin, B., Ali, S. M. F., Abedi, J. (2017). Case Histories of Solvent Use in Thermal Recovery. *Society of Petroleum Engineers*. Western Regional Meeting; Bakersfield, California, USA, 23 April 2017.

Babak, P., Mendoza, A. M., Kantzas, A. (2018). Iterative slope and intercept method for diffusion estimation in binary liquids. *Chem. Eng. Sci.*, 181, 286-297.

Bird, R.B., Stewart, W.E., Lightfoot, E. N. (2002). *Transport Phenomena*, 2nd edition, Jon Wiley & Sons, New York, USA.

BP Statistical Review of World Energy, *(2018)*. Retrieved from: https://www.bp.com/en/global/corporate/energy-economics/statistical-review-of-world-energy.html

Casas, Y. (2017). Settling Rate of Asphaltenes and Solids from Diluted Bitumen, Master of Science thesis, University of Calgary, Calgary, Canada.

Castellanos-Diaz, O., Verlaan, M. L., Hedden, R. (2016). Solvent Enhanced Steam Drive: Results from the First Field Pilot in Canada. *Society of Petroleum Engineers*. SPE EOR Conference at Oil and Gas West Asia; Muscat, Oman, 21-23 March 2016.

Chen, S., Davis, H. T., Evans, D. F. (1981). Tracer diffusion in polyatomic liquids. II. *J. Chem. Phys.,* 75, 1422-1426.

Chen, S., Seib, B., Ben-Zvi, A., Robinson, T. (2018). Christina Lake Early Rise Rate Solvent Aided Process Pilot. *Society of Petroleum Engineers*. SPE Canada Heavy Oil Technical Conference; Calgary, Alberta, Canada, 13-14 March 2018.

Coelho, L., Oliveira, J. D., Tavares, F., Matthews, M. (2002). Role of attractive forces in self-diffusion and mutual diffusion in dense simple fluids and real substances. *Fluid Phase Equilibria*, 194-197, 1131-1140.

Crank, J. (1975). *The mathematics of Diffusion*, 2nd edition, Oxford University Press, London, Britain.

Cussler, E.L. (2009). Diffusion: *Mass Transfer in Fluid Systems*, 3rd edition, Cambridge, New York, USA.

Darken, L.S. (1948). Diffusion, Mobility and Their Interrelation Through Free Energy in Binary Metalic Systems. *Transactions of the American Institute of Mining and Metallurgical Engineers*, 175, 184-201.

Diedro, F., Bryan, J., Kryuchkov, S., Kantzas, A. (2015). Evaluation of Diffusion of Light Hydrocarbon Solvents in Bitumen. *Society of Petroleum Engineers*. SPE Canada Heavy Oil Technical Conference, Calgary, Alberta, Canada, 9-11 June 2015.

Dullien, F.A.L. 1971. Statistical Test of Vignes Correlation of Liquid-Phase Diffusion Coefficients. *Indus. Eng. Chem. Fund.,* 10,41-49.

Duran, J. (2018). Personal communication. Calgary, Alberta, Canada,

Fayazi, A., Kryuchkov, S., Kantzas, A. (2017). Evaluating Diffusivity of Toluene in Heavy Oil Using Nuclear Magnetic Resonance Imaging. *Energy & Fuels*, 31, 1226-1234.

Fadaei, H., Shaw, J. M., Sinton, D. (2013). Bitumen–Toluene Mutual Diffusion Coefficients Using Microfluidics. Energy & Fuels, 27, 2042-2048.

Fletcher, C.A.J. (1991). Computational Techniques in Fluid Dynamics: Volume 1, 2nd Ed., Springer-Verlag: Berlin, Germany.

Fu, B. Phillips, C. (1979). New Technique for Determination of Diffusivities of Volatile Hydrocarbons in Semi-Solid Bitumen, *Fuel*, 58, 557-560

Funk, E.W. (1979): Behavior of Tar Sand Bitumen with Paraffinic Solvents and its Application to Separations for Athabasca Bitumen, *Can. J. Chem. Eng.*, 57, 333-341.

Ghai, R.K., Erlt, H., Dullien, F.A.L. (1973.) Liquid Diffusion in Nonelectrolytes. AIChE Journal, 5, 881-900.

Gagliano, A. J., Lasalle, D. D., Olivo, J. A., Sabas, R. A., Ali, S. M. F. (1996). Enhanced Oil Recovery Pilot Project, Catriel Oeste Field. *Society of Petroleum Engineers*,20,82-93.

Geet, A. L., Adamson, A. W. (1965). PREDICTION OF DIFFUSION COEFFICIENTS FOR LIQUID n-ALKANE MIXTURES. *Ind. & Eng. Chem.*, 57, 62-66.

Ghanavati, M. (2013). Application of Taylor Dispersion Technique to Measure Molecular Diffusion Coefficient of Hexane-Bitumen System, Master of Science thesis, University of Calgary, Calgary, Canada.

Ghanavati, M., Hassanzadeh, H., Abedi, J. (2014). Critical review of mutual diffusion coefficient measurements for liquid solvent bitumen/heavy oil mixtures. *Cana. J. Chem. Eng.*, 92, 1455-1466.

Ghanavati, M., Hassanzadeh, H., Abedi, J. (2014a). Application of taylor dispersion technique to measure mutual diffusion coefficient in hexane bitumen system. *AIChE J.*, 60, 2670-2682.

Gray, M. R. (2015). Upgrading oilsands bitumen and heavy oil. Edmonton, Alberta, Canada: Pica Pica Press, an imprint of The University of Alberta Press.

Gupta, S. C., Gittins, S. D. (2006). Christina Lake Solvent Aided Process Pilot. *Petroleum Society of Canada*,45,15-18.

Guerrero-Aconcha, U. E., (2009). The Diffusion Coefficient of Liquid and Gaseous Solvents in Heavy Oil and Bitumen, Master of Science thesis, University of Calgary, Calgary, Canada.

Guerrero-Aconcha, U. E., Salama, D., Kantzas, A. (2008). Diffusion Coefficient of n Alkanes in Heavy Oil. *Society of Petroleum Engineers*. SPE Annual Technical Conference and Exhibition, Denver, Colorado, USA, 21-24 September 2008.

Hall, L. D. (1953). An Analytical Method of Calculating Variable Diffusion Coefficients. *J. Chem. Phys.,* 21, 87-89.

Hayduk, W., Cheng, S.C. (1971). Review of Relation Between Diffusion and Solvent Viscosity in Dilute Liquid solutions. *Chem. Eng. Sci*., 26, 635.

Hayduk, W., Minhas, B.S. (1982). Correlation for Prediction of Molecular Diffusivities in Liquids. *Can. J. Chem. Eng.*, 60, 295-299.

Johnston, K. A., Schoeggl, F. F., Satyro, M. A., Taylor, S. D., Yarranton, H. W. (2017). Phase behavior of bitumen and n-pentane. *Fluid Phase Equilibria*, *442*, 1–19.

Kantzas, A. (2018). Personal communication. Calgary, Alberta, Canada,

Leffler, J., Cullinan, H. T. (1970). Variation of Liquid Diffusion Coefficients with Composition. Dilute Ternary Systems. *Indus. Eng. Chem. Fund.,* 9, 88-93.

Lin, L., Ma, H., Zeng, F., Gu, Y. (2014). A Critical Review of the Solvent-Based Heavy Oil Recovery Methods. *Society of Petroleum Engineers*. SPE Heavy Oil Conference-Canada; Calgary, Alberta, Canada, 10-12 June 2014.

Li, J.C.M., Chang, P. (1955). Self-Diffusion Coefficient and Viscosity in Liquids. *J. Chem. Phys*., 23, 518-520.

Lundberg, J. L., Wilk, M.B., Huyett, M.J. 1963. Sorption Studies Using Automation and Computation. *Indus. Eng. Chem. Fund.*, 2, 37-43.

Luo, H., Kantzas, A. (2008). Study of Diffusivity of Hydrocarbon Solvent in Heavy Oil Saturated Sands Using X-Ray Computer Assisted Tomography. *Petroleum Society of Canada*. Canadian International Petroleum Conference, Calgary, Alberta, Canada, 17-19 June 2008.

Luo, H., Kryuchkov, S., Kantzas, A. (2007). The Effect of Volume Changes Due to Mixing on Diffusion Coefficient Determination in Heavy Oil and Hydrocarbon Solvent System. *Society of Petroleum Engineers*. SPE Annual Technical Conference and Exhibition, Anaheim, California, U.S.A.,11-14 November 2007.

Maini, B.B. (2016). Personal communication. Calgary, Alberta, Canada,

Mancilla-Polanco, A. A. (2017). The Phase Behavior of Heavy Oil and Propane Mixtures, Master of Science thesis, University of Calgary, Calgary, Canada.

McKenna, A. M., Marshall, A. G., Rodgers, R. P. (2013). Heavy petroleum composition. 4. Asphaltene compositional space. *Energy & Fuels*, 27, 1257–1267.

Motahhari, H., Satyro, M. A., Yarranton, H. W. (2011). Predicting the Viscosity of Asymmetric Hydrocarbon Mixtures with the Expanded Fluid Viscosity Correlation. *Ind. & Eng. Chem. Res.*, 50, 12831-12843

Motahhari, H., Satyro, M. A., Taylor, S. D., Yarranton, H. W. (2013a). Extension of the Expanded Fluid Viscosity Model to Characterized Oils. *Energy & Fuels*, 27, 1881-1898

Motahhari, H., Schoeggl, F., Satyro, M., Yarranton, H. (2013b). Viscosity Prediction for Solvent-Diluted Live Bitumen and Heavy Oil at Temperatures Up to 175-deg-C. *J. Can. Petr. Tech.*, 52, 376-390.

Motahhari, H., Schoeggl, F.F., Satyro, M.A., Yarranton, H.W. (2013c). The Effect of Solvents on the Viscosity of an Alberta Bitumen at In Situ Thermal Process Conditions. *Society of Petroleum Engineers*. SPE Heavy Oil Conference Canada, Calgary, Alberta, Canada, 11-13 June 2013

Motahhari, H. (2013d). Development of Viscosity Model for Petroleum Industry Applications. Ph. D. Thesis, University of Calgary, Calgary, Alberta, Canada.

Natural Resources Canada (2018). Energy Fact Book of Natural Resources Canada, *2016-2017*. Retrieved from: *https://www.nrcan.gc.ca/energy/resources/17923*

NIST. (2018). *Standard Reference Database*. Gaithersburg, MD. Retrieved from: https://webbook.nist.gov/chemistry/

Nortz, R.L., Baltus, R.E., Rahimi, P. (1990). Determination of the Macroscopic Structure of Heavy Oils by Measuring Hydrodynamic Properties, *Ind. Eng. Chem. Res.*, 29, 1968-1976.

Nourozieh, H., Kariznovi, M., Abedi, J. (2014). Pentane as a Potential Candidate for ES-SAGD and Hybrid Processes: Its Phase Behaviour with Bitumen. *Society of Petroleum Engineer*. SPE Heavy Oil Conference-Canada; Calgary, Alberta, Canada, 10-12 June 2014.

Oballa, V., Butler, R. M. (1989). An Experimental Study Of Diffusion In The Bitumen-Toluene System. *J. Can. Petr. Technol.,* 28, 62-69.

Perlau, D., Jaafar, A. E., Boone, T., Dittaro, L. M., Yerian, J. A., Dickson, J. L., Wattenbarger, C. (2013). Findings from a Solvent-Assisted SAGD Pilot At Cold Lake. *Society of Petroleum Engineer*. SPE Heavy Oil Conference-Canada, Calgary, Alberta, Canada,11-13 June 2013.

Poling, B.E., Prausnitz, J.M., O'Connell, J.P. (2001), *The Properties of Gases and Liquids*, 5th edition, McGraw-Hill, New York, USA.

Ramos-Pallares, F., Schoeggl, F. F., Taylor, S. D., Satyro, M. A., Yarranton, H. W. (2016a). Correction to Predicting the Viscosity of Hydrocarbon Mixtures and Diluted Heavy Oils Using the Expanded Fluid Model. *Energy & Fuels,* 30, 6178-6178.

Ramos-Pallares, F., Taylor, S. D., Satyro, M. A., Marriott, R. A., Yarranton, H. W. (2016b). Prediction of Viscosity for Characterized Oils and Their Fractions Using the Expanded Fluid Model. *Energy & Fuels*, 30, 7134-7157.

Ramos-Pallares, F., Schoeggl, F. F., Taylor, S. D., Satyro, M. A., & Yarranton, H. W. (2015). Predicting the Viscosity of Hydrocarbon Mixtures and Diluted Heavy Oils Using the Expanded Fluid Model. Energy & Fuels, 30, 3575-3595.

Ramos-Pallares, F. (2017). The Viscosity and Thermal Conductivity of Heavy Oils and Solvents. Ph. D. Thesis, University of Calgary, Calgary, Alberta, Canada.

Reimschüssel, W., Hawlicka, E. (1977). Self-Diffusion in Benzene-Toluene and Benzene-Cyclohexane Solutions. Berichte Der Bunsengesellschaft Für Physikalische Chemie, 81, 1221-1224.

Riazi, M.R. (1996). A New Method for experimetnal Measurment of Diffusivity Coefficients in Reservoir Fluids. *J. Petr. Sci. & Eng.*, 14, 235-250.

Richardson, W. D. (2017). Diffusivity of Light Hydrocarbon Gases in Bitumen, Ph.D. Dissertation, University of Calgary, Calgary, Canada.

Richardson, W. D., Schoeggl, F.F., Maini, B., Kantzas, A., Shawn, T., Yarranton, H., (2018a). Diffusivity of Gas into Bitumen: Part I Analysis of Pressure Decay Data with Swelling. *Society of Petroleum Engineers J.* 1-49. Paper under revision to be published.

Richardson, W. D., Schoeggl, F.F., Maini, B., Kantzas, A., Shawn, T., Yarranton, H., (2018b). Diffusivity of Gas into Bitumen: Part II Dataset and Correlation. *Society of Petroleum Engineers J.* 1-49. Paper under revision to be published.

Rodriguez-Leon, S. L. (2018). The Stability of Visbroken Heavy Oil Against Asphaltene Precipitation, Master of Science thesis, University of Calgary, Calgary, Canada.

Sadighian, A., Becerra, M., Bazyleva, A., Shaw, J. M. (2011). Forced and Diffusive Mass Transfer between Pentane and Athabasca Bitumen Fractions. *Energy & Fuels, 25*, 782-790.

Salama, D., Kantzas, A. (2005). Monitoring Of Diffusion Of Heavy Oils With Hydrocarbon Solvents In The Presence Of Sand. *Society of Petroleum Engineers*. SPE International Thermal Operations and Heavy Oil Symposium, Calgary, Alberta, Canada, 1-3 November 2005.

Sanchez-Lemus, M. C. (2015). Extended Distillation and Property Correlations for Heavy Oil. Ph.D. Dissertation, University of Calgary.

Sarafianos, N. (1986). An analytical method of calculating variable diffusion coefficients. *J. Mater. Sci.*, 21, 2283-2288.

Saryazdi, F., Motahhari, H., Schoeggl, F.F., Taylor, S.D., Yarranton, H.W. (2013). Density of Hydrocarbon Mixtures and Bitumen Diluted With Solvents and Dissolved Gasses. *Energy & Fuel.* 27. 3666-3678.

Sheikha, H., Pooladi-Darvish, M., Mehrotra, A.K. (2005). Development of graphical methods for estimating the diffusivity coefficients of gases in bitumen from pressure-decay data. *Energy & Fuels*, 19, 2041-2049.

Stark, S. D. (2013). Cold Lake Commercialization of the Liquid Addition to Steam for Enhancing Recovery (LASER) Process. *International Petroleum Technology Conference*; Beijing, March 26-28, 2013.

Tang, J. (2001). On the Determination of Diffusivities of Volatile Hydrocarbons in Semi-Solid Bitumen, *Can. J. Chem. Eng*., 79, 164-168.

Tang, J., Zhang, P. X. (2000). Method to Determine Molecular Diffusivities of Phenol in Bitumen, *Can. J. Chem. Eng.*, 78, 1175-1180.

Taylor, G.I. (1953): Dispersion of soluble matter in solvent flowing slowly through a tube, *Royal Society London Series A*, 219 186–203.

Taylor, G. I. (1954): Conditions under which dispersion of a solute in a stream of solvent can be used to measure molecular diffusion, *Royal Society London Series A*, 225, 473–477.

Tharanivasan, A. (2012). Asphaltene Precipitation from Crude Oil Blends, Conventional Oils, and Oils with Emulsified Water. Ph. D. Thesis, University of Calgary, Calgary, Alberta, Canada.

Verlaan, M. L., Hedden, R., Castellanos-Díaz, O., Lastovka, V., Giraldo Sierra, C. A. (2015). Solvent Enhanced Steam Drive: Experiences from the First Field Pilot in Canada. *Society of Petroleum Engineers*. SPE Kuwait Oil and Gas Show and Conference, Mishref, Kuwait, 11-14 October 2015.

Vignes, A. (1966). Diffusion in Binary Solutions: Variation of Diffusion Coefficient with Composition. *Indus. Eng. Chem. Fund.,* 5, 189-199.

Wen, Y., Kantzas, A., Wang, G. J. (2004). Estimation of Diffusion Coefficients in Bitumen Solvent Mixtures Using X-Ray CAT Scanning and Low Field NMR. *Petroleum Society of Canada*. Canadian International Petroleum Conference, Calgary, Alberta, Canada; 8-10 June 2004.

Wen, Y., Bryan, J., Kantzas, A. (2005). Estimation of Diffusion Coefficients in Bitumen Solvent Mixtures as Derived From Low Field NMR Spectra. *J. Can. Petr. Technol*, 44, 29-35.

Wen, Y. W., Kantzas, A. (2005). Monitoring Bitumen−Solvent Interactions with Low-Field Nuclear Magnetic Resonance and X-ray Computer-Assisted Tomography. *Energy & Fuels*, 19, 1319-1326.

Wen, Y., Bryan, J., Kantzas, A. (2003). Estimation of Diffusion Coefficients in Bitumen Solvent Mixtures as Derived From Low Field NMR Spectra. *Petroleum Society of Canada*. Canadian International Petroleum Conference, Calgary, Alberta, Canada, 10-12 June 2003.

Wilke, C. R., Chang, P. (1955). Correlation of diffusion coefficients in dilute solutions. *AIChE J.*, 1, 264-270.

Yarranton, H. W., Satyro, M. A. (2009). Expanded Fluid-Based Viscosity Correlation for Hydrocarbons. *Ind. & Eng. Chem. Res*., 48, 3640-3648.

Yaws, C. L. (2018). Transport Properties of Hydrocarbons. Norwich, NY: William Andrew Inc. Retrieved from: https://app.knovel.com/web

Zhang, X., Shaw, J. (2007). Liquid-Phase Mutual Diffusion Coefficients for Heavy Oil + Light Hydrocarbon Mixtures, *J. Petr. Sci. Technol*., 25, 773- 790.

Zhang, X., Fulem, M., Shaw, J. (2007). Liquid-Phase Mutual Diffusion Coefficients for Athabasca Bitumen + Pentane, *J. Chem. Eng. Data*, 52, 691-694.

Appendix A: Density and Viscosity of WC-B-A3 Bitumen

Temperature °C	Pressure MPa	Viscosity mPa·s	Density kg/m³
50.00	0.1	5401.8	990.2
50.01	2.5	5996.4	991.6
50.02	5	6632.3	993.0
50.02	7.5	7329.1	994.4
50.02	10	8029.2	995.7
75.05	0.1	698.7	974.4
75.05	2.5	755.8	975.8
75.05	5	810.1	977.3
75.05	7.5	861.6	978.8
75.05	10	924.9	980.3
99.99	0.1	169.9	958.4
99.99	2.5	181.5	960.1
99.98	5	191.7	961.7
99.98	7.5	202.6	963.3
99.98	10	215.2	965.0
125.04	2.5	62.6	944.1
125.04	5	66.1	945.9
125.04	7.5	69.3	947.6
125.04	10	73.0	949.5
150.04	2.5	28.1	928.5
150.04	5	29.4	930.5
150.04	7.5	30.7	932.4
150.04	10	32.2	934.4
175.05	2.5	15.1	912.7
175.05	5	15.6	915.0
175.05	7.5	16.3	917.3
175.05	10	16.9	919.6

Appendix B: Validation of One-Dimensional Diffusion

In Chapter 4, it was assumed that radial diffusion was negligible compared to axial diffusion because the initial interface between the two fluids was flat and the diffusion fronts were always parallel to the initial interface. To test this assumption, several diffusion experiments were conducted in glass tubes. Known masses of bitumen and solvent are brought into contact inside a glass tube, using the same procedure as explained in Chapter 3 for the liquid-liquid diffusion experiments. Then, the position and the shape of the interface were tracked over time.

Figure B1 shows one of the glass tube experiments conducted in a 2.8 cm graduated cylinder. Once the fluids were brought in contact (Figure B1a), the interface was flat and there was no evidence of wall effects (curve interface near the walls). Over time, the diffusion fronts rose parallel to the initial interface and again there was no evidence of wall effects.
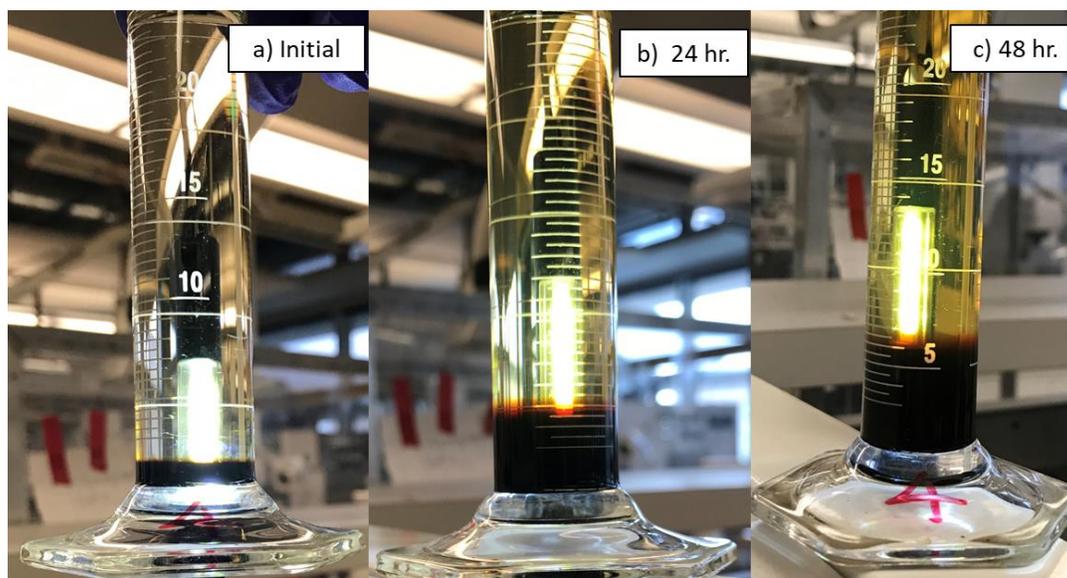

Figure B1. Solvent/bitumen interface tracking in a 2.8 cm diameter glass tube for a toluene/bitumen system at ambient conditions.

Figure B2 shows the position of the interface over the time for glass tube experiments conducted in graduated cylinders with diameters ranging from 1.1 to 4.1 cm. All of the points follow the same

line, suggesting that the diameter of the cell did not affect the diffusion process over this range of diameters. Recall that the diffusion apparatus has a 3.8 cm diffusion cell; therefore, it is expected to not have any wall effects in the experiments performed in this thesis.
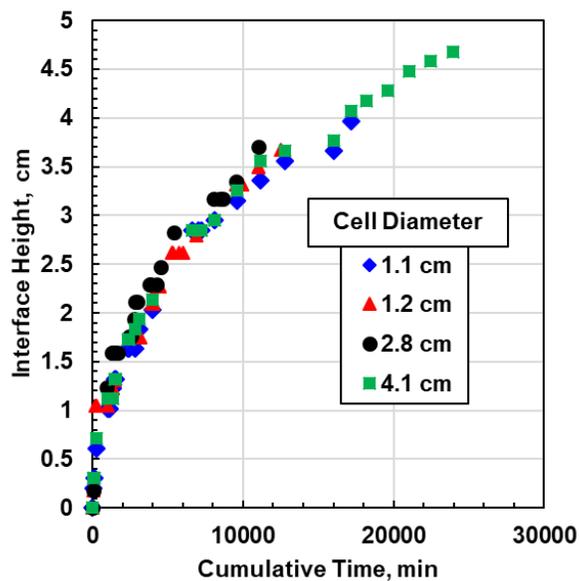

Figure B2. Effect of the diameter on the position of the interface versus time for a toluene/bitumen system at ambient conditions.

Appendix C: Concentration Profiles Versus $X/\sqrt{t}$ for Toluene/Maltenes, *n*-Heptane/ Maltenes, and *n*-Pentane/Bitumen Systems
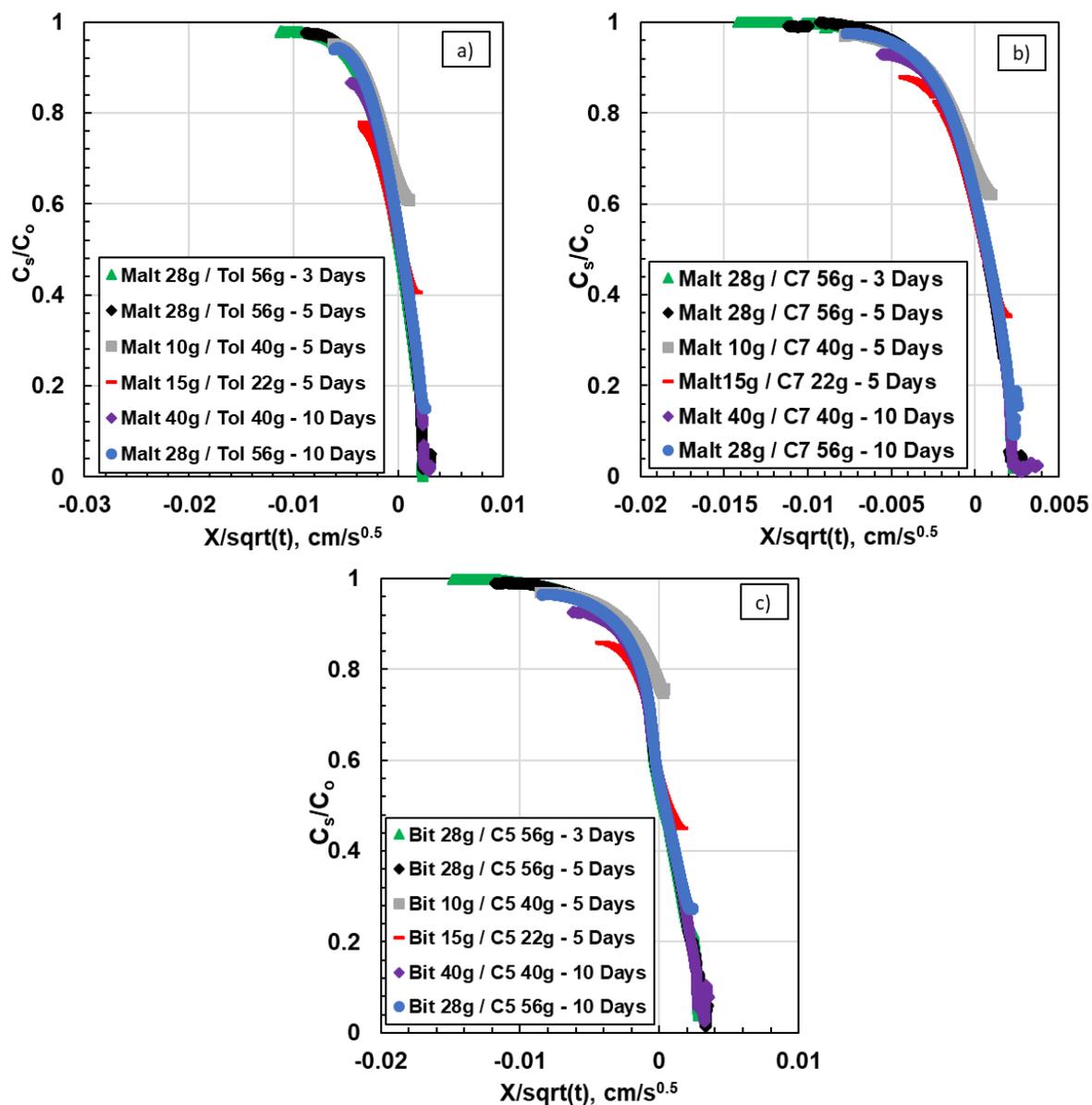

Figure C1. Concentration profiles plotted against $X/\sqrt{t}$ for: a) toluene/maltenes systems; b) *n*-heptane/maltenes systems; c) *n*-pentane/bitumen systems.

**Appendix D: Concentration Profiles Versus $X/\sqrt{t}$, $X/\sqrt[3]{t}$ and $X/\sqrt[4]{t}$**
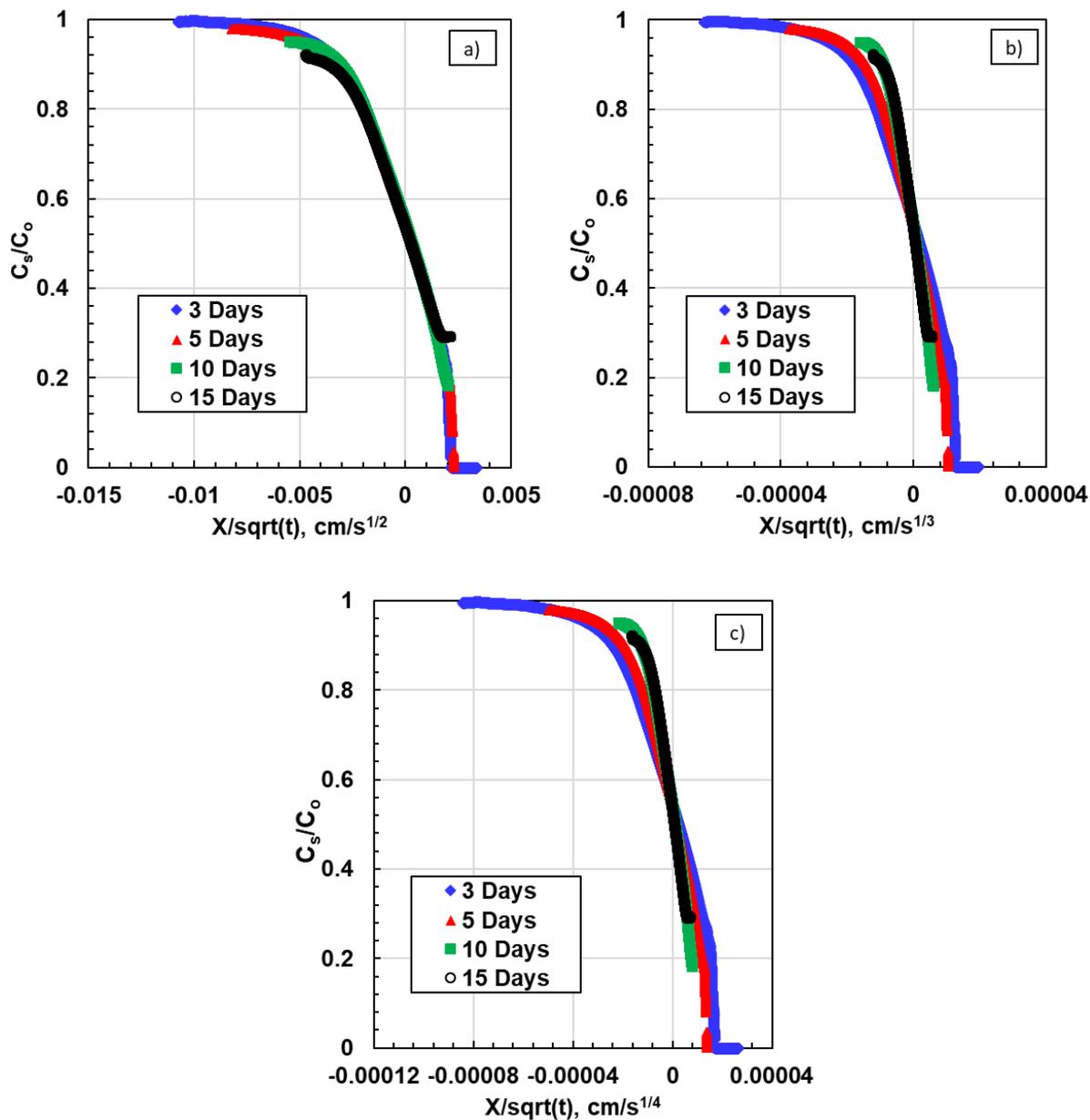
Figure D1. Concentration profiles of toluene/bitumen system at ambient conditions plotted against: a) $X/\sqrt{t}$; b) $X/\sqrt[3]{t}$; c) $X/\sqrt[4]{t}$

Appendix E: Settling Rate Profile Calculations

In Chapter 5, settling rate profiles were used to evaluate the effect of asphaltenes precipitation on the mass transfer rate at different dilution conditions. The profiles were calculated using the Stoke's law, given by (Bird *et al.*, 1960):

$$u(x) = \frac{g(\rho_{asp} - \rho_{mix}(x))d_{asp}^2}{18\mu_{mix}(x)} \tag{D1}$$

where u is the settling rate at a given position x, ρ_{asp} is the asphaltenes density, ρ_{mix} and μ_{mix} are the density and viscosity of the mixture at a given position x, d_{asp} is the diameter of the asphaltenes particles, and g is the gravitational acceleration. Therefore, to calculate settling rate profiles, the concentration, density, and viscosity profiles as well as the diameter of the asphaltenes particles and the asphaltene density are required.

The concentration profiles were generated using the numerical model presented in Chapter 4. The initial masses of solvent and bitumen, temperature, pressure, and diffusion time for the *n*-alkane/bitumen experiments were the inputs to the model. The Modified Hayduk and Cheng equation (Eq.5.4) was used to account for the concentration dependant diffusivity with the fluid parameters A_p and *n* from Table 5.4. Figure E1 shows the calculated concentration profiles for average solvent mass contents of 50, 59, 67, and 80 wt%.

At each concentration, the density was calculated from the density mixing rule (Eq. 4.43) and the viscosity from the EF model (Eq.4.53) to obtain the density and viscosity profiles shown in Figure E2. Finally, the diameter and the density for the asphaltenes particles were obtained from Duran (2018). The density for the asphaltenes was set to 1.2 g/cm³. Precipitated asphaltenes aggregate and therefore have a distribution of sizes. However, they settle as a zone and their settling rate can be determined using their volume mean diameter (Duran, 2018). It was assumed that the asphaltenes aggregated during the experiment. The diameter was set to 260 micrometers (0.026 cm), the maximum expected diameter of an asphaltene aggregate Duran (2018). Hence, the settling calculation will determine the maximum expected settling rate.
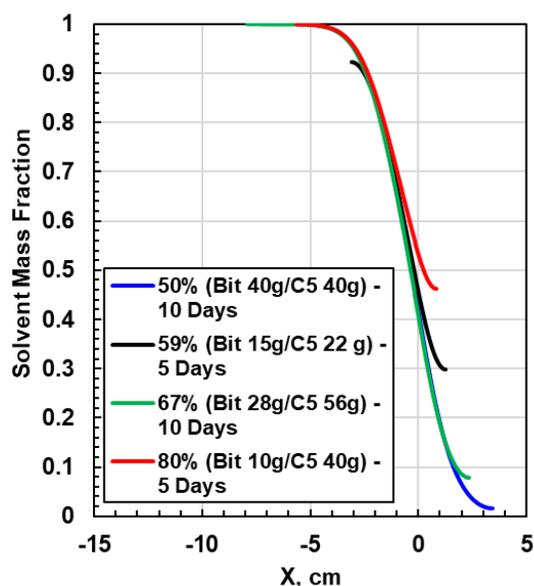
Figure E1. Calculated mass fraction profiles for n-pentane/bitumen systems at ambient conditions with average n-pentane contents from 50 to 80 wt% and diffusion times of 5 and 10 days.
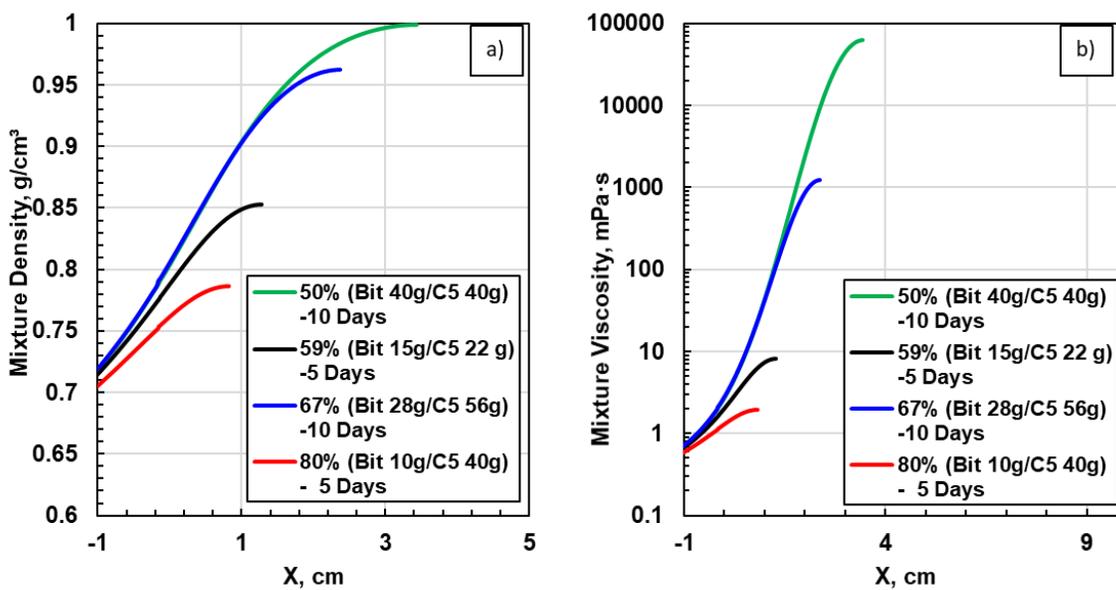

Figure E2. Calculated density (a) and viscosity profiles (b) for n-pentane/bitumen systems at ambient conditions with average n-pentane contents from 50 to 80 wt% and diffusion times of 5 and 10 days.